

Vilde Arild Thomassen

A Study of Soil Contamination by Residues of Single-use Face Masks

Master's thesis in Civil and Environmental Engineering

Supervisor: Rao Martand Singh

Co-supervisor: Rafaela Cardoso

June 2023

Vilde Arild Thomassen

A Study of Soil Contamination by Residues of Single-use Face Masks

Master's thesis in Civil and Environmental Engineering
Supervisor: Rao Martand Singh
Co-supervisor: Rafaela Cardoso
June 2023

Norwegian University of Science and Technology
Faculty of Engineering
Department of Civil and Environmental Engineering



Vilde Arild Thomassen

A Study of Soil Contamination by Residues of Single-use Face Masks

Lisboa, June 2023

Master Thesis

Supervisor: Professor Rafaela Cardoso, NTNU

Supervisor: Professor Rao Martand Singh, IST

Department of Civil and Environmental Engineering
Norwegian University of Science and Technology (NTNU)

Preface

The Norwegian University of Science and Technology (NTNU) in Trondheim and Instituto Superior Técnico (IST) collaborated to complete this master's thesis as a component of the master's program in Civil and Environmental Engineering originally carried out at NTNU in Trondheim. The study was supervised by Professor Rao Martand Singh at NTNU and Professor Rafaela Cardoso at IST, who also suggested the topic of the thesis. The laboratory work and research were carried out during spring of 2023 at IST, and the thesis was written as a joint effort between IST and NTNU for the specialization course TBA 4900 in Geotechnics at NTNU. I would like to express my gratitude to my supervisors for their guidance and support throughout this project.

Lisboa, 2023-06-11



Vilde Arild Thomassen

Acknowledgements

I would like to take this opportunity to express my sincere gratitude to the individuals and organizations who have played a crucial role in the successful completion of this thesis. Firstly, I would like to thank my supervisors, Professor Rao Martand Singh at NTNU and Professor Rafaela Cardoso at IST, for their invaluable support, guidance, and encouragement throughout this project. Their expertise and insights have been instrumental in shaping my research and understanding of the subject matter. A special thanks to Prof. Rafaela for committing this collaboration with NTNU.

I would also like to extend my thanks to Jorge Pontes at the laboratory of the Civil Department at IST for his valuable assistance with preparations for the experimental work.

Special thanks go to the Mining lab at IST, Professor Manuel Francisco Costa Pereira from the Civil, Architecture and Georesources department, and Professor Maria Paula Mendes from the research unit Civil Engineering Research and Innovation for Sustainability. Their generous offer of equipment necessary to shred face masks into smaller particles simulating microplastics was extremely helpful. I would also like to thank Gabriel Calebe from the Masters in Environmental Engineering for his assistance.

I would like to thank the staff at NOVA School of Science and Technology (FCT NOVA) for their expert assistance with laboratory testing of water and soil samples. Their dedication have been essential in conducting the research and achieving meaningful results. Thank you for your contribution to this project.

Finally, I want to emphasize that this experience has been instrumental in shaping my perspective on the environmental challenges faced by the engineering industry. Through this project, I have come to realize the crucial role of research and development in tackling environmental problems, and the need for a holistic approach that takes into account the bigger picture. I believe that the topic of this thesis is of utmost importance in the context of the current environmental crisis, and its relevance will only grow in the future. I am excited to apply the knowledge and skills gained from this project to contribute to the ongoing efforts towards sustainability and environmental awareness in my future career endeavours.

VT

Abstract

With plastic waste posing a significant threat to terrestrial and aquatic ecosystems, the increased usage of single-use face masks during the COVID-19 pandemic has created environmental challenges due to their polymer-based composition and potential contribution to microplastic (MP) pollution. MPs, defined as particles ranging from 1 micron to 5 millimetres, result from the degradation of plastic waste from various sources, including industrial production, domestic use, and improper disposal. While the impact of MPs on marine ecosystems has been extensively studied, their potential effects on terrestrial environments, particularly from a geotechnical engineering standpoint, remain largely unexplored. This master's thesis aims to provide a comprehensive overview of the environmental consequences associated with the disposal of single-use face masks in soil during the pandemic. It involves a laboratory study that examines the influence of incorporating shredded face masks into soil under simulated natural conditions, taking into account geotechnical engineering soil parameters.

The experimental procedure involved subjecting soil samples, with and without shredded face masks, to UV exposure for a duration of two and six weeks. The collected samples underwent analysis to assess their physical and hydraulic properties, as well as the chemical composition of the soil and water. Additionally, the presence of face mask fibers in both the soil and the submerged water was examined. The data obtained from the experimental work were analysed, and the effects of face mask fibers on soil properties were evaluated by comparing samples with and without the presence of shredded face masks.

The results of the laboratory investigation offer insights into the potential environmental impact of single-use face masks in terrestrial environments. Notably, the presence of mask fibers was found to decrease permeability and increase water retention capacity in the soil. Moreover, prolonged degradation impacted the pore structure of the soil and the void ratio, indicating possible degradation of both soil and face mask fibers. The degradation of the mask fibers themselves was less obvious, though, as the particle size distribution of the fibers were essentially the same in samples exposed to UV light and those that were not.

These findings can contribute to raise public awareness regarding the responsible disposal of single-use face masks. Furthermore, the study emphasizes the need for further research in this field and underscores the significance of considering the broader environmental impacts of plastic waste on soil and water systems from a geotechnical engineering perspective.

Sammendrag (Norwegian)

Med plastavfall som utgjør en betydelig trussel mot terrestriske og akvatiske økosystemer, har den økte bruken av engangs munnbind under COVID-19-pandemien skapt miljøutfordringer på grunn av deres polymerbaserte sammensetning og mulige bidrag til mikroplastforurensning. Mikroplast (MP), definert som partikler i størrelsesorden 1 mikron til 5 millimeter, oppstår som et resultat av nedbrytningen av plastavfall fra ulike kilder, inkludert industriell produksjon, bruk i hjemmet og feilaktig avfallshåndtering. Mens virkningen av mikroplast på marine økosystemer har blitt grundig studert, er deres potensielle effekter på terrestriske miljøer, spesielt fra et geoteknisk ingeniørperspektiv, i stor grad utforsket. Denne masteroppgaven har som mål å gi en omfattende oversikt over de miljømessige konsekvensene forbundet med håndtering av engangs ansiktsmasker i jord under pandemien. Den omfatter en laboratorieundersøkelse som undersøker påvirkningen av å tilsette kuttet ansiktsmasker i jord under simulerte naturlige forhold, med hensyn til geotekniske jordparametere.

Den eksperimentelle prosedyren involverte eksponering av jordprøver, med og uten fiber fra engangs munnbind, for UV-lys i to og seks uker. De innsamlede prøvene ble analysert for å vurdere deres fysiske og hydrologiske egenskaper, samt kjemisk sammensetning av jordprøven og vannet. Videre ble tilstedeværelsen av munnbinds-fiber i både jordprøven og vannet som omringet jordprøven undersøkt. Dataene fra forsøket ble analysert, og effektene av oppkuttet munnbind på jordegenskapene ble evaluert ved å sammenligne prøver med og uten tilstedeværelse av disse fibrene fra munnbind.

Resultatene fra laboratorieundersøkelsen gir innsikt i den potensielle miljøpåvirkningen av engangs munnbind i terrestriske miljøer. Spesielt ble det funnet at tilstedeværelsen av munnbinds-fiber reduserte permeabiliteten og økte vannretensjonskapasiteten i jorden. Videre påvirket langvarig nedbrytning porestrukturen i jorden og porevolumet, noe som indikerer mulig nedbrytning av både jord- og munnbinds-fiber. Nedbrytningen av maskens fibre i seg selv var imidlertid mindre tydelig, da partikkelfordelingen av fibrene var i hovedsak den samme i prøver som var eksponert for UV-lys og de som ikke var det.

Disse funnene kan bidra til å øke bevisstheten blant allmennheten om ansvarlig avfallshåndtering av engangs munnbind. Videre understreker studien behovet for ytterligere forskning på dette feltet og betydningen av å vurdere de bredere miljøkonsekvensene av plastavfall på jord- og vannsystemer fra et geoteknisk ingeniørperspektiv.

Table of Contents

Preface	I
Acknowledgements	II
Abstract	III
Sammendrag (Norwegian)	IV
Table of Contents	V
List of Figures	VIII
List of Tables	XII
1 Introduction.....	1
1.1 Background	1
1.2 Motivation.....	2
1.3 Aim and objective	3
1.4 Limitations.....	4
1.5 Structure of the Thesis	5
2 Literature review.....	6
2.1 Plastic.....	6
2.2 Face Mask.....	8
2.2.1 Types of Face Masks.....	8
2.2.2 Manufacturing of Single-use Face Masks	10
2.2.3 Use and Disposal of Single-use Face Masks.....	11
2.2.4 The Increased Use and Disposal of Single-use-plastic due to the COVID-19 Pandemic	14
2.2.5 Environmental impact of surgical (single-use) face masks	18
2.3 Microplastics Sourced from Single-use Face Masks.....	19
2.3.1 Microplastics caused by environmental weathering of plastics.....	20
2.3.2 Presence of microplastics in the water systems	22
2.3.3 Presence of microplastics in sediments.....	23
2.3.4 Health aspects of microplastics.....	24
2.3.5 Identifying microplastics	25

3	Experimental work.....	27
3.1	Methodology.....	27
3.1.1	General overview.....	27
3.1.2	Conducted tests.....	27
3.2	Soil.....	28
3.2.1	Soil characterization.....	28
3.2.2	Specific Gravity of the particles.....	29
3.2.3	Grading size distribution and consistency limits.....	30
3.2.4	Optical Microscope and Mineral analysis of the soil.....	32
3.3	Shredded Face Masks.....	34
3.3.1	Shredding process.....	34
3.3.2	Grading size distribution of the face mask fibers.....	35
3.4	Procedure for Experimental Work.....	36
3.4.1	Sample preparation.....	36
3.4.2	Experimental setup.....	38
3.4.3	Temperature.....	39
3.5	Characterization of Compacted Samples.....	41
3.5.1	Initial water content.....	41
3.5.2	Saturated permeability.....	42
3.5.3	Water retention curve.....	42
3.6	Ageing Tests and Results.....	49
3.6.1	Dry volumetric weight.....	49
3.6.2	Mercury intrusion porosimetry tests.....	51
3.6.3	Chemical analysis of the water.....	53
3.6.4	Optical microcope.....	54
3.6.5	Scanning electron microscope.....	56
4	Joint Analysis of the Results and Discussion.....	60
4.1	Visual Observations.....	60
4.1.1	Soil.....	60

4.1.2	Water.....	61
4.2	Mask effect on the Physical and Hydraulic Properties.....	63
4.2.1	Saturated permeability (k).....	63
4.2.2	Water retention curves.....	64
4.3	Void Ratio and Effects on Soil Structure.....	67
4.3.1	Mercury Intrusion Porosimetry.....	67
4.3.2	Void ratio	70
4.3.3	SEM Analysis	73
4.3.4	Chemical water analysis.....	74
4.3.5	Environmental impact of single-use face masks in soils.....	77
5	Conclusions and Recommendations for Further Work	78
5.1	Conclusions	78
5.2	Recommendations for further work.....	80
	References.....	81
	Appendix A.....	86
	Appendix B.....	87
	Appendix C.....	88
	Appendix D	89

List of Figures

Figure 1.1. Discarded single-use face mask observed in various environments in Lisbon, 2023. ...2

Figure 2.1 Illustration of three types of face masks commonly used during the pandemic (adapted from *Qualities to Look for in Face Mask Protection - Safe'N'Clear, Inc. | The Communicator™ Clear Face Mask*, n.d.)9

Figure 2.2. Schematic view of a medical mask, composed by three TNT layers, two spunbond and the internal meltblown (adapted from Armento et al., 2021)..... 10

Figure 2.3. Process map of single-use surgical face mask (adapted from A.W. Lee et al., 2021) ... 12

Figure 2.4. Breakdown of generated waste from raw material extraction to the end-of-life. The waste generated at EoL was not added to the total amount of waste generated. As a result, a stapled line separates the waste generated at EoL from the other categories, indicating the updated value for waste generated following the incineration process (adapted from A.W. Lee et al., 2021) 13

Figure 2.5. Schematic diagram of the incineration process (adapted from Moharir et al., 2019). 13

Figure 2.6. A general description on the fate of microplastcs (MPs) in the environment originating from the surgical face masks (adapted from Akber Abbasi et al., 2020) 18

Figure 2.7. Mask collected at the Soko Islands by OceanAsia after the beginning of the COVID-19 pandemic (*COVID-19 Facemasks & Marine Plastic Pollution*, 2020)..... 19

Figure 2.8. The source and fate of microplastics (MPs) (adapted from Xiang et al., 2022) 20

Figure 2.9. Illustration of MPs detected in water bodies such as drinking water and their potential source from various plastic items, including single-use plastics. (Adapted from *Growing Plastic Pollution in Wake of COVID-19*, 2020; *WHO Publish Report on Microplastics in Drinking Water*, 2019) 23

Figure 3.1. Illustration of the soil collected from construction site in Tagus Park, Lisbon. 29

Figure 3.2. Grading size distribution chart for the soil used in the experiment. 31

Figure 3.3. Graph for liquid limit test. The liquid limit value is the water content on 25 hammer blows. 32

Figure 3.4. Microscopic photo of the soil sample in resolution 2.5 mm to the left and 5 mm to the right. 32

Figure 3.5. XRD pattern of soil sample from construction site in Lisbon. A 2θ step size of 0.0330 with scan step time of 74 sec was used with Cu as anode material. 33

Figure 3.6. Illustration of the face mask used in the shredder (1) and the RTECH 2000 cutting mill used to shred face mask with cutting blades (2,3) and bottom sieve (4)..... 34

Figure 3.7. Grading size distribution of face mask fibers subjected to no degradation (MH T0) and long-term degradation with UV exposure (MH, UV T2).....	35
Figure 3.8. Filtering placed from fine to coarse at the bottom of the sample to allow water to flow through the sample.	39
Figure 3.9. Experimental setup of samples suffering UV exposure to the left and no UV exposure to the right.....	39
Figure 3.10. WRC for NM (0 % face mask concentration).....	45
Figure 3.11. WRC for ML (1 % face mask concentration).	46
Figure 3.12 WRC for MH (5 % face mask concentration).....	46
Figure 3.13. Experimental setup of the procedure of the water retention curve. Samples NM, ML and MH were placed in jars with different NaCl solutions. Red labels correspond to samples left to be dried and blue labels corresponds to samples left to be wetted.....	47
Figure 3.14. WRC for ML,m (low mass of mask fibers).	48
Figure 3.15. WRC for MH,m (high mass of mask fibers).....	48
Figure 3.16. Pore size distribution curve for soil samples with 0 % face mask fiber concentration that was subjected to long-term UV degradation (T2) and no degradation (T0) using MIP.....	52
Figure 3.17. Pore size distribution curve for soil samples with 1 % face mask fiber concentration that was subjected to long-term UV degradation (T2) and no degradation (T0) using MIP.....	52
Figure 3.18. Pore size distribution curve for soil samples with 5 % face mask fiber concentration that was subjected to short- and long-term degradation (T1 and T2, respectively) and no degradation (T0) using MIP. This sample had some lacking data and thus MH T2 has flat areas along the curve.....	52
Figure 3.19. Microscopic images obtained with scale 4x 0.10 mm for samples NM, ML and MH (from the left to the right column) subjected to no degradation (T0).....	55
Figure 3.20. Microscopic images obtained with scale 4x 0.10 mm for samples MH (top row) and ML (bottom row) subjected to long-term degradation and UV exposure (UV T2).....	55
Figure 3.21. SEM views of sample containing no mask fiber concentration subjected to no degradation (NM T0) and long-term degradation with UV (NM, UV T2). Scaling of the SEM view is 150x 200 μm , 300x 100 μm and 1500 x 20 μm from left to right, respectively.	57
Figure 3.22. SEM views of sample containing 1 % mask fiber concentration subjected to no degradation (ML T0), long-term degradation without UV (ML T2) and long-term degradation with UV (ML, UV T2). Scaling of the SEM view is 150x 200 μm for the higher row and 300x 100 μm for the lower row.....	57
Figure 3.23. SEM views of sample containing 5 % mask fiber concentration subjected to no degradation (MH T0), long-term degradation without UV (MH T2) and long-term degradation	

with UV (MH, UV T2). Scaling of the SEM view is 150x 200 μm for the higher row and 300x 100 μm for the lower row.....	58
Figure 3.24. EDS spectrum (to the right) detected at the area marked with yellow for sample containing a high concentration of mask fibers with no degradation. Elements detected are Pd, Au and C (a) and O, C, Si, Al, Fe, Mg, Ti, Ca and K (b).	59
Figure 3.25. EDS spectrum (to the right) detected at the area marked with yellow for sample containing a high concentration of mask fibers subjected to long-term degradation and UV exposure. Elements detected are C, O, Fe, Si, Al, Ti, Mg and Ca (a) and O, C, Si, Al, Fe, Ti, Mg, Ca and K (b).	59
Figure 4.1. Photograph of the samples after the first period (T1) of the experiment showing that less soil was found accumulated on the bottom of the container for high concentration of masks (1, right photo) and not subjected to UV-exposure (2, left photo).....	60
Figure 4.2. From left, ML and NM to the right. MH at the top (T1 period).	62
Figure 4.3. From NM to MH (top to bottom). Left column had UV exposure and right column had not (T2 period).....	62
Figure 4.4. The effect of adding different concentrations of microplastics on soil saturated saturated permeability (k). Results of this experimental work using MP of size 2 mm (shredded face mask fibers) with concentrations of 0, 1, and 5 % in silty soil in the present study are shown in Bar A. In clayey soil in Keshan County, China, MP (polypropylene microfibers) of size 0.5 mm with concentrations of 0, 1, and 6 % are represented by Bar B in research results (Guo et al., 2022).....	64
Figure 4.5. Water retention curve (WRC) obtained for samples containing concentration of 0, 1 and 5 % mask fibers and solely low- and high mask fiber mass, corresponding to NM, ML, MH, and ML,m and MH,m, respectively.	66
Figure 4.6. Water retention curve (WRC) obtained for samples with mask fiber concentrations of 0, 1 and 5 %, corresponding to NM, ML and MH, respectively.....	66
Figure 4.7. Distribution of pore sizes through the soil samples containing different concentrations of face mask fibers. NM, ML and MH corresponding to 0, 1 and 5 % concentration of face mask fibers. T0 indicates no degradation of the samples.....	68
Figure 4.8. Distribution of pore sizes through the soil samples containing different concentrations of face mask fibers. NM, ML and MH corresponding to 0, 1 and 5 % concentration of face mask fibers. T2 correspond to long-term degradation and UV indicates that the sample has been exposed to UV during this period.....	69
Figure 4.9. Changes in pore sizes and distribution with the presence of water and degradation in the upper row, and the presence of mask fibers and degradation in the lower row.....	70

Figure 4.10. Void ratio in samples with different concentration of shredded face mask fibers with MH, ML and NM corresponding to 5,1 and 0 % respectively for sub-samples extracted from both top and bottom of cylindrical samples used in the experimental work. MH,UV, ML,UV and NM,UV are samples suffering UV exposure. T1 represents first degradation period of 2 weeks and T2 represents second degradation period of 6 weeks. 71

Figure 4.11. Concentrations of inorganic compounds (mg/l) of water samples submerging soil with varying concentrations of face mask fibers (NM, ML, and MH), subjected to various degradation processes such UV exposure and short- and long-term aging (T1 and T2)..... 76

Figure 4.12. Concentrations of inorganic compounds (mg/l) of water samples submerging soil with varying concentrations of face mask fibers (NM, ML, and MH), subjected to various degradation processes such UV exposure and short- and long-term aging (T1 and T2)..... 76

Figure 4.13. Concentrations of inorganic compounds (mg/l) in samples of water mixed with face mask fibers of concentrations (ML and MH), subjected to different degradation mechanisms such as long-term aging (T2) and UV exposure. 76

List of Tables

Table 2.1. Basic characteristics of different face masks (<i>Comparison of Mask Types for COVID-19 / Safe Work Australia, 2022</i>).....	9
Table 2.2. Reported COVID-19 cases, and estimated total plastic waste generation by region, measured in tonnes (adapted from Benson et al., 2021).	15
Table 2.3. Estimated daily COVID-19 facemasks and global plastic waste generation by country prior to management (adapted from Benson et al., 2021).	16
Table 2.4. Summary of experimental conditions and release of microplastics (MPs) from experimental studies (Wang et al., 2021)	21
Table 2.5. An overview of the identification and quantification of MPs with analytical methods (Cashman et al., 2022; Fu et al., 2020; Xiang et al., 2022)	26
Table 3.1. Pattern list of the minerals identified by XRD in the soil sample collected from construction site in Lisbon.....	33
Table 3.2. Sample names and their corresponding concentrations of added face masks.....	37
Table 3.3. An overview of the sample numbers with the related volume, solid mass, amount of water and amount of shredded face masks. Plan-column determines which kind of degradation mechanism the samples are exposed to.	37
Table 3.4. Temperatures at different measurement times under different simulated environmental conditions.	40
Table 3.5. Initial water content with corresponding dry density and void ratio for samples subjected to different degradation periods and mechanisms.	41
Table 3.6. Saturated permeability of samples with different concentrations of shredded face masks corresponding to 0, 1 and 5 % for NM, ML and MH, respectively.....	42
Table 3.7. Relative humidity (RH) with corresponding soil suction (ψ). The suction corresponds to the concentration of the NaCl.	44
Table 3.8. Curve-fitting constants for soil samples with 0, 1 and 5 % concentration of face mask fibers corresponding to NM, ML and MH, respectively.	45
Table 3.9. Curve-fitting constants for soil samples for low and high mass of face mask fibers corresponding to ML,m and MH,m, respectively.	47
Table 3.10. Void ratio obtained from porosimetry of samples suffering degradation with and without UV exposure for period T1. NM, ML and MH corresponds to soil with concentrations 0, 1 and 5 %, respectively of shredded face masks.	50

Table 3.11. Void ratio obtained from porosimetry of samples suffering degradation with and without UV exposure for period T2. NM, ML and MH corresponds to soil with concentrations 0, 1 and 5 %, respectively of shredded face masks. 51

Table 3.12. List of inorganic component concentrations found in submersion water leachates (mg/l). "Non-detected" is represented by N.D. With degradation durations T0, T1, and T2, the symbols NM, ML, and MH represent soil concentrations of face mask fibers of 0, 1, and 5%, respectively. w corresponds to samples containing only water and mask fibers..... 53

Table 4.1. Change in volume (Δvol) based on the difference between air void space between top and bottom sample (Δe) and the initial void ratio before any degradation (e_{init}) for period T1 and T2. 72

1 Introduction

1.1 Background

The widespread use of plastic products in our daily lives has resulted in significant environmental challenges with plastic waste being a major contributor to pollution in both terrestrial and aquatic ecosystems (Jambeck et al., 2015). Plastic waste can take hundreds of years to degrade, and during this time, it can break down into smaller particles known as microplastics (MPs). MPs refer to small plastic particles with sizes between 1 micron to 5 millimetres, and they can be generated from a variety of sources, including industrial production, domestic use, and disposal of plastic products (Benson et al., 2021a; Kumar et al., 2020). Roughly 8 million metric tons of plastic waste enters the ocean annually (Fava, 2022), and as much as 80 % of this waste comes from land-based sources (Jambeck et al., 2015).

MPs have a rising environmental impact because they can migrate to diverse environmental media, including as water bodies and soil, where they can remain and accumulate, providing a risk to both animal and human health. Multiple habitats, including seas, freshwater systems, soil, and air, have been shown to contain MPs (Pizarro-Ortega et al., 2022). They can be ingested by organisms, causing physical damage and reducing their ability to feed or reproduce, and moreover end up in the human food chain and ultimately impact human health. A study conducted by Horton et al. (2017) found that MPs were present in 72 % of global tap water samples, which highlights the extent of the problem of MP pollution in relation to water pollution. Additionally, MPs can serve as carriers for contaminants like persistent organic pollutants (POPs), which can build up in tissues of organisms and thus threaten human health (Sarijan et al., 2021).

The COVID-19 pandemic has led to a significant increase in the use of single-use face masks as a means of preventing the transmission of the virus. By the start of the pandemic, face masks have contributed to the global plastic production by almost 370 million ton (Saliu et al., 2021). While these masks are essential in protecting public health, their widespread use has resulted in environmental concerns, particularly regarding the improper disposal of face masks, such as littering or dumping in landfills. Single-use face masks are made of polymer-based materials, which classify them as single-use plastics. Plastic waste in the environment can be transported by rivers, storms, winds, or directly dumped into terrestrial or aquatic systems (Pizarro-Ortega et al., 2022). Interaction with environmental conditions such as biological degradation, UV-radiation,

CHAPTER 1

temperature and contact with water, will eventually lead to fragmentation, and potentially give rise to micro pollutants such as MPs (Kumar et al., 2020). A laboratory study conducted by Saliu et al. (2021) found that single-use face masks release up to 173,000 MP fibers per day when exposed to simulated environmental conditions, which may result in contamination of the land and water. Face mask disposal can thus exacerbate the issue of plastic waste and MP pollution, leading to potential harm to human health and ecosystems (Pizarro-Ortega et al., 2022).



Figure 1.1. Discarded single-use face mask observed in various environments in Lisbon, 2023.

1.2 Motivation

The objective of the master's thesis is to provide a comprehensive review of the existing research on the environmental impacts of single-use face masks in soils, during the COVID-19 pandemic. Additionally, this thesis includes a laboratory study that investigates the effects of the presence of shredded face masks in soils, focused on changes on saturated permeability, water holding capacity, and the void ratio of the soil. These properties are among those that characterize the leaching potential of soils, and therefore their ability to store or spread contaminants.

Overall, the impact of single-use face masks on the environment and human health is a critical issue that requires further investigation. This thesis aims to contribute to a better understanding

of the environmental implications of the widespread use and disposal of single-use face masks during the COVID-19 pandemic by combining a literature review with original laboratory work. By studying the impact of face masks on soil contamination, this research can inform strategies for mitigating the environmental impact of these masks and raising public awareness about the importance of waste management systems, not only during the current pandemic, but also in the future.

1.3 Aim and objective

Single-use face masks have become a significant source of plastic pollution in the environment. While their impact on marine ecosystems has been widely studied, their potential impact on terrestrial environments remains largely unexplored, especially from the perspective of geotechnical engineering. In addition, it is important to investigate the potential migration of MPs from the soil medium to the surrounding water bodies. This thesis aims to assess the impact of shredded face masks in soils physical and hydraulic properties, as well as their potential to degrade under different environmental conditions. Specifically, the study addresses the following objectives:

- Investigate the impact of adding shredded face masks on the physical and hydraulic properties of soils.
- Assess the potential degradation of shredded face masks in soil under different environmental conditions.
- Examine the influence of microplastics (MPs) on the leaching of contaminants from the soil medium into surrounding water bodies.

By addressing these objectives, this thesis will contribute to our understanding of the potential impact of single-use face masks on terrestrial environments, as well as their role in the migration and fate of MPs in soil and water systems.

1.4 Limitations

In this master's thesis, there are several limitations to consider when interpreting the results. Firstly, due to limitation in time and resources, only one type of soil was used in the experiment. While this was done to simplify the study and reduce variables, it is possible that different types of soil could have different degradation rates and impacts on the environment. Therefore, the results of this study should be applied with caution and further research with a wider range of soil types is recommended.

Secondly, this experiment only simulates soil contamination in the surface layer using residues mixed with the soil in known quantities. As a result, the findings of this investigation may not represent all the environmental consequences of single-use face masks on soil from natural contamination, where the residues concentrations will vary depending on depth.

Thirdly, the study performed focuses only on the changes on the soils' hydraulic properties and not on the possible impact of the residues on their mechanical properties, and therefore the study has this limitation from a geotechnical engineering perspective.

Lastly, identifying and quantifying MPs sourced from single-use face masks can be complicated due to their small size. This means that precise and developed equipment is necessary to achieve accurate results. However, this equipment can be time-consuming to use and expensive to access. Therefore, the methods used in this study may not have identified all the MPs present in the soil samples.

Also worth noting is that using fibers from shredded face masks to mimic degraded face masks in the environment is a simplification. Due to the time required for degradation, an experiment involving genuine face masks in soil would be time-consuming. In addition, it would be less controllable considering the fragment sizes from degradation would be difficult to anticipate and, thus, control to have any supported theory for the experimental task.

These limitations are taken into account when interpreting the results of this study and applying them to the wider context of the environmental impacts of single-use face mask. Further research with a wider range of soil types and depths and more precise MP identification and quantification methods is recommended to provide more comprehensive understanding of the environmental impacts of these masks.

1.5 Structure of the Thesis

Chapter 1	Introduction <i>First chapter introduces the thesis and discusses its context, motivation and problem formulation.</i>
Chapter 2	Literature Review <i>Includes an overview of the literature on plastic, face masks made of plastic, and the effects of their disposal on the environment.</i>
Chapter 3	Laboratory Work <i>Chapter 3 presents the laboratory work, including its methodology, procedure, and results.</i>
Chapter 4	Joint Analysis of the Results and Discussion <i>The discussion of the laboratory results in respect to prior research and expectations is covered in this chapter.</i>
Chapter 5	Conclusions and Recommendations for further work <i>Chapter 5 concludes the findings and makes suggestions for additional research.</i>

2 Literature review

A preliminary literature review was carried out in the beginning of 2023. The aim of the review was to synthesize available information on the environmental impact of single-use face masks, including potential release of microplastics (MPs), and to promote proper disposal practices to mitigate the potential harm caused by plastic waste. While studies have explored the impact of MPs on various environmental media, there are lacking studies specifically investigating the environmental impact of single-use face masks. Research on detecting MPs in the environment have been conducted, however the majority of these studies are focusing on MP detection from plastic waste in general, rather than from single-use face masks. Thus, the importance of the review was to gather information of MP contamination from face masks specifically while considering existing information of contamination of general plastics.

2.1 Plastic

2.1.1 The History of Plastics

The plastic industry started to grow in the middle of the 1900s. Before this, the most important type of thermoplastics, the cellulosic, were made from vegetable sources. Thermoplastics are plastics that can be melted and reshaped without undergoing chemical change and can be divided into three groups including commodity plastics (high-volume, low-cost plastics), engineering plastics (higher-performance plastics with improved properties) and specialty plastics (highly specialized materials with exceptional properties) (Gilbert, 2017). After World War II, the main raw material for the European plastic industry was coal, and today, the plastic industry is dominated by raw materials from petroleum (Gilbert, 2017). The most significant petroleum product is ethylene, and the manufacture of ethylene results in the production of propylene as a by-product. Vinyl chloride, styrene, ethylene oxide, and ethylene glycol are produced when ethylene combines with other reactants, and these organic compounds serve as the basis for the well-known polymers PVC, PS and polyesters.

From 1950 to 2015 the plastic production increased exponentially from 2.3 million tons to 448 million tons and by 2050 the production is expected to double (Parker, 2019). However, the

problem is not only related to the production. Plastics are synthetic polymers from petroleum products and are considered as a non-biodegradable materials, meaning that they do not break down by living organisms into natural elements or substances in the environment over a period of time (*From Pollution to Solution*, 2022). Different studies have reported that among the amount of plastics we are dealing with by 2017, more than 6.9 billion tons have become plastic waste and 91 % of this waste never made it to the recycling bin (*University of Georgia*, 2017).

2.1.1 Problems with Plastics

Every aspect of daily life uses plastic, including various enterprises, forms of transportation, buildings, and the medical industry. Plastics are almost universally used and are present almost everywhere on earth. The average amount of plastic consumed per capita worldwide in 2005 was 30 kg (Statista, 2016) and as plastic production has increased rapidly over the years, this average consumption is likewise anticipated to rise. It is worth noting that plastic consumption differs significantly between nations and regions, with the United States having the highest consumption levels followed by Western Europe (Gilbert, 2017).

As mentioned, an immense amount of the produced plastic ends up as waste in the environment. With time, the plastic pieces will start to break down into smaller particles when exposed to different degradation mechanisms and eventually cause a source to MPs. This is what poses the greatest threat from plastic waste since such tiny particles are so easily dispersed and transported to other environmental media including the air, soil, river, and ocean. These particles might be consumed by the local wildlife and organisms, ultimately entering the human food chain. Millions of creatures are killed each year by plastic trash, and reports indicate that MPs are found in more than 100 aquatic species, including fish, shrimp, and mussels, all of which frequently consumed by humans (Parker, 2019).

According to a [video](#) by the United Nations Environment Programme UNEP (2022) titled "Plastic Pollution: Harmful Chemicals in Our Plastics," the threat of plastic pollution goes beyond its physical impact on the environment. Plastic products contain over 10,000 chemicals, commonly referred to as "forever chemicals," that are used to enhance their properties depending on the intended use. These chemicals have been linked to detrimental effects on human health, as many of them are non-biodegradable and can accumulate in the environment and persist for generations.

One area of concern that requires immediate attention is the use of single-use face masks, which have become ubiquitous during the COVID-19 pandemic. These masks are made of various types of plastics, and their disposal has raised concerns about their contribution to the plastic waste crisis. The following chapters will delve into the environmental impact of single-use face masks and explore potential solutions to reduce their ecological footprint. It is essential to address the issue of single-use face masks, as they represent a microcosm of the larger plastic waste problem and highlight the need for a more sustainable approach to plastic production and consumption.

2.2 Face Mask

Due to the global pandemic of COVID-19 having its outburst in March 2020, a worldwide recommendation from the government was to wear personal protective equipment (PPE) to avoid transmission of infection (Shekaraiah & Suresh, 2021). Among different types of PPE, face masks have been identified as the most effective protective equipment by providing a physical barrier preventing virus transmission (Armentano et al., 2021).

2.2.1 Types of Face Masks

There is a large variety of face mask products, however in this context, three main categories of face masks can be defined: fabric mask, respirator mask, and surgical (single-use) masks. Table 2.1 presents an overview of the three mask types with their basic characteristics, developed by Safe Work Australia (2022) and a picture of the different masks are illustrated in Figure 2.1. Fabric masks (cloth face coverings) are reusable masks made from textiles. Their efficiency is lower compared with surgical masks and respirators, depending on the particle filtering capacity of the fabric (*The Norwegian Directorate of Health, 2020*). However, they have the advantage of being reusable if proper cleaning and sanitizing is done. Respirator masks, in general, are close-fitting masks that prevents inhalation of harmful particles while breathing. Due to filter materials with large pores, they are not active in virus contamination, however, certain respirator masks approved by the European and the U.S standards including FFP2, FFP3 and N95 respectively, are guaranteed protection for infective virus particles (Armentano et al., 2021). Surgical face masks usually worn by health care workers are single-use devices. They work as a physical barrier

CHAPTER 2

between the people and the environment and are further divided into three categories based on their bacterial filtration efficiency (Type I, Type II and Type IIR) (Konda et al., 2020). For common use, surgical masks are immensely popular as they provide safety against infections, are easy to wear and easily accessible. Moreover, these are the type of face masks that are commonly observed discarded into the environment and will hence be considered in this study.

Table 2.1. Basic characteristics of different face masks (Comparison of Mask Types for COVID-19 | Safe Work Australia, 2022).

Mask	Protection	Type	Use
Fabric/ cloth mask	<ul style="list-style-type: none"> - Helps prevent infectious people from spreading COVID-19 - Provides the user with a lower level of protection 	Not medical grade	<ul style="list-style-type: none"> - Reusable - Manufactured/homemade - Should have a minimum of 3 layers of washable fabrics
Surgical mask	<ul style="list-style-type: none"> - Prevents the spread of COVID-19 - Protects against splashes and large droplets or sprays from reaching the user's mouth/nose 	Medical grade	<ul style="list-style-type: none"> - Single use - 3 layers - Has three grading levels of protection and fluid resistance
P2/N95 Respirator	<ul style="list-style-type: none"> - Prevents the spread of COVID-19 - Provides the user with the greatest protection from exposure to biological particles in the air such as viruses and bacteria 	Medical grade	<ul style="list-style-type: none"> - Single use - Requires fit test and fit check

Note. Type I (level 1) surgical masks are acceptable for general use/patient care, and higher protection gradings are preferred in higher-risk settings such as healthcare, aged care, and disability sectors, quarantine, police, and security. Fabric/cloth masks are suitable for public/community use and general workplace settings, but not for medical settings.

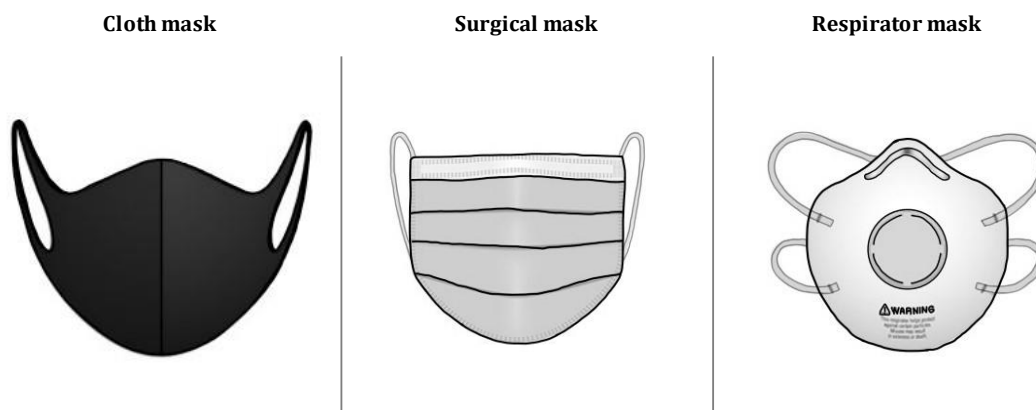


Figure 2.1 Illustration of three types of face masks commonly used during the pandemic (adapted from *Qualities to Look for in Face Mask Protection - Safe'N'Clear, Inc. | The Communicator™ Clear Face Mask*, n.d.)

Disposable face masks are commonly developed from synthetic thermoplastic polymers such as polypropylene (PP), polyurethane (PU), polyacrylonitrile (PAN), polystyrene (PS), polycarbonate (PAC), polyethylene (PET), or polyester (PET) (Armentano et al., 2021). Surgical masks with the protection suitable for daily use, often consist of three layers with a non-woven PP fabric sandwiching a filtering material in the middle made of melt-blown PP, as illustrated in Figure 2.2 (Shekaraiah & Suresh, 2021).

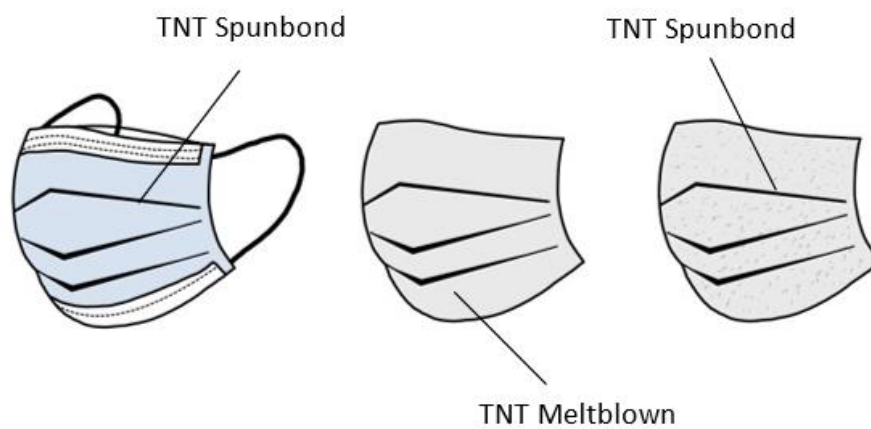


Figure 2.2. Schematic view of a medical mask, composed by three TNT layers, two spunbond and the internal meltblown (adapted from Armento et al., 2021)

2.2.2 Manufacturing of Single-use Face Masks

Face masks makes a composite of diverse layers of non-woven fabrics made from polymeric fibres. The fiber dimension and pattern can be related to the protective efficiency of the face mask. Hence, the manufacturing processes of fabrics is important for the quality of the end product (Armentano et al., 2021). Spunbonding and meltblowing are methods in fabric development used in the production of surgical face masks.

Spunbond method

This method mainly consists of two steps including fiber production and different bonding techniques. First, the polymers are extruded and stretched to form the fiber, then, all fibers are attached using self-adhering, thermal or chemical bonding (Armentano et al., 2021). The result is

a non-woven fabric, often consisting of more soft fibers than fabrics made using the meltblown method.

Meltblown method

The meltblown method is a simple and versatile one-step process for converting polymers into non-woven fabrics. This technique leads to fabrics containing fibers with smaller diameter and thus an improved filter efficiency. Hence, the meltblown process is suitable for producing fabrics for the main filter of the face mask, that is, the middle layer. The polymers are directly transformed in membranes using five constituents; the extruder, metering pump, die assembly, web formation and winding in order to obtain a nonwoven web (Drabek & Zatloukal, 2019).

2.2.3 Use and Disposal of Single-use Face Masks

A study comparing the life cycle assessment of surgical face masks and reusable face masks (face cloth) proceeded by Wei Lun Lee (2021) with the intention of mapping the environmental impact from manufacturing, usage, and disposal of the face masks, developed a process map (Figure 2.3) showing the stages from cradle to grave. The surgical face mask considered in the study consisted of:

- an aluminium nose piece;
- a polyurethan ear loop;
- a composite of melt-blown PP covered with a layer of spunbond PP covering both sides.

Hence, a typical composition of regular face masks commonly used during the pandemic, as illustrated in Figure 2.2.

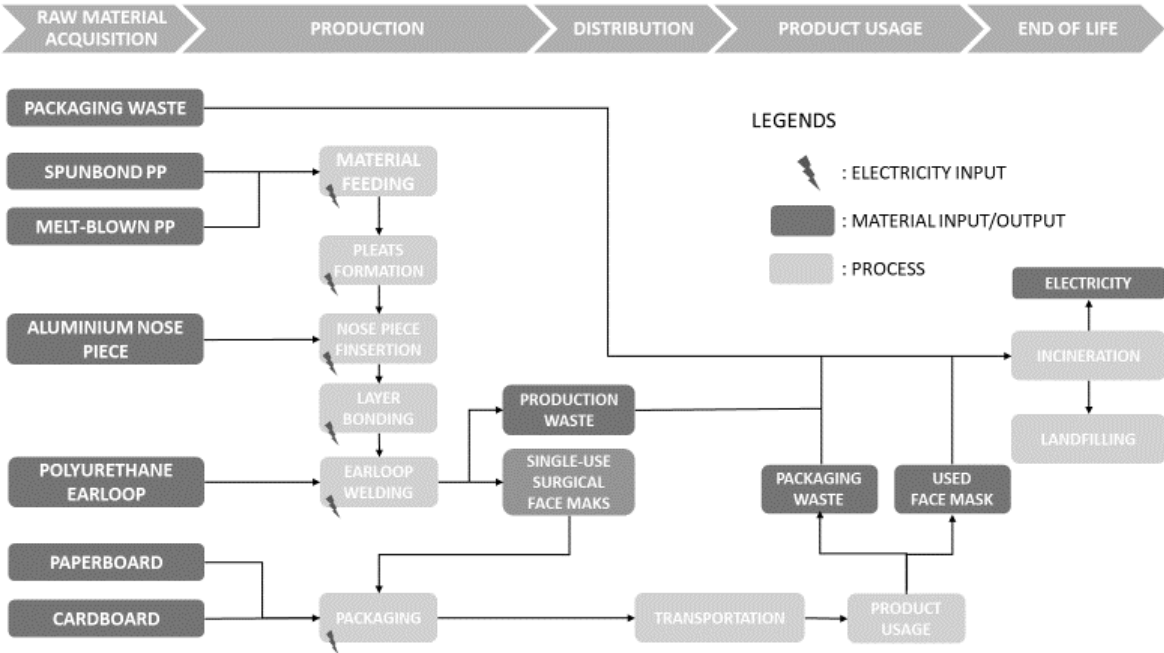


Figure 2.3. Process map of single-use surgical face mask (adapted from A.W. Lee et al., 2021)

The process map gives information about all the stages from raw material acquisition to end-of-life and is thus an important tool for understanding how the face masks are manufactured and treated after their usage stage. As surgical face masks are polymer based, mask production, generation and disposal make a source of plastic waste. Wei Lun lee (2021) presented the contribution of waste generated from raw material extraction to the end-of-life stage shown in Figure 2.4. Values in the usage stage correlates with the quantity of materials used in the production phase of the face mask. Thus, 86.5 % of the used materials to produce a surgical face mask ends up as generated waste in the usage stage. The dotted line indicates the updated value of cumulated waste generated after the incineration process, thus after waste management treatment is proceeded.

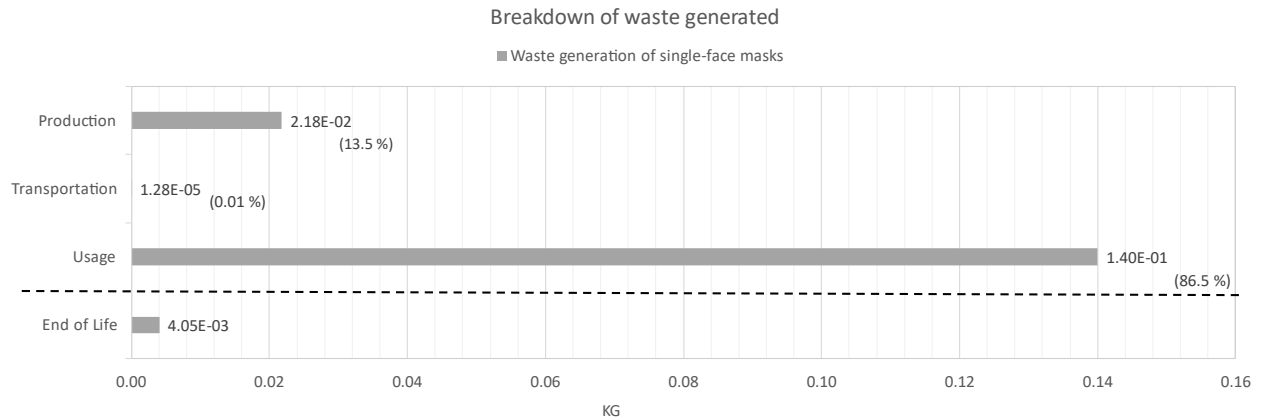


Figure 2.4. Breakdown of generated waste from raw material extraction to the end-of-life. The waste generated at EoL was not added to the total amount of waste generated. As a result, a stapled line separates the waste generated at EoL from the other categories, indicating the updated value for waste generated following the incineration process (adapted from A.W. Lee et al., 2021)

If the process map for face masks is followed as described in Figure 2.4 will discarded masks be considered as municipal waste and further incinerated in a waste-to-energy plant. Incineration is a process where waste is combusted while heat is produced resulting in biproducts including ash, heat, and combustion gases (Moharir et al., 2019). A schematic diagram of a typical incineration process is shown in Figure 2.5. Incineration of inorganic content, such as plastics, will contribute to the formation of ashes and toxic gases. Thus, they are likely to increase the risk of plastic environmental pollution if they are not treated correctly. Heat generation of plastic waste typically produce air pollutant gasses like CO_x, NO_x and SO_x (Gupta et al., 2022). However, the consequences of leaving the waste in the environment in comparison to use waste treatment processes are likely to be worse due to problematics with the degradation process of plastic, which will be further discussed in Chapter 2.3.

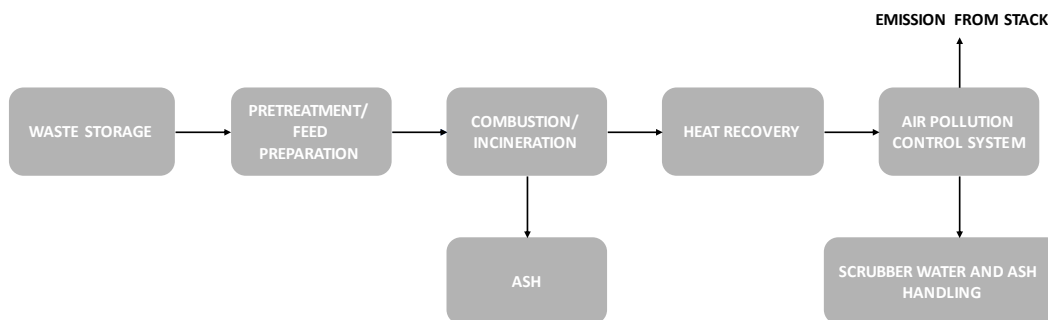


Figure 2.5. Schematic diagram of the incineration process (adapted from Moharir et al., 2019)

2.2.4 The Increased Use and Disposal of Single-use-plastic due to the COVID-19 Pandemic

Due to the COVID-19 pandemic, governments around the world have recommended the use of personal protective equipment (PPE) to control the spread of the SARS-CoV-2 virus. This has led to a surge in production and usage of single-use PPE, including face masks, gloves, and medical gowns, which are primarily made from non-woven polymeric materials (Benson et al., 2021b). Despite the existence of waste treatment processes for disposed face masks, studies show that the generation of waste from single-use plastics, particularly in developing countries with poor waste management systems, remains significant (*United Nations Environment Programme, 2021*). Moreover, the increased demand for PPE, including face masks, has reversed the ongoing battle against plastic pollution, as improper disposal of these PPEs can lead to their accumulation in the environment, exacerbating the existing problem of plastic pollution in marine and terrestrial systems.

A research study by Benschol *et al.* (2021) developed one year after the outbreak of COVID-19, estimated that since March 2020, 1.6 million tonnes of plastic waste was generated daily and an estimation of 3.4 billion single-use face masks was discarded daily. Among these numbers, Asia was projected to contribute with the largest quantity of discarded facemasks with approximately 1.8 billion face masks per capita per day, followed by Europe (445 million) and Africa (411 million). Despite the similar numbers of disposed face masks in Europe and Africa, estimated plastic waste generated from masks in Europe is almost the half of the projected waste generation in Africa (Table 2.2). This is an indication of Europe generally having better waste management systems and knowledge about recycling than Africa, as expected in higher-income regions. Additionally, from Table 2.3 it can be observed that the ASEAN (Association of Southeast Asian Nations) region are outstanding in terms of total estimated plastic waste compared to estimated face masks discarded daily. Comparing Bangladesh with Turkey with both similar numbers of daily discarded face masks, Bangladesh has over the half of waste production than Turkey. Same goes for the Philippines compared with France. This emphasizes the importance of having good waste management systems to be able to avoid increasing the problem of plastic pollution due to the pandemic.

The numbers presented in both tables are estimated values based on the total population of the country retrieved from Worldometers (2020) and an arbitrary percent of face mask acceptance rate by the urban population (hypothetical data). All values are thus representing an estimated scenario of the use and disposal of plastic waste during the first year of the ongoing pandemic. Recent studies have projected that the demand for PPE is expected to remain high in the future

CHAPTER 2

with an estimated increase in the production of disposable face mask of 20 % between 2020 and 2025 (N. Singh et al., 2020), meaning the trend of increased plastic waste generation will continue if mitigation measures are not made.

Table 2.2. Reported COVID-19 cases, and estimated total plastic waste generation by region, measured in tonnes (adapted from Benson et al., 2021).

Region	Population	Total COVID-19 cases	Facemask acceptance rate by population (%)	Avg. facemask /capita/ day	Estimated daily facemask disposed	Estimated plastic waste generates (tonnes)	Estimated plastic waste generated /day (tonnes)
Africa	1,340,598,147	212,271	70	1	411,814,854	100,544,861	275,465
Asia	4,641,054,775	1,470,640	80	1	1,875,181,681	348,079,108	953,641
Europe	747,636,026	2,149,248	80	1	445,022,934	56,072,702	153,623
South America	653,952,454	1,267,858	75	1	380,414,703	49,046,434	134,373
North America	368,869,647	2,361,458	80	1	244,335,150	27,665,223	75,795
Oceania	42,677,813	8,896	75	1	21,682,379	3,200,836	8,769
Total					3,378,451,702	584,609,165	1,601,666

CHAPTER 2

Table 2.3. Estimated daily COVID-19 facemasks and global plastic waste generation by country prior to management (adapted from Benson et al., 2021).

Rank	Country	Population	Urban population (%)	Facemask acceptance rate by population (%)	Avg. facemask /capita/day	Estimated facemask discarded	Total estimated plastic waste (tonnes)
1	China	1,439,323,776	61	80	1	702,390,002	107,949,283.20
2	India	1,380,004,385	35	80	1	386,401,228	103,500,328.90
3	United States	331,002,651	83	80	1	219,785,760	24,825,198.80
4	Brazil	212,559,417	88	75	1	140,289,215	15,941,956.30
5	Indonesia	273,523,615	56	80	1	122,538,579	20,514,271.10
6	Japan	126,476,461	92	80	1	93,086,675	9,485,734.58
7	Russia	145,934,462	74	80	1	86,393,201	10,945,084.70
8	Mexico	128,932,753	84	75	1	81,227,634	9,669,956.48
9	Nigeria	206,139,589	52	70	1	75,034,810	15,460,469.20
10	Pakistan	220,892,340	35	80	1	61,849,855	16,566,925.50
11	Bangladesh	164,689,383	39	80	1	51,383,087	12,351,703.70
12	Turkey	84,339,067	76	80	1	51,278,153	6,325,430.03
13	Iran	83,992,949	76	80	1	51,067,713	6,299,471.18
14	Germany	83,783,942	76	80	1	50,940,637	6,283,795.65
15	United Kingdom	67,886,011	83	80	1	45,076,311	5,091,450.83
16	France	65,273,511	82	80	1	42,819,423	4,895,513.33
17	Philippines	109,581,078	47	80	1	41,202,485	8,218,580.85
18	South Korea	51,269,185	82	80	1	33,632,585	3,845,188.88
19	Italy	60,461,826	69	80	1	33,374,928	4,534,636.95
20	Argentina	45,195,774	93	75	1	31,524,052	3,389,683.05
21	Egypt	102,334,404	43	70	1	30,802,655	7,675,080.30
22	Colombia	50,882,891	80	75	1	30,529,735	3,816,216.83
23	Spain	46,754,778	80	80	1	29,923,058	3,506,608.35
24	Vietnam	97,338,579	38	80	1	29,590,928	7,300,393.43
25	DR Congo	89,561,403	46	70	1	28,838,772	6,717,105.23
26	Thailand	69,799,978	51	80	1	28,478,391	5,234,998.35
27	South Africa	59,308,690	67	70	1	27,815,775	4,448,151.75
28	Canada	37,742,154	81	80	1	24,456,916	2,830,661.55
29	Ukraine	43,733,762	69	80	1	24,141,037	3,280,032.15
30	Iraq	40,222,493	73	80	1	23,489,935	3,016,686.98
31	Saudi Arabia	34,813,871	84	80	1	23,394,921	2,611,040.33
32	Algeria	43,851,044	73	70	1	22,407,883	3,288,828.30
33	Malaysia	32,365,999	78	80	1	20,196,383	2,427,449.93
34	Peru	32,971,854	79	75	1	19,535,824	2,472,889.05
35	Poland	37,846,611	60	80	1	18,166,373	2,838,495.83

CHAPTER 2

According to the UNICEF (2021) article "Disposing of face masks: The next environmental problem?" published on their website, plastics like surgical face masks have the potential to persist in the environment for up to 450 years if not disposed properly, causing significant environmental harm. The article also cites the author Poudel (2021), who states that the proper method of discarding disposable face masks is still being disregarded. The stakeholders, including the government should address its safe disposal and develop guidance for the public to become aware of the problem and how it can be mitigated. Several face mask-users lacks information on how to dispose face masks safely. Observations has shown that used face masks are being discarded all over the streets, in parks and on coastlines (Fadare & Okoffo, 2020). In fact, it was estimated that only 12 % of the plastic waste from face masks were incinerated, 9 % recycled, and the rest ended up in landfills or other environmental medias (Geyer et al., 2017). A study reported by the World Wide Fund for Nature (WWF) stated that the amount of incorrect disposal of face masks every month was equivalent to 30-40 tons of plastic waste dispersed in the environment, equivalent to 10 million face masks (Kwak & An, 2021).

The question will rather be, what is the safe and proper method of discarding face masks? The World Health Organisation (WHO) recommends discarding face masks in the "correct" rubbish bin immediately after use and not reusing them (CORPORATIVA, n.d.), but due to the masks still having the risk of virus transmission, they are not recommended disposed in the recycling bins.

A recommendation of correct disposal given by the Brazilian Sanitary and Environmental Engineering Association (ABES) issued that the used materials should be placed into two smaller plastic bags before they can be disposed with the general domestic waste ('Disposing of disposable masks properly', 2022). However, this solution will only lead to an increase of plastic waste. As the quality of waste treatment systems varies from country to country based on their knowledge and legislations from the government, a risk of such waste being dumped in open areas and roadsides are significant. As any other services, solid waste services have a cost in resources, skilled personnel, appropriate equipment, suitable location, proper maintenance and operation (Guerrero et al., 2013). Thus, the presence of solid waste treatment systems will depend on the financial situation of the country and its interest in waste management issues. It can be presumed that developing countries are likely to suffer from a shortage of waste management systems due to their economic constraints. Moreover, such countries often have large populations as seen in Table 2.2 and Table 2.3, and the problem of plastic waste is thus immense in such countries. This is however not only a problem for the country itself, but countries nearby could also be affected, as a lot of developing countries, especially in the ASEAN regions, are coastal, and the risk of plastic waste spreading into the marine environment and being transported through wind and streams is plausible.

2.2.5 Environmental impact of surgical (single-use) face masks

The generation of hazardous plastic waste, including surgical face masks, has become a pressing issue worldwide. In 2018, the World Health Organization (WHO) reported that low-income countries generate approximately 0.2 kg/day of hazardous plastic waste, while high-income countries generate around 0.5 kg/day. The degradation of surgical face masks, like other plastic waste, can result in the production of MPs, posing a threat to terrestrial and aquatic environments and ultimately impacting living organisms, including human health. MPs can infiltrate the soil medium and eventually reach groundwater, which serves as a vital source of freshwater and drinking water (Agence européenne pour l'environnement (Organisme et agence de l'UE), 2022). This contamination of groundwater can lead to the ingestion of MPs by aquatic species, entering the human food chain and introducing toxic pollutants (Du et al., 2022). Figure 2.6 provides an illustration of the process from the breakdown of surgical face masks to the presence of MPs in environmental media.

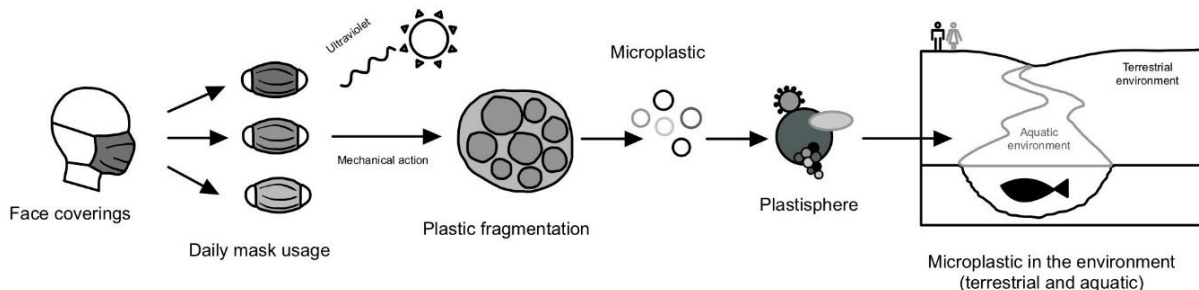


Figure 2.6. A general description on the fate of microplastics (MPs) in the environment originating from the surgical face masks (adapted from Akber Abbasi et al., 2020)

Use and disposal of surgical face masks can have negative environmental impacts that go beyond physical waste. As they contain plastics, they contribute to climate change due to carbon emission. According to Fadare Okoffo (2022), the carbonaceous materials in the single-use face masks have a high capacity to absorb and retain other pollutants, which can lead to release of greenhouse gases into the atmosphere. The production of a single mask consumes approximately 10-30 Wh of energy and releases 59 g CO₂-eq greenhouse gas emissions into the environment (Selvaranjan et al., 2021). Thus, both the production and disposal of face mask contribute to carbon emissions and global warming.



Figure 2.7. Mask collected at the Soko Islands by OceanAsia after the beginning of the COVID-19 pandemic (*COVID-19 Facemasks & Marine Plastic Pollution*, 2020)

2.3 Microplastics Sourced from Single-use Face Masks

The COVID-19 pandemic has witnessed a substantial surge in the global production of disposable face masks, with an estimated demand of 89 million masks per month according to the WHO (2020). Unfortunately, improper disposal practices and inadequate waste management have led to the environmental contamination of single-use plastic products like face masks (Fadare & Okoffo, 2020). As face masks degrade, they break down into small particles, contributing to the accumulation of plastic fibers. These fibers fall into the category of MPs, which are further divided into primary and secondary MPs. Primary MPs enter the environment directly from sources such as microbeads in cosmetics, while secondary MPs are formed through the breakdown of larger plastic items and include small particles derived from discarded face masks (Benson et al., 2021b). These MPs can accumulate in ecosystems and be ingested by wildlife and potentially by humans. Figure 2.8 illustrates the journey of MPs from their sources to their ultimate impact on the environment, emphasizing the critical need to reduce the use of single-use plastics, including face masks.

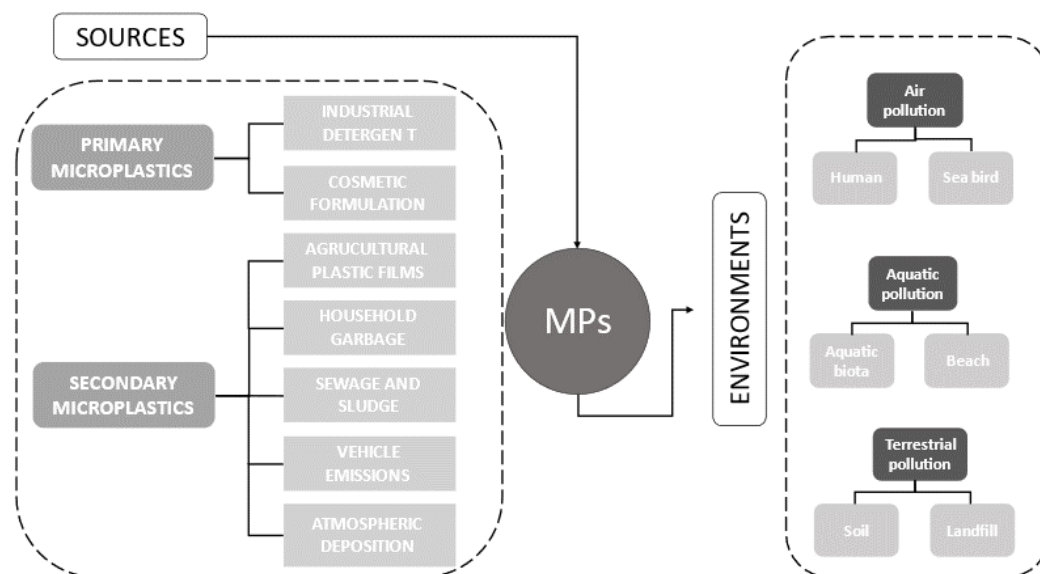


Figure 2.8. The source and fate of microplastics (MPs) (adapted from Xiang et al., 2022)

2.3.1 Microplastics caused by environmental weathering of plastics

Degradation of plastic is an extremely slow process, but with time, interaction with environmental conditions such as biological degradation, UV-radiation, temperature and contact with water, will eventually lead to fragmentation, and potentially give rise to MPs (Kumar et al., 2020). Environmental weathering of plastics undergoes through abiotic and biotic processes. Abiotic factors such as sunlight, temperature, wind and mechanical forces leads to physical and chemical changes of the material, whereas biotic factors refer to weathering due to physical processes of organisms and biochemical processes (Zhang et al., 2021). As a result, changes of the plastic properties occur, and eventually, fragmentation happens. According to a study by Pizarro-Ortega *et al.* (2022), the release of MPs from surgical face masks was examined through different weathering methods, which were mainly classified into chemical and physical degradation. The experimental conditions for these methods are summarized in Table 2.4.

Chemical degradation

Irreversible changes in the chemical characteristics of plastics could be caused by UV-radiation over time, causing oxidation of the polymer structure (Pizarro-Ortega et al., 2022). This is also expected to be the case for face masks. Another property of plastic refers to its crystallinity which further influences the chemical, optical, thermal, and mechanical properties, and moreover, its

fracture mechanism. The degree of crystallinity is affected by its exposure to UV-radiation and aquatic environments with time, and in accordance with Chen *et al.* (2021) it was observed an increase of the degree of crystallinity of PE plastics until 23 weeks of exposure. Since disposable face masks are polymer-based, it could be helpful to investigate such degradation results of “regular” plastics and use this as a starting point for expected degradation of disposable face masks.

Physical degradation

Chemical degradation of plastics can lead to degradation of physical properties and may further affect the mechanical properties that refers to its behaviour to load application, such as tensile strength or elongation at break (Pizarro-Ortega *et al.*, 2022). Low values of elongation at break and tensile strength will likely lead to fragmentation under natural conditions due to a more brittle behaviour of the plastic, and the fragmentation mechanism will again be determined by the chemical properties of the material (Pizarro-Ortega *et al.*, 2022).

Table 2.4. Summary of experimental conditions and release of microplastics (MPs) from experimental studies (Wang *et al.*, 2021)

Type of mask	Experimental condition	Microplastic release (MP)
Disposable surgical	Virgin face mask placed in an aqueous solution and shaken for 24 h	483,888 MPs per mask
	Virgin face mask exposed to UV-radiation, placed in an aqueous solution and shaken for 24 h	1,566,560 MPs per mask
	Virgin face mask exposed to UV-radiation, placed in an aqueous solution in the presence of sand and shaken for 24 h	16,001,943 MPs per mask

2.3.2 Presence of microplastics in the water systems

Studies have shown that the presence of MPs in aquatic systems, such as ponds, lakes, rivers, and oceans, has become a potential source of pollution. In particular, the detection of MPs has been conducted in various farm settings, with the results indicating their growing impact on the aquatic environment (Xiang et al., 2022). A review paper developed by Gabisa and Gheewala (2022) considered the abundance of MPs in the ASEAN region with the conclusion of commonly finding the presence of secondary MPs with most of the observed fragments coming from polyethylene (PE), polystyrene (PS) and polypropylene (PP). MPs are emitted by a variety of anthropogenic activities including industrial and agricultural processes, transportation, waste management and construction, among others. Thus, the exact sources are difficult to determine. However, it is detected that MPs in water bodies usually are sourced from runoffs, wind, atmospheric deposition, rivers, and tides.

The review paper by Gabisa and Gheewala (2022) reported that wells from groundwater in Indonesia contained concentrations of MPs ranging from 0.25 to 0.95 items/L. These MPs were mainly sourced from landfills located near the wells. Leachate and atmospheric deposition are the main transportation modes of MPs from landfills to the water systems. Moreover, landfill leachates are able to transport up to among 81 MPs/day to the aquatic environment (Nurhasanah et al., 2021). Consequently, the construction of more landfill facilities may exacerbate the issue of MP contamination in groundwater. Furthermore, inadequate management of leachate from household wastewater can lead to contaminated groundwater (Gabisa & Gheewala, 2022). However, results from the study revealed that MPs were more abundant in surface water than in groundwater, with a higher concentration of MPs nearby urban areas with extensive commercial activity. It is thus reasonable to assume that this is caused by irresponsible use of single-use plastics and lack of social awareness about waste management.



Figure 2.9. Illustration of MPs detected in water bodies such as drinking water and their potential source from various plastic items, including single-use plastics. (Adapted from *Growing Plastic Pollution in Wake of COVID-19*, 2020; WHO Publish Report on *Microplastics in Drinking Water*, 2019)

2.3.3 Presence of microplastics in sediments

Generally, most plastic waste is discarded and disposed directly into the terrestrial systems before reaching the aquatic systems. As a result, a significant portion of plastic waste remains in the terrestrial environment and inland waters (Su et al., 2022). MPs sourced from plastic waste in soils can be transported both laterally and vertically to other environmental medias. Lateral transportation occurs through processes such as runoff, wind, soil movement or erosion (Gabisa & Gheewala, 2022). Vertical transport of MPs can occur through soil ploughing, bio-disturbance, or wet-dry cycles, allowing them to reach deeper layers of the soil medium and potentially reach the groundwater system (Su et al., 2022; Zhou et al., 2020).

When considering long-term perspective, it becomes evident that MPs are more frequently detected in sediments than in water bodies due to the sediments' limited movement and circulation. Studies on sediments have revealed that courser materials have a higher affinity for MPs, resulting in the highest concentrations being found in the upper layers of the sediment (Gabisa & Gheewala, 2022). Analyses of coastal sediment cores in Australia have shown that the highest concentration of MPs is typically found in the upper layers, specifically at depths of 15 cm and above (Yao et al., 2019). Secondary MPs sourced from polymers like polyethylene (PE) and polypropylene (PP) are commonly observed in the studied sediments within aquatic environments (Gabisa and Gheewala, 2022).

The concentration of MPs in a particular area is significantly influenced by the level of plastic contamination. Areas directly exposed to plastic pollution exhibit MP concentrations that are up to 200 times higher than those in protected areas. However, even protected areas are not immune to MP contamination, as the buoyancy of MPs allows them to be transported by wind and surface currents (Asadi et al., 2019). Sediments, therefore, serve as both sources and sinks for MPs and play a crucial role in regulating the distribution of MPs within aquatic systems (Yao et al., 2019). Considering the increasing attention towards plastic pollution in terrestrial environments and the accumulation of MPs in soils from urban areas and agricultural fields, where they may be retained permanently or temporarily, it is imperative to conduct further research on the abundance of MPs in sediments (Su et al., 2022).

2.3.4 Health aspects of microplastics

As MPs are present in different environments such as air, soil and water, they also have been found in our food and drinking water. This can harm human health in various ways. The ingestion of MPs can cause damage to the digestive systems, leading to inflammation and changes in gut biota. Additionally, MPs can release harmful chemicals into the body, and these can cause reproductive problems, developmental delays, and cancer (Campanale et al., 2020). Over time, MPs can moreover accumulate in the body, including the heart tissue and blood vessels, leading to increased inflammation and development of atherosclerosis which previously have been reported as the leading cause of death in the United States (Kontrick, 2018; Kuller, 1969).

Considering MP concentrations are already known to be present in sediments and surrounding bodies of water, groundwater, a component of water that interacts with soil, is expected to be similarly affected. Furthermore, MPs are poisons that are regularly identified in groundwater sources (S. Singh & Bhagwat, 2022), raising serious concerns about human health. Because groundwater or underground water supplies 25% of the world's water supply (Panno et al., 2019), it is critical to keep this resource safe and uncontaminated.

2.3.5 Identifying microplastics

The extensive use of plastic materials today, and especially during the COVID-19 pandemic, has led to an immense accumulation of plastic wastes which through various degradation mechanisms has created a source of MPs in the environment (Xiang et al., 2022). Developing good techniques for detection, identification and localisation of MP is thus essential for predicting the impacts of MPs, and further mitigate the problem of MP abundance in different environmental medias. The common methods for MP detection are either directly in environmental samples such as aerosols, sediments, and water columns, or within organisms that are originated from different environments. However, the wide range of MPs makes them difficult to extract, quantify and identify (Cashman et al., 2022).

Conversely, some techniques for identifying MPs have been developed and tested, among others:

- Visual observation
- Fourier Transform Infrared (FT-IR)
- Raman Spectroscopy

Detection and characterisation of MPs usually involves three steps including, extraction, separation and characterisation and/or identification (Fu et al., 2020). Xiang *et al.* (2022) developed recommendations for the main steps of MP detection in the aquaculture environment with the aim to achieve as accurate results as possible. When identifying MPs, he emphasised the importance of combining various techniques instead of using a single method and additionally the importance of establishing standards for qualitative and quantitative MP analyses. A similar study by Fu et al. (2020) covering quantification and identification methods for MPs and nanoplastics (NPs) in the environment provided a guideline in selecting proper methodologies and techniques for MPs research in different sample matrices. An overview of the three methods mentioned above are presented in Table 2.5 covering their procedures, advantages and disadvantages (Cashman *et al.*, 2022; Fu *et al.*, 2020; Xiang *et al.*, 2022).

Table 2.5. An overview of the identification and quantification of MPs with analytical methods (Cashman et al., 2022; Fu et al., 2020; Xiang et al., 2022)

Method	Visual Observation	FT-IR	Raman Spectroscopy
Procedure	- MPs are manually identified and sorted before being counted according to their physical characteristics; colour, shape and hardness	- Three modes including ATR ¹ , reflection and transmission are applied - Provides the chemical bond information of compounds	- Vibrational spectroscopy technique based on the inelastic scattering of light - Provides information about molecular structure of substances which can be compared with a known reference spectrum.
Advantage	- Simple operation - Low cost and no chemical hazards - Used for pre-separation before spectral analysis - MPs source, degradation stage type, colour and shape are easily detected	- Simple operation - Generates chemical information and mapping - Accurate identification	- No damage of the sample - Identifies MPs in both solid and liquid samples (no interference from water) - Higher spatial resolution (about 1µm)
Disadvantage	- Time consuming and high error rate - Size limitation to particles >1 mm - Many similar substances to MPs can cause over/underestimation	- Time consuming - Requires dry samples that must be prepared as thin films or ground powders - Size limitation to particles > 2µm	- Detection time higher than FT-IR - Presence of colour, fluorescence, additives and contaminants in the sample could disturb the result - Low concentration substances are difficult to measure

1 Attenuated total reflection (ATR)

In a study quantifying MPs in sediments from Narragansett Bay in Rhode Island, a hybridized method for the extraction of MPs was developed using density separation and Raman Spectroscopy (Cashman et al., 2022). The hybrid extraction procedure was used to assess the efficacy of extracting MPs from sediments. Sediments from Long Island Sound in New York and Narragansett Beach in Rhode Island were each spiked with known quantities (100 MP per sample) of five types of MPs. The plastic-amended sediments were mixed for at least 48 hours before MPs were extracted using a two-step density separation technique with two sodium bromide solutions. The extracted microplastics were collected on four filters representing two sieve classes and two density separation steps. The filters containing the spiked MPs were visually inspected using a microscope to count the spiked MPs retained on the filters. The recovered MPs were then compared to the initial spiked values to determine the percent recovery. Environmental MPs extracted from the sediments were identified and quantified using Raman Spectroscopy, and particles with a confirmed polymer match and an acceptable hit quality index (HQI) were accepted as a MP particle and further analysed for their physical properties (shape, size and colour). This extraction method was designed for 40-1000µm in diameter, meaning that particles of smaller sizes were left out. Thus, the problem of MPs in environment is even more complicated as smaller particles (like microfibers) also threatens the environment but are not easy to detect due to their small size.

3 Experimental work

3.1 Methodology

3.1.1 General overview

The experimental work performed was conceived to simulate the degradation process of face masks in soil submerged in water under natural conditions. The soil tested is collected from a construction site in Lisbon, Portugal, and the main work were carried out in the geotechnical laboratory of the department of Civil Engineering of IST (Instituto Superior Técnico) in Lisbon from March to May 2023. The soil was chosen from the specified construction site because it contained fragments of different grading sizes such as clay, silt, sand, and gravel, making it a natural soil that most likely represents the soil type that face masks are commonly discarded into. Prior to the main experiment, standardized testing was carried out on the soil to obtain information about its physical and hydraulic properties. Additionally, experimental work in the mining department of IST were carried out to collect the shredded single-use face masks that was going to be added to the soil. The experimental work was conducted over a period of approximately 2 and 6 weeks, corresponding to time periods T1 and T2, respectively. T0 is also used as a term in this study and corresponds to neither degradation nor water submersion of the soil sample. These periods were chosen due to time limitations to complete the experiment and obtain results before the end of the master's program, while still allowing for a sufficient interval between the two periods to detect any potential differences in degradation. This approach provides a perspective on the impact of face masks on soil quality and the resulting environmental consequences.

3.1.2 Conducted tests

The methodology employed in this master's thesis encompassed a comprehensive array of tests and analyses to characterize both the soil and face mask fiber samples. For the soil, the grading size distribution was determined through sieving, adhering to the standard LNEC - E239 "Granulometric Analysis by Sieving." Laser diffraction analysis, following international standards

such as ISO 13320, USP 429, and EP 2.9.31, was utilized to obtain the particle size distribution of the face mask fibers. A goniometer instrument was employed to conduct a mineral analysis of the soil, while the liquid limit, plastic limit, and plasticity index were determined using the standardized test method D 4318-17. The specific gravity of the soil solids was determined using the water pycnometer method outlined in ASTM D 854-02. The desired initial water content, dry density, and void ratio were adjusted through a water content control procedure. Saturated permeability was determined through a permeability test following the method specified in ASTM D 5084-16a. The water retention curve was determined for both the soil and face mask fibers using the adsorption and desorption method. Volumetric dry density (porosimetry), employing the Archimedes principle and the "Paraffin method," characterized the pore structure of the soil. Mercury intrusion porosimetry was used to determine the pore size distribution and porosity of the soil samples. Chemical analysis was conducted on water samples from the submersion water of the soil samples. Scanning electron microscopy provided microstructural information about the soil and face mask fiber samples, while an optical microscope generated microscopic images of the soil samples at a detailed level.

3.2 Soil

3.2.1 Soil characterization

The soil utilized in this study was collected from a construction area in Tagus Park, Lisbon, to as closely resemble natural conditions as feasible. At first glance, the soil appears to be rusty and brownish with some larger gravel fragments and clay clusters, as seen in Figure 3.1. Its colour gives thus the impression that it is rich in iron and/or aluminium and contains traces of organic matter (Queensland;, n.d.). The soil was air-dried, passed through a sieve to remove large debris, and dried for at least 24 hours at 105°C to remove any remaining water. A sub-sample was retained for characterization and analysis, which included determining the soil's physical properties, such as particle size distribution, consistency limits, initial water content and grain specific gravity. These tests were conducted according to established laboratory standards and procedures.



Figure 3.1. Illustration of the soil collected from construction site in Tagus Park, Lisbon.

3.2.2 Specific Gravity of the particles

Procedure for oven-dried specimens in Method B of the Standard Test Method for Specific Gravity of Soil Solids by Water Pycnometer was utilized. As a simplification, the G_s for the sample preparation for the experiment was set at 2.5. The initial water content of a test sample was measured, and the mass of the dried soil was adjusted to make the experimental value of the G_s equal the fixed value since the soil samples were not completely dry when the testing took place. Thus, it was established that the three soil samples examined had an average specific gravity (G_s) of:

$$G_s = 2.46 \cong 2.5$$

It should be emphasized that all prepared samples utilized in the experimental setup, including samples with various amounts of shredded face mask, use the fixed value of the G_s . This is only a simplification, though, as determining the G_s of face mask fibers is challenging given their low weight and density. Therefore, it is expected that the real G_s of soil samples containing these fibers will decrease as the amount of face mask fibers increases.

3.2.3 Grading size distribution and consistency limits

Results of the grading size distribution chart are presented in Figure 3.2 which illustrates the particle distribution of the sample. The curve covers a wide range of particles from fines to gravel with the majority of the particles being in the size range of 1 – 4 mm. The percentage of sand particles is 82% and gravel is 15%, with only 3% of fines.

The uniformity (C_U) and the curvature (C_c) coefficients can be determined by using the information from the grain size distribution and the following formula:

$$C_U = \frac{D_{60}}{D_{10}} = 6$$

(1)

$$C_c = \frac{D_{30}^2}{D_{60}D_{10}} = 2$$

(2)

The percentage of sand particles is 82% and gravel is 15%, with only 3% of fines. With the obtained values for C_U and C_c , the soil classifies as a well-graded sand with little or no fines in accordance with the Unified Soil Classification System by ASTM D-2487 (D18 Committee, n.d.).

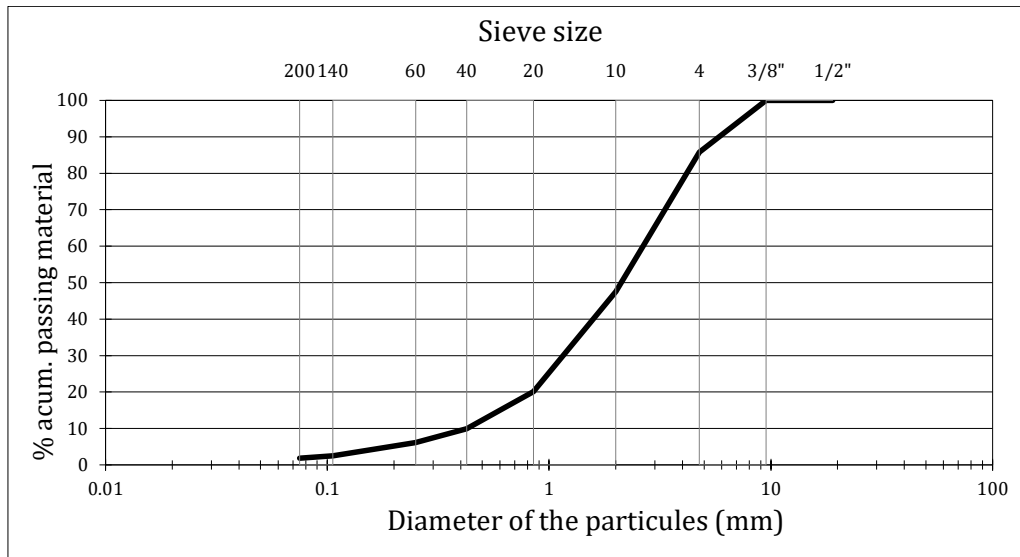


Figure 3.2. Grading size distribution chart for the soil used in the experiment.

The consistency limits were determined although the low percentage of fines because the presence of clayey minerals was noticed. The liquid limit (LL) can be determined from the diagram in Figure 3.3 as the water content at 25 drops using a logarithmic regression.

$$LL = 46 \%$$

The plastic limit (PL) is determined by finding the average water content of all four trials and determined using:

$$PL = \frac{\text{Average water content (\%)}}{\text{Number of trial points}} = 28 \%$$

(3)

Plasticity index (PI) is determined by the difference of LL and PL:

$$PI = LL - PL = 18 \%$$

Due to the values being generally low for PL and PI, the fine fraction of the soil classifies as a low plastic clay (CL).

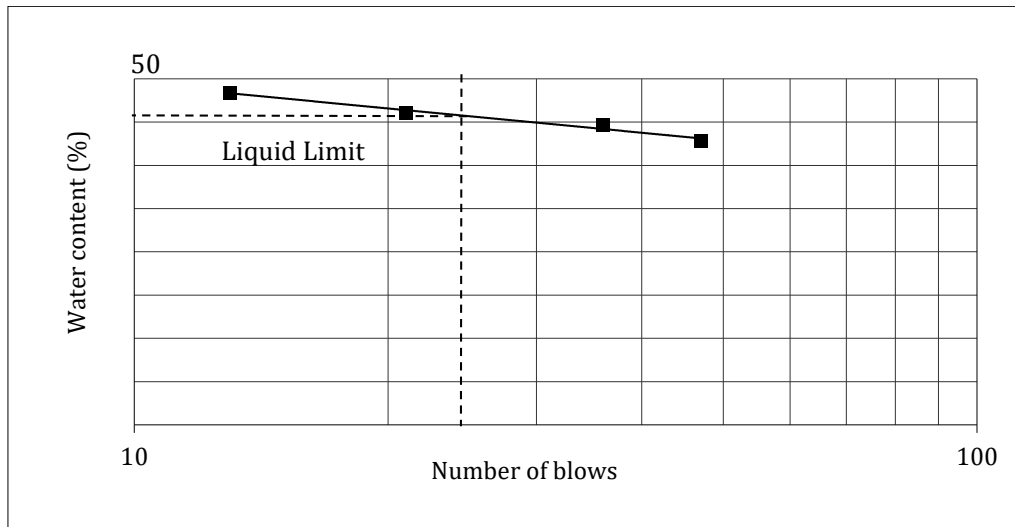


Figure 3.3. Graph for liquid limit test. The liquid limit value is the water content on 25 hammer blows.

3.2.4 Optical Microscope and Mineral analysis of the soil

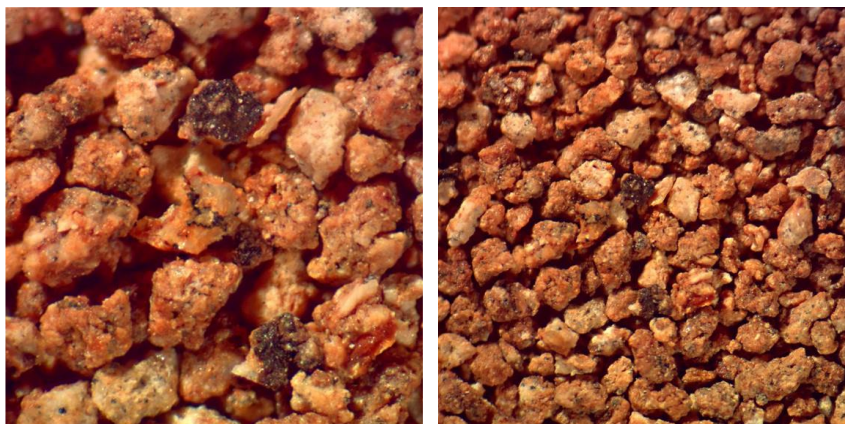


Figure 3.4. Microscopic photo of the soil sample in resolution 2.5 mm to the left and 5 mm to the right.

Figure 3.4 presents microscopic images of the soil with both 2.5- and 5-mm resolutions. A mineral analysis using a goniometer instrument to measure the reflectance angles on the surface of the soil sample after being sieved in the nr. 4 sieve size (4.75 mm) was carried out to characterize the soil and its anticipated behavior by learning more about the mineral composition of the soil. Soil samples with mask fibers prevented analysis since the fibers might produce reflected angles that resembled minerals that were not actually present in the soil. Table 3.1 displays the results for magnetic and non-magnetic minerals. Magnetic minerals are unlikely to have as much of an impact on the classification of the soil's minerology as they made up only about 6% of the overall sample.

CHAPTER 3

The discovery of some expanding clay, including montmorillonite and illite, suggests that the soil has some swelling capacity in contact with water. The X-ray diffraction XRD pattern of the soil sample is shown in Figure 3.5.

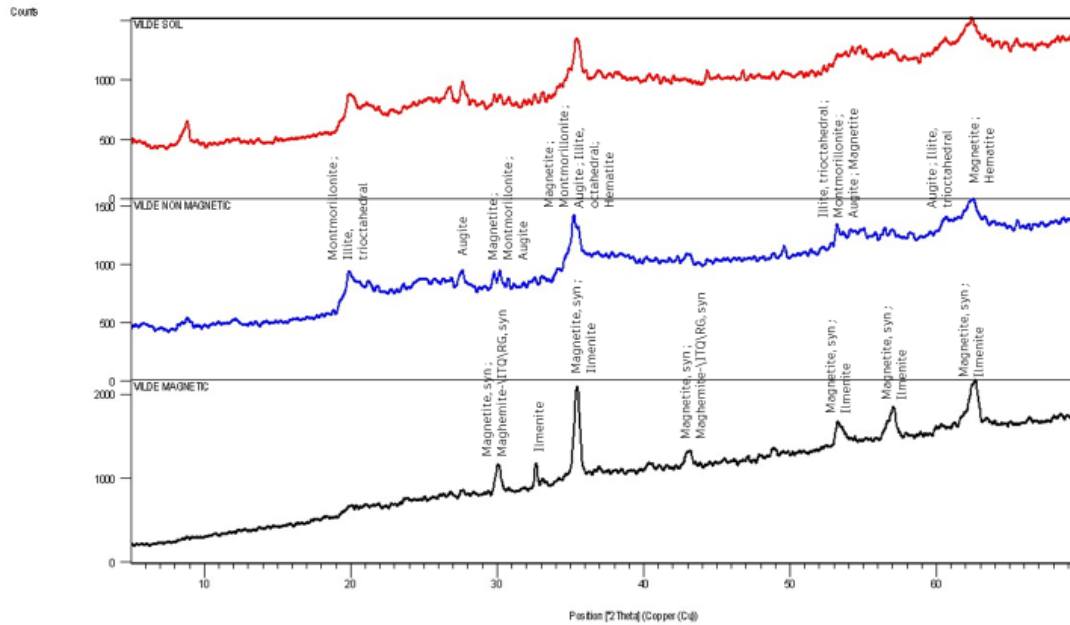


Figure 3.5. XRD pattern of soil sample from construction site in Lisbon. A 2θ step size of 0.0330 with scan step time of 74 sec was used with Cu as anode material.

Table 3.1. Pattern list of the minerals identified by XRD in the soil sample collected from construction site in Lisbon.

Mineral group		Compound name	Scale Factor	Chemical Formula
Magnetic	Non-magnetic			
x		Magnetite, syn	0.980	$Fe_3 O_4$
x		Ilmenite	0.473	$Fe Ti O_3$
x		Illite	0.074	$K_4 Mg_3 Al_2 (Si_{24} O_{64}) (OH)_8$
x		Maghemite\ITQ\RG, syn	0.512	$Fe_2 O_3$
	x	Magnetite	0.759	$Fe_3 O_4$
	x	Montmorillonite	0.739	$Mg O Al_2 O_3 (5Si O_2) \cdot x H_2 O$
	x	Augite	0.547	$Ca (Fe, Mg) Si_2 O_6$
	x	Hematite	0.398	$Fe_2 O_3$
	x	Illite, trioctahedral	0.269	$K_{0.5} (Al, Fe, Mg)_3 (Si, Al)_4 O_{10} (OH)_2$

3.3 Shredded Face Masks

3.3.1 Shredding process

The face masks used in this study were commercially available, single-use face masks type IIR, made from polypropylene (PP). The middle layer of the mask was made of meltblown PP while the two other layers were made of spunbond PP. The material was then shredded using a heavy-duty cutting mill *RETCH SM 2000* with a bottom sieve of size 2 mm (Figure 3.6). Prior to shredding, the metallic nose piece and ear bands were removed to prevent damaging the machine. The SM 2000 is a universal standard model cutting mill that is suitable for grinding a variety of materials, including soft, medium-hard, tough, elastic, fibrous, and heterogeneous mixtures. The machine is designed with double-acting cutting bars for optimum cutting effects and has a defined final fineness due to bottom sieves with aperture sizes ranging from 0.25 to 20 mm (*Cutting Mill SM 200 - Retsch - Operational Safety and Convenience*, n.d.).

It is assumed that the face mask fibers are the size of the filter used in the machine. It should be noted that smaller or larger fractions may not have been captured during shredding and may not be represented in the final analysis. The shredding process produced small fibers and a significant amount of dust and finer fragments, which were collected for further analysis.

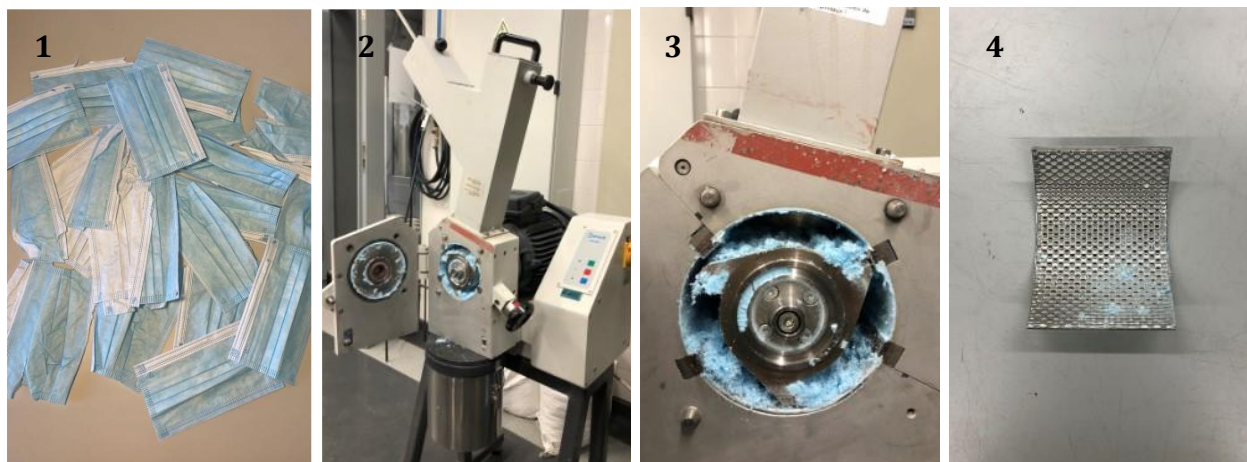


Figure 3.6. Illustration of the face mask used in the shredder (1) and the RTECH 2000 cutting mill used to shred face mask with cutting blades (2,3) and bottom sieve (4).

3.3.2 Grading size distribution of the face mask fibers

Laser diffraction was used to obtain the particle size distribution of the face mask fibers subjected to no degradation and for the degradation of period T2 with UV. To determine the diameters that correspond to a specific proportion of the referenced population, a quantitative size distribution of entire particles was obtained. The analysis showed the size distribution by volume, but as the dry unit weight of the mask fiber, γ_{mask} , is assumed to remain constant, the ratio between the mass and the volume is also assumed to remain constant, and the mask fiber volume and mask fiber mass are therefore regarded as being equal. To compare the fiber diameters in proportion to the soil diameter, the particle size distribution of the shredded face mask fiber samples is shown in Figure 3.7.

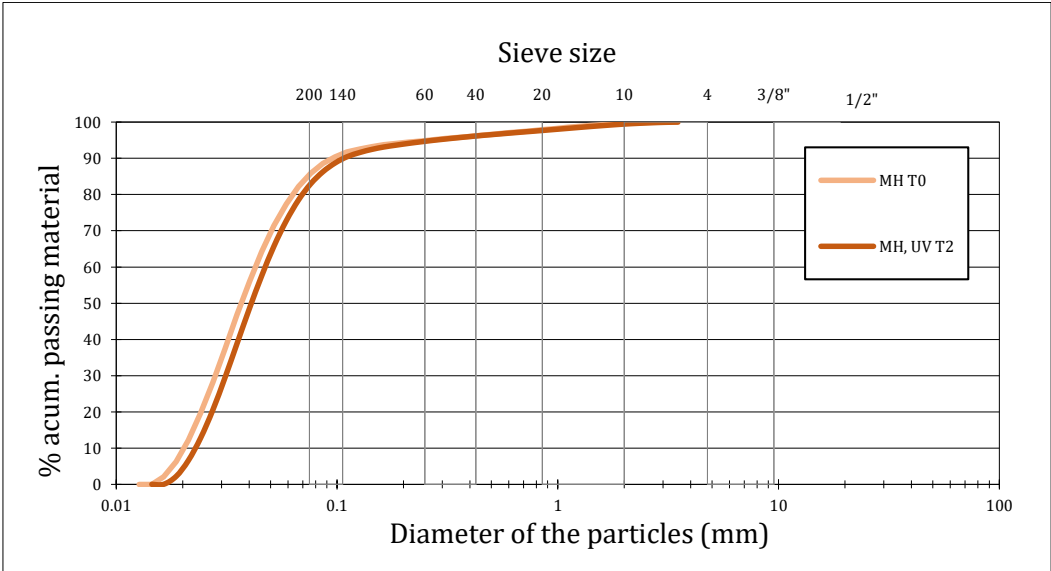


Figure 3.7. Grading size distribution of face mask fibers subjected to no degradation (MH T0) and long-term degradation with UV exposure (MH, UV T2).

3.4 Procedure for Experimental Work

3.4.1 Sample preparation

To investigate the potential mitigation of shredded face masks in the soil, 12 soil samples were prepared with and without the addition of shredded face masks. The concentration of shredded face masks added was determined as a certain percentage of volume, corresponding to 1% and 5% of the soil volume for the low and high values, respectively (see Table 3.2 and Table 3.3). The soil dried and sieved was compacted into cylindrical plastic containers with dimensions of approximately 7 cm in diameter and 6 cm in height, with six containing different concentrations of shredded face masks and six without. The volume of soil for each cylinder was determined using a suggested dry density of 15 kN/m^3 and a water content of 15%, by using empirical values of similar soil.

The soil was then compacted into three layers using a circular cylinder weight, with each layer subjected to 20 hammer-blows, thus with less compaction energy typically used in the standard Proctor Test (ASTM D698-12). The excess soil material that did not fit into the cylinder after compaction was weighed and left in the oven to dry for at least 48 hours to adjust the dry density and void ratio based on the accurate water content. Initially, this process was only performed on one sample without mask fibers to determine whether the real water content matched the supplied water content. Because the findings showed a larger water content than what was initially applied to the soil, the samples containing shredded mask were also controlled and adjusted to the water content intended. The initial water content with corresponding dry density is presented in Chapter 3.5.1, Table 3.5.

It was observed that the shredded masks occupied a lot of volume of the soil, especially for the high number of masks, resulting in a large volume of material not fitting into the cylinder during compaction. Additionally, the larger amount of added mask fibers resulted in the soil drying up faster compared to the prepared samples without masks. Thus, the compaction had to be proceeded rapidly to avoid the soil to dry out.

CHAPTER 3

Table 3.2. Sample names and their corresponding concentrations of added face masks.

Mask concentration ¹ (%)	Sample type
0	NM
1	ML
5	MH

Note 1: Mask concentration equals to the percentage of the solid mass to each soil sample placed in a cylinder.

Table 3.3. An overview of the sample numbers with the related volume, solid mass, amount of water and amount of shredded face masks. Plan-column determines which kind of degradation mechanism the samples are exposed to.

Nr.	Sample	V (cm^3)	M_s (g)	M_w (g)	$M_{s,L}$ (g)	$M_{w,L}$ (g)	$M_{s,H}$ (g)	$M_{w,H}$ (g)	$M_{m,L}$ (g)	$M_{m,H}$ (g)
1	MH	227.1	340.6	51.1	337.2	50.6	323.6	48.5	3.4	17.0
2	MH	227.1	340.6	51.1	337.2	50.6	323.6	48.5	3.4	17.0
3	NM, UV	227.1	340.6	51.1	337.2	50.6	323.6	48.5	3.4	17.0
4	ML	223.2	334.8	50.2	331.5	49.7	318.1	47.7	3.3	16.7
5	ML,UV	230.9	346.4	52.0	342.9	51.4	329.0	49.4	3.5	17.3
6	ML, UV	234.8	352.1	52.8	348.6	52.3	334.5	50.2	3.5	17.6
7	NM, UV	227.1	340.6	51.1	337.2	50.6	323.6	48.5	3.4	17.0
8	NM	215.5	323.3	48.5	320.0	48.0	307.1	46.1	3.2	16.2
9	MH,UV	227.1	340.6	51.1	337.2	50.6	323.6	48.5	3.4	17.0
10	NM	219.4	329.0	49.4	325.8	48.9	312.6	46.9	3.3	16.5
11	ML	219.4	329.0	49.4	325.8	48.9	312.6	46.9	3.3	16.5
12	MH,UV	227.1	340.6	51.1	337.2	50.6	323.6	48.5	3.4	17.0
17 ¹	NM	215.5	323.3	48.5	320.0	48.0	307.1	46.1	3.2	16.2
18 ¹	ML	219.4	329.0	49.4	325.8	48.9	312.6	46.9	3.3	16.5
19 ¹	MH	227.1	340.6	51.1	337.2	50.6	323.6	48.5	3.4	17.0

Note 1: Samples 17, 18 and 19 were prepared identically to 8, 11 and 1 for conducting a saturated permeability test.

In addition to the samples indicated in the table above, three samples (NM, ML, and MH) were compacted in a smaller cylindrical container with a diameter of 7 cm and a height of 2 cm, with significantly less compaction energy than described in the standard Proctor Test to not over-compact the sample due to its decreased height. Ten blows were utilized per layer, for a total of three layer. These samples were prepared in order to measure the water retention capacity of the soil samples with different mask fiber concentration. The remaining compacted soil samples were

then examined to determine their physical and hydraulic properties, including their initial water content, saturated permeability, volumetric dry density and mercury intrusion porosimetry (MIP). Additionally, the samples were analysed using optical microscope, scanning electron microscopy (SEM) and chemical analysis. These tests with their corresponding results are further described in Chapter 3.5 and 3.6.

3.4.2 Experimental setup

To simulate the effect of soil suffering degradation in natural conditions, sample 1-12 was submerged in water and placed in containers both with- and without UV-exposure for period T1 and T2. Throughout the experimental procedure, samples were retrieved at regular intervals for subsequent analysis, and water was refilled weekly to account for evaporation. One of the UV-lamps failed after approximately one week, but a replacement lamp was installed to provide consistent UV exposure during subsequent periods. When the UV lamp failed twice at the end of T1, it was decided to use just one light bulb on the remaining samples. As the experimental setting for T2 was changed by positioning the samples adjacently, it was assumed that the remaining samples received roughly the same amount of UV exposure with a single lamp as they did with two lamps during T1. As a result, for the duration of the trial, all samples experienced nearly the same level of exposure.

The compacted specimens were placed with three different filtering sizes from fine to coarse at the bottom of the sample (Figure 3.8) and placed in a circular plastic container with a volume of approximately 1.5 litres, as seen in the experimental setup (Figure 3.9). All tests were submerged in distilled water with a volume of approximately 600 mL, depending on the size of the sample. Half of the tests were placed in a light-isolated room underneath two UV lamps, and the other half was placed in a laboratory without any UV exposure. Additionally, four samples of shredded face masks only mixed with water were prepared to observe the degradation of the fragments themselves. The temperatures in both the room and water were controlled using a laboratory thermometer prior to the experiment in order to monitor the conditions during the experiment.

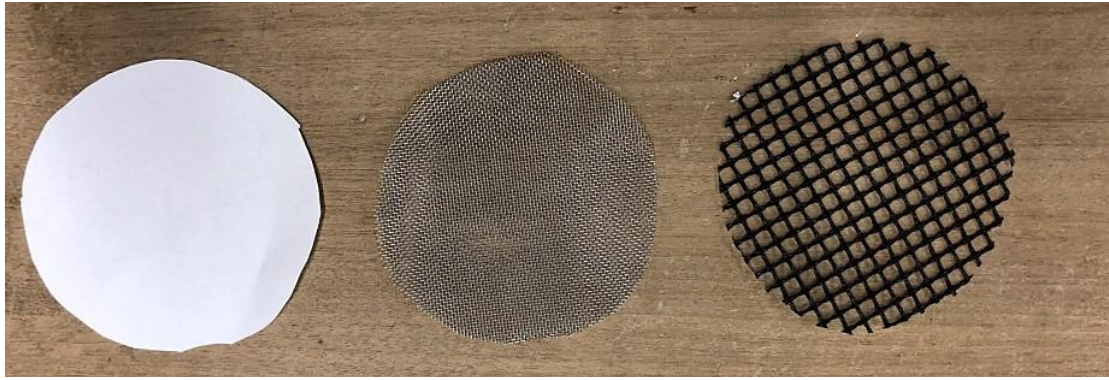


Figure 3.8. Filtering placed from fine to coarse at the bottom of the sample to allow water to flow through the sample.



Figure 3.9. Experimental setup of samples suffering UV exposure to the left and no UV exposure to the right.

3.4.3 Temperature

Throughout the experiment, measurements of the lab's temperature as well as the conditions of the water and air inside the enclosed area with the UV lamps were taken at regular intervals. The temperature was shown to increase with time, as would be expected given the warming weather outdoors. But within the UV-lit room, there was a noticeable increase in temperature. Since heat is regarded as a deterioration process for the samples, such temperature variances should be

CHAPTER 3

taken into consideration when analysing the samples. The temperature variations between the start of the experiment and its end are shown in the table below:

Table 3.4. Temperatures at different measurement times under different simulated environmental conditions.

Location	Experiment start (°C)	Week 2 (°C)	Week 3 (°C)	Week 4 (°C)	Experiment end (°C)
Laboratory	18.5	20.5	20.5	20.5	20.5
Room with UV lamp	18.5	21.5	23	26	24
Water in room with UV lamp	19	25	26	27.5	28.5

3.5 Characterization of Compacted Samples

3.5.1 Initial water content

To achieve the correct initial water content for each prepared sample, a water content control was proceeded with results presented in Table 3.5. It can be noticed that the average water content is at approximately 19 % which is larger than the actual water content of 15 % added to each sample during compaction. A possible reason for this is due to the soil not being completely dry before proceeding compaction. However, this is not a problem as the dry density (γ_d) and void ratio (e) were adjusted after correction of the real water content.

Table 3.5. Initial water content with corresponding dry density and void ratio for samples subjected to different degradation periods and mechanisms.

Sample nr.	Sample	Period	w (%)	$\gamma_{d,adjusted}$ (kN/m^3)	$e_{adjusted}$ (-)
1	MH	T1	19.7	11.4	1.2
2	MH	T2	17.3	10.8	1.3
19	MH	T0	21.8	9.1	1.8
9	MH,UV	T1	20.3	12.5	1.0
12	MH,UV	T2	21.3	12.3	1.0
4	ML	T2	20.2	12.8	1.0
11	ML	T1	19.9	12.6	1.0
18	ML	T0	26.0	8.2	2.0
5	ML,UV	T1	19.7	12.1	1.1
6	ML,UV	T2	20.0	12.9	0.9
8	NM ¹	T1	17.9	13.2	0.9
10	NM ¹	T2	17.9	12.2	1.0
17	NM	T0	15.7	8.2	2.0
7	NM,UV ¹	T2	17.9	12.7	1.0
3	NM,UV ¹	T1	17.9	11.9	1.1

Note 1: Samples are assumed having the same water content as they were compacted the same day and had the same amount of time drying in the oven. Thus, only real water content of sample 10 was collected and adapted to the others mentioned.

3.5.2 Saturated permeability

To achieve information about the soil's ability of transmitting water, the saturated permeability was found by proceeding a permeability test with falling water head. The samples were not degraded prior to testing, and they were prepared using compaction as described in Chapter 3.4.1 for samples without added shredded masks (NM), samples with added shredded masks in low concentration (ML), and samples with added shredded masks in high concentration (MH). Table 3.6 displays the findings. Saturated permeability, k , from falling-head test is given as:

$$k = \frac{aL}{At} \ln \frac{H_0}{H}$$

(4)

- a – cross-sectional area of standpipe
- A – cross-sectional area of soil cylindrical soil sample
- L – distance the water travels in the soil (height of cylinder)
- t – elapsed time during test
- H_0 – total head in the beginning of the test
- H – total head at the end of the test

Table 3.6. Saturated permeability of samples with different concentrations of shredded face masks corresponding to 0, 1 and 5 % for NM, ML and MH, respectively.

Sample type	Sample nr.	Saturated permeability, k (m/s)
NM	17	9×10^{-7}
ML	18	3×10^{-8}
MH	19	5×10^{-7}

3.5.3 Water retention curve

The water retention curve (WRC) of a soil is a crucial aspect that depicts the relationship between soil-water potential and volumetric soil-water content (Novák & Hlaváčiková, 2019). In this study, water potential is quantified in megapascals (MPa) and represents the force needed to extract

CHAPTER 3

water from the soil, commonly referred to as suction. The WRC provides valuable insights into how water moves through the soil and can be related to its permeability. To measure the WRC, the adsorption and desorption method was employed, and a curve-fitting model was used for data analysis.

To prepare the soil samples for testing, the initial water content and dry density were determined by averaging the information presented in Chapter 3.4.1. The specific gravity (G_s) of the soil was set to 2.5, resulting in a void ratio of 2.2, which was utilized during data processing. To establish different suctions, the samples were placed in containers with solutions of varying NaCl concentrations. The relationship between relative humidity (RH) and suction followed Kelvin's law (M. D. Fredlund et al., 2016), which can be described as in equation (5). The control of RH was achieved by using unsaturated NaCl solutions, and the corresponding values of RH and suction for each NaCl concentration are presented in Table 3.7.

$$\psi = -\frac{RT\rho_w}{\omega_v} \ln\left(\frac{u_v}{u_{v0}}\right)$$

(5)

ψ	–	total suction/ soil suction (kPa)
$\frac{u_v}{u_{v0}}$	–	relative humidity (RH %)
R	–	universal molar gas constant (i.e., 8.31432 J/(molK))
T	–	absolute temperature (K)
ρ_w	–	density of the water (i.e., 998 kg/m ³ at t = 20°C)
ω_v	–	molecular mass of water vapor (i.e. 18.016 kg/(molK))

CHAPTER 3

Table 3.7. Relative humidity (RH) with corresponding soil suction (ψ). The suction corresponds to the concentration of the NaCl.

RH (%)	ψ (MPa)
0.996	0.5
0.978	3
0.895	15
0.744	39

To compute the WRC, the Van Genuchten water retention equation (Van Genuchten, 1980) was employed in combination with the relation of water content and saturation, which utilizes specific constants.

$$Sr = \left(1 + \left(\frac{s}{\rho} \right)^{\frac{1}{1-\gamma}} \right)^{-\gamma}$$

$$Sr = \frac{Gs}{e \cdot w}$$

(6)

Sr	–	saturation (%)
ρ, γ	–	empirical shape-defining parameters (Mpa), (-)
s	–	metric suction (MPa)
Gs	–	specific gravity of soil particles (-)
e	–	void ratio (-)
w	–	water content (%)

The constants used in the equation were determined through fitting the Van Genuchten equation to experimental data obtained from the soil sample's WRC. By adjusting these constants, the equation can accurately represent the soils water retention behaviour. The constants used is presented in Table 3.8. Through this comprehensive approach, including the test by vapor equilibrium, the use of NaCl solutions to control RH, and the application of the Van Genuchten equation, the WRC for each soil sample (NM, ML, and MH) was determined. Figure 3.10, Figure 3.11 and Figure 3.12 illustrates the obtained WRCs for each sample, obtained through curve-

CHAPTER 3

fitting during the data analysis phase. This methodology allowed for a thorough characterization of the soil's water retention properties and its relationship with suction and RH.

Table 3.8. Curve-fitting constants for soil samples with 0, 1 and 5 % concentration of face mask fibers corresponding to NM, ML and MH, respectively.

	Drying Branch			Wetting Branch		
	NM	ML	MH	NM	ML	MH
ρ (MPa)	0.13	0.15	1	0.02	0.07	0.1
γ	0.35	0.33	0.4	0.3	0.30	0.35

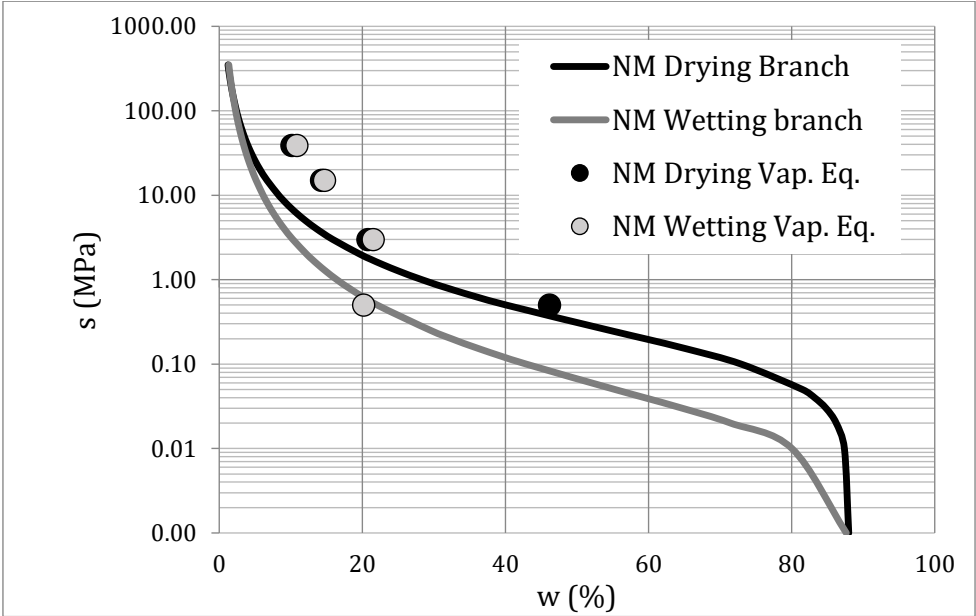


Figure 3.10. WRC for NM (0 % face mask concentration).

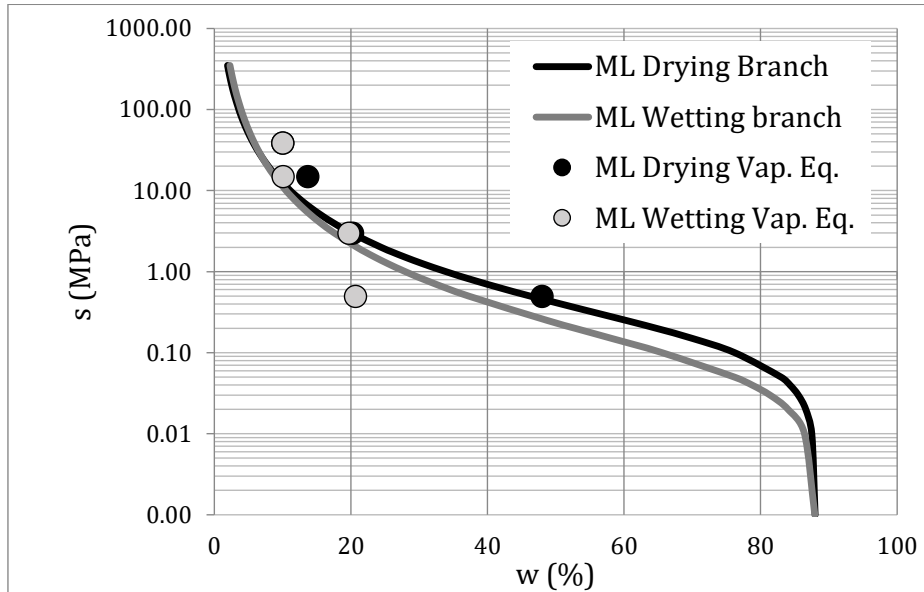


Figure 3.11. WRC for ML (1 % face mask concentration).

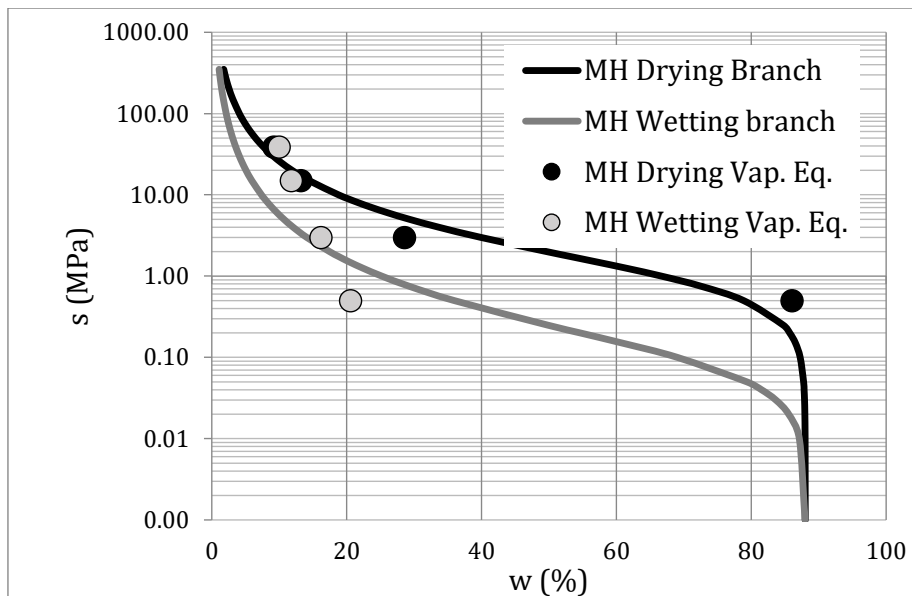


Figure 3.12 WRC for MH (5 % face mask concentration).

The identical process used for the soil was repeated for low and high masses of shredded face masks to investigate the fibers' ability for retaining water. Figure 3.13 is an illustration of the experimental setup. The estimated values for the low- and high-mask fiber masses (ML,m and MH,m) were 0.2 and 0.4 g, respectively. Although the water holding capacity for low- and high-mask masses should be equivalent, it was decided to continue the analysis in both scenarios.

CHAPTER 3

A specific gravity (G_s) of 0.9 and a dry density (γ_d) of 0.9 g/cm³ were used to obtain the water retention curve to the face mask fibers. These values correspond to typical values for PP plastic, which is the primary component of the experiment's face masks (Kundra, 2022; 'Polyolefins • Plastics Europe', n.d.). The void ratio as a consequence was 1.2. However, this void ratio corresponds to the PP itself and not clusters of shredded face masks. By using curve-fitting in the data treatment of the WRC plots, a void ratio of 8 was implemented to match the drying and wetting branch curves to the corresponding vapour equilibrium points. The curve-fitting constants used to obtain the WRC of ML,m and MH,m is presented in Table 3.9 and their corresponding WRC are illustrated in Figure 3.14 and Figure 3.15.



Figure 3.13. Experimental setup of the procedure of the water retention curve. Samples NM, ML and MH were placed in jars with different NaCl solutions. Red labels correspond to samples left to be dried and blue labels corresponds to samples left to be wetted.

Table 3.9. Curve-fitting constants for soil samples for low and high mass of face mask fibers corresponding to ML,m and MH,m, respectively.

	Drying Branch		Wetting Branch	
	ML,m	MH,m	ML,m	MH,m
ρ (MPa)	2.5	3	0.01	0.01
γ	0.6	0.6	0.5	0.5

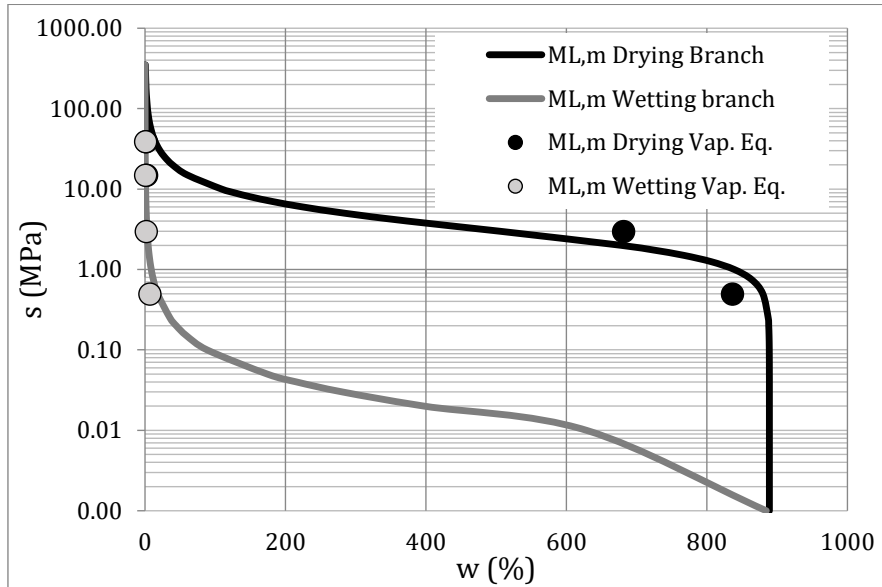


Figure 3.14. WRC for ML,m (low mass of mask fibers).

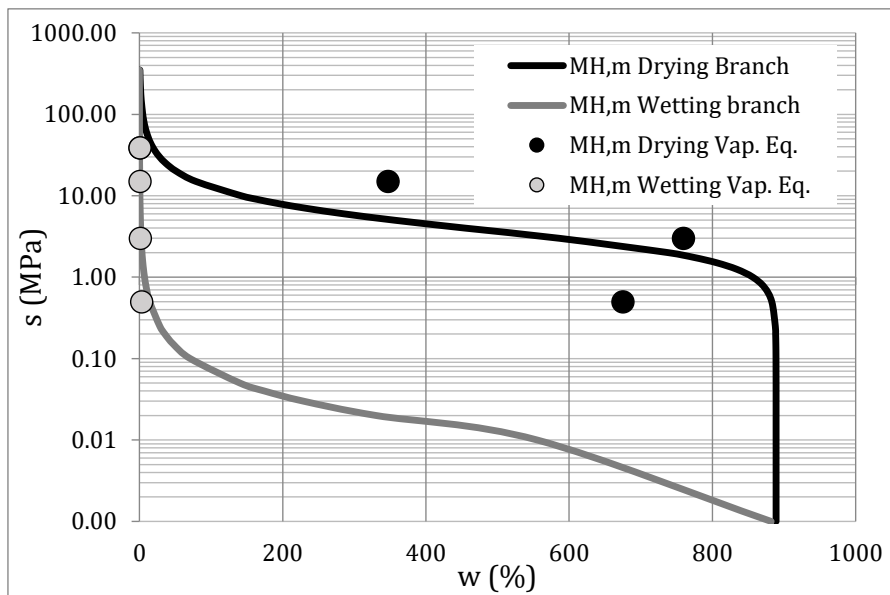


Figure 3.15. WRC for MH,m (high mass of mask fibers).

3.6 Ageing Tests and Results

3.6.1 Dry volumetric weight

A method to determine the pore structure of the soil, including its pore size and pore size distribution, by intrusion of a liquid (Haugen & Bertoldi, 2017). The test method used for obtaining the porosimetry is based on the Archimedes principle (water immersion). The porosimetry is proceeded using the standardised method referred to as “Paraffin method” where melted paraffin is applied to each sample before fully submerged in water to secure that no water leaks into any pores of the soil sample. Soil used in the testing was extracted from both the top- and bottom part of the cylindrical samples. All samples from the different time intervals of the experiment are tested to compare the results of the soil’s pore structure suffering different degradation mechanisms. The dry density and void ratio of the soil (Table 3.10 and Table 3.11) is calculated based on equation (7) using the relation between unit weight (γ) and void ratio (e) as in equation (8) and (9). Considering that this analysis involves numerous phases where precision always will be a difficulty due to human error, experimental errors should be taken into account.

$$\gamma_h = \frac{\frac{M_{air}}{M_{paraffin,air} - M_{paraffin,submerged}}}{\gamma_w}$$

(7)

M_{air} and $M_{paraffin,air}$	–	mass of the sample without and with paraffin cover respectively
$M_{paraffin,submerged}$	–	mass of the sample submerged with paraffin cover
γ_w and $\gamma_{paraffin}$	–	volumetric weight of water (10kN/m ³) and paraffin (9kN/m ³)
γ_h	–	buoyant unit weight (kN/m ³)

$$\gamma_d = \rho_d \cdot g$$

(8)

$$e = \frac{G_s}{\gamma_d - 1}$$

(9)

Where ρ_d is the dry density of the soil and an be related to the volume of the soil, V , which again relates to wet weight of the soil and the buoyant dry density γ_h . G_s used in these equations are 2.5.

Table 3.10. Void ratio obtained from porosimetry of samples suffering degradation with and without UV exposure for period T1. NM, ML and MH corresponds to soil with concentrations 0, 1 and 5 %, respectively of shredded face masks.

Period T1												
	Top sample						Bottom sample					
Nr.	MH	ML	NM	MH, UV	ML, UV	NM, UV	MH	ML	NM	MH, UV	ML, UV	NM, UV
γ_h (kN/m^3)	7.9	5.5	7.0	6.1	7.4	7.3	5.4	6.8	6.3	6.6	7.0	7.1
γ_d (kN/m^3)	13.7	9.3	11.5	10.4	12.3	12.6	9.2	12.1	10.7	13.2	12.0	12.4
e_{final} (-)	0.8	1.7	1.2	1.4	1.0	1.0	1.7	1.1	1.3	0.9	1.1	1.0

Table 3.11. Void ratio obtained from porosimetry of samples suffering degradation with and without UV exposure for period T2. NM, ML and MH corresponds to soil with concentrations 0, 1 and 5 %, respectively of shredded face masks.

Period T2												
Nr.	Top sample						Bottom sample					
	MH	ML	NM	MH, UV	ML, UV	NM, UV	MH	ML	NM	MH, UV	ML, UV	NM, UV
γ_h (kN/m^3)	8.3	5.0	6.3	6.7	7.5	7.5	5.9	8.0	7.0	5.6	6.1	8.5
γ_d (kN/m^3)	12.9	8.2	10.1	10.2	12.7	12.7	10.0	13.7	11.8	10.5	10.5	14.4
e_{final} (-)	0.9	2.1	1.5	1.5	1.0	1.0	1.5	0.8	1.1	1.4	1.4	0.7

3.6.2 Mercury intrusion porosimetry tests

The Mercury Intrusion Porosimetry (MIP) process is used to determine the pore size distribution and porosity of the soil samples based on the amount of mercury intruded at each pressure increment. Thus, using the Washburn equation, the pore diameter can be determined in relation with the pressure conducted (Watt-Smith et al., 2007).

MIP was applied to selected samples from the time intervals T1 and T2, as well as additional samples without degradation (T0). Based on anticipated sample differences due to degradation exposure, a select group of samples was chosen. On a AutoPore IV 9500 porosimeter, the MIP test was performed with a mercury pressure that was raised constantly between 0.5 psi and 33000 psi. The MIP specimens were taken from each sample, both from the top and bottom, and cut into cubes before being air dried to remove any water out of the pores. Specific gravity (Gs) was set to 2.5, resulting in a void ratio of 2.2 based on the average dry unit weight of the soil samples. This was utilized in the data processing. The pore volume distribution plots for the different samples are presented in Figure 3.16, Figure 3.17 and Figure 3.18 comparing the different degradation mechanism for each concentration of face mask fibers. The figures also illustrate the span of what is defined as micro-, meso- and macro pores in this study. Sample MH UV T2 had an error during the analysis and had to be disregarded in the presentation of the obtained results.

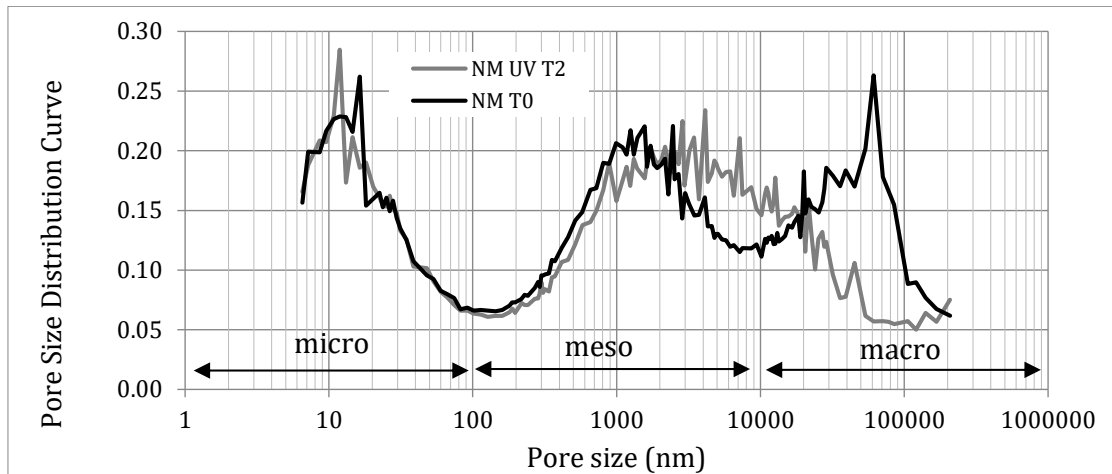


Figure 3.16. Pore size distribution curve for soil samples with 0 % face mask fiber concentration that was subjected to long-term UV degradation (T2) and no degradation (T0) using MIP.

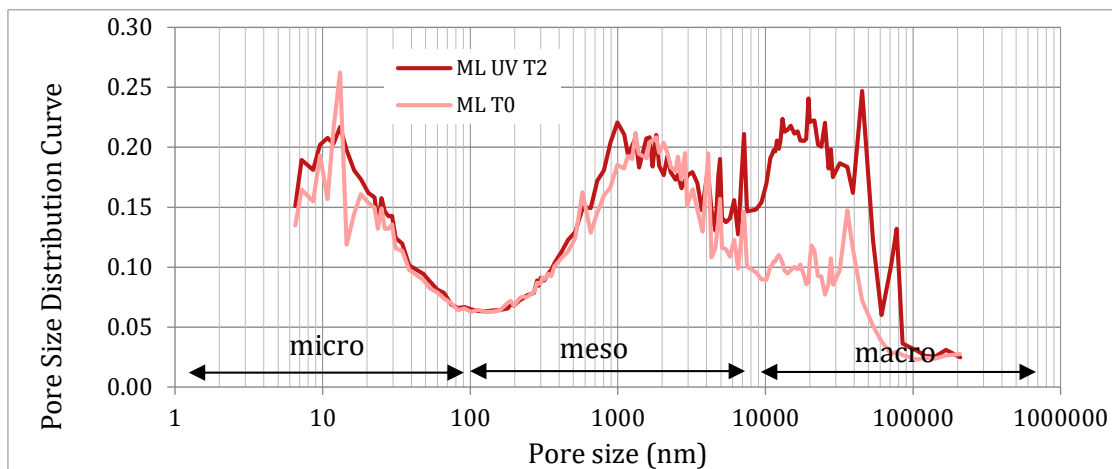


Figure 3.17. Pore size distribution curve for soil samples with 1 % face mask fiber concentration that was subjected to long-term UV degradation (T2) and no degradation (T0) using MIP.

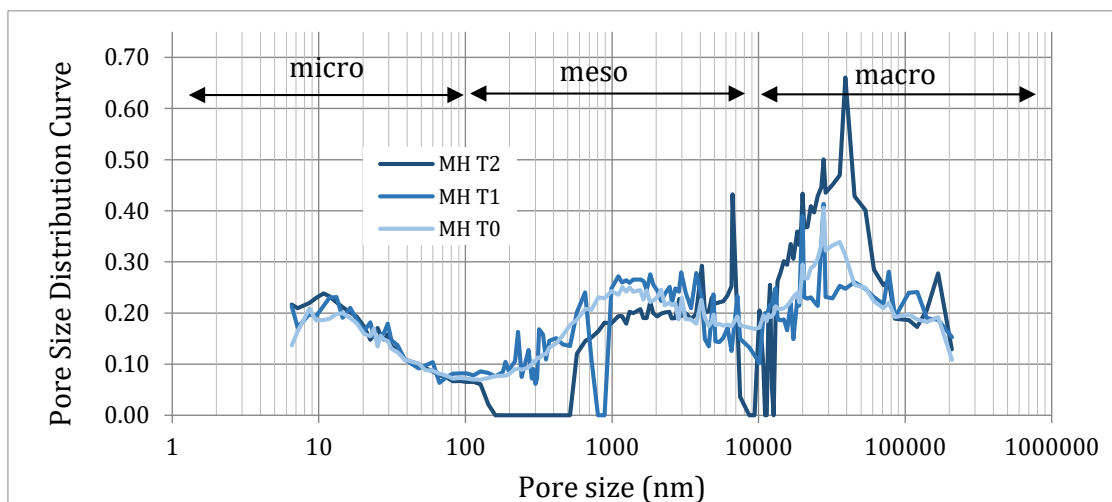


Figure 3.18. Pore size distribution curve for soil samples with 5 % face mask fiber concentration that was subjected to short- and long-term degradation (T1 and T2, respectively) and no degradation (T0) using MIP. This sample had some lacking data and thus MH T2 has flat areas along the curve.

3.6.3 Chemical analysis of the water

12 water samples were sent to Nova FCT's chemical lab for an investigation of inorganic components in order to study the submersion water of the soil samples. The selection of inorganic compounds was based on previous research that investigated leachate water from single-use face masks to examine the concentrations of different elements developed during various degradation phases. Table 3.12 for periods T0, T1 and T2 presents the resulting released concentrations in mg/l (Liu et al., 2022; Sendra et al., 2022). Negative values can be considered an error and are not considered in the interpretation of these results. Relative standard deviation (% RSD) and net intensity could be found in Appendix C.

Table 3.12. List of inorganic component concentrations found in submersion water leachates (mg/l). "Non-detected" is represented by N.D. With degradation durations T0, T1, and T2, the symbols NM, ML, and MH represent soil concentrations of face mask fibers of 0, 1, and 5%, respectively. w corresponds to samples containing only water and mask fibers.

		Concentrations (mg/l)															
Sample		Al	Ba	Cd	Co	Cr	Cu	Fe	Mn	Ni	P	Pb	Sr	Si	Ti	V	Zn
Control	T0	-	N.D	N.D	N.D	N.D	-	N.D	N.D	0.01	N.D	0.01	N.D	N.D	N.D	N.D	N.D
		0.01					0.05										
NM	T1	1.44	0.02	N.D	0.01	N.D	-	0.97	0.01	0.01	0.08	0.02	0.05	7.01	0.13	0.01	N.D
							0.05										
NM,UV	T2	0.05	0.05	N.D	N.D	N.D	-	0.03	N.D	0.01	0.03	0.02	0.11	8.26	N.D	0.01	N.D
							0.05										
ML	T1	0.58	0.04	N.D	N.D	N.D	-	0.46	0.01	0.01	0.06	0.02	0.08	7.27	0.06	0.01	N.D
							0.05										
ML,UV	T1	0.10	0.07	N.D	N.D	N.D	-	0.03	N.D	0.01	0.01	0.02	0.15	7.79	0.01	0.01	N.D
							0.05										
ML (w)	T2	N.D	N.D	N.D	N.D	N.D	-	N.D	N.D	0.02	0.04	0.02	0.01	0.17	N.D	N.D	0.18
							0.05										
ML, UV (w)	T2	N.D	0.01	N.D	N.D	N.D	-	N.D	0.01	0.02	0.09	0.02	0.01	0.30	N.D	N.D	0.12
							0.05										
MH, UV	T1	0.18	0.02	N.D	N.D	N.D	-	0.12	N.D	0.01	0.03	0.02	0.07	5.68	0.02	0.01	N.D
							0.06										
MH, UV	T2	0.03	0.09	N.D	N.D	N.D	-	0.01	N.D	0.01	0.02	0.02	0.16	8.07	N.D	0.01	N.D
							0.06										
MH	T2	0.16	0.07	N.D	N.D	N.D	-	0.08	N.D	0.01	0.02	0.02	0.13	5.45	0.02	N.D	N.D
							0.05										
MH (w)	T2	-	N.D	N.D	N.D	N.D	-	N.D	N.D	0.01	0.02	0.02	N.D	0.05	N.D	N.D	0.03
		0.01					0.06										
MH,UV (w)	T2	N.D	0.01	N.D	N.D	N.D	-	N.D	0.01	0.02	0.02	0.02	0.01	0.32	N.D	N.D	0.13
							0.05										

3.6.4 Optical microscope

The optical microscope Amscope with an achromatic objective lens 4x scale 0.10 mm was utilized to generate microscopic images of soil samples NM, ML and MH subjected to no degradation (T0) and long-term degradation with UV exposure (UV T2) (Figure 3.19 and Figure 3.20). Although it is difficult to distinguish any variations between the degradation of the soil and the face mask fibers, it should be noted that the soil particles tend to collect around the face mask fiber clusters as seen in Figure 3.20 a, c, d, and f.

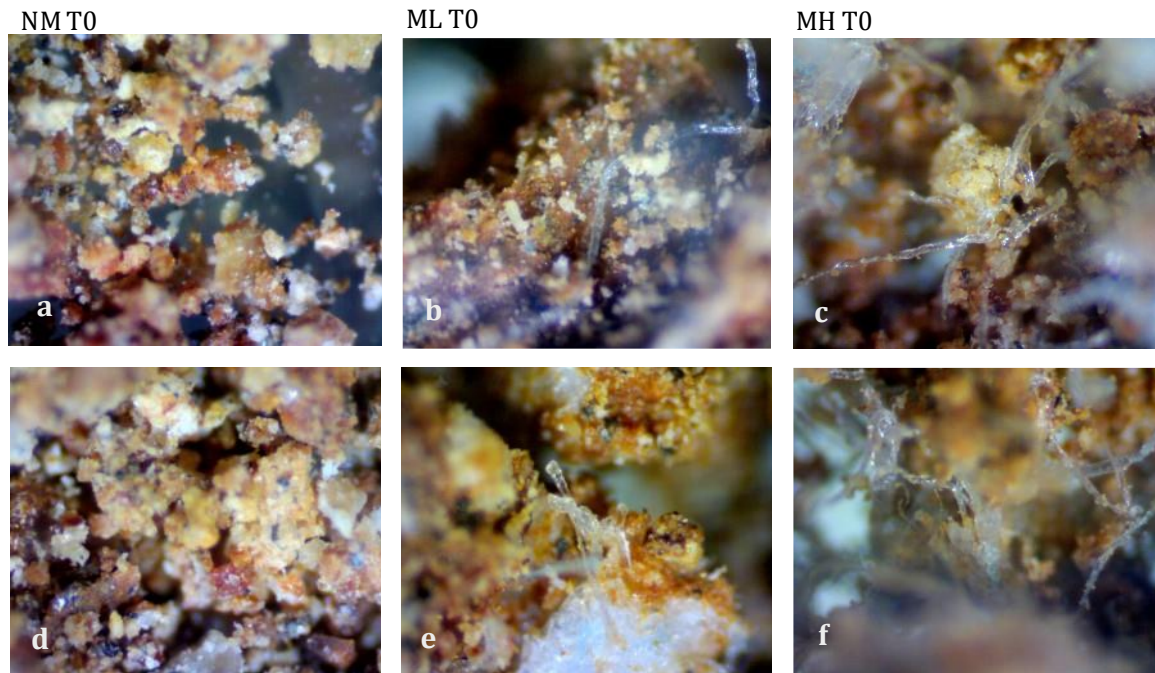


Figure 3.19. Microscopic images obtained with scale 4x 0.10 mm for samples NM, ML and MH (from the left to the right column) subjected to no degradation (T0).

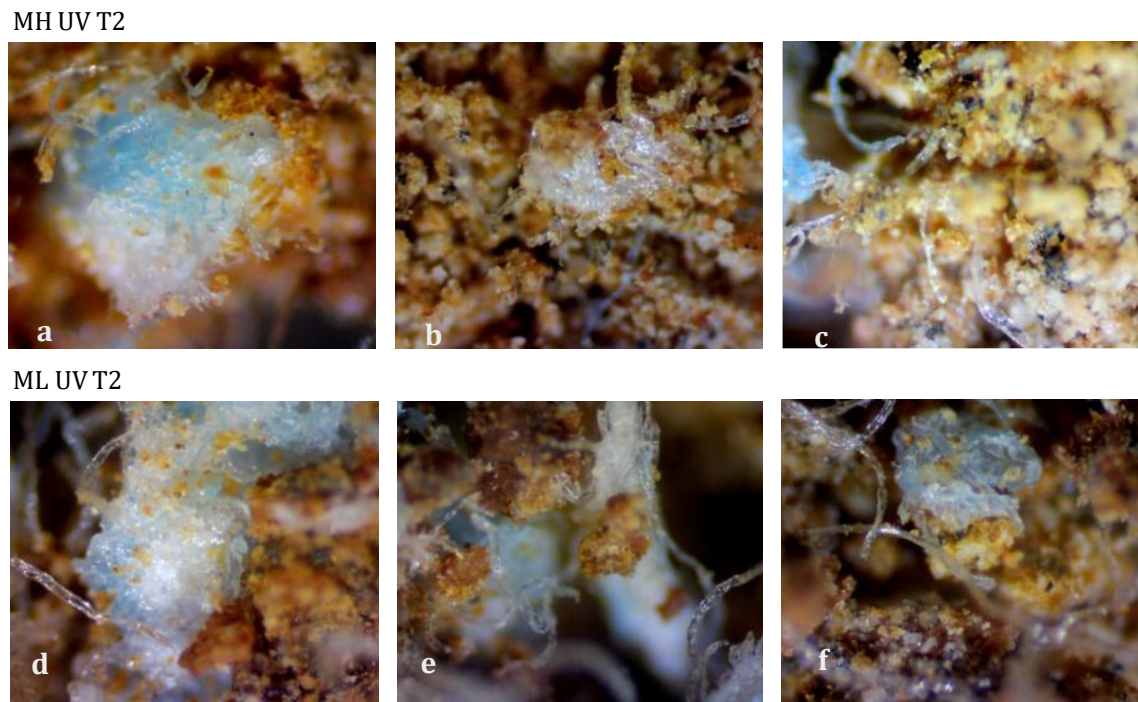


Figure 3.20. Microscopic images obtained with scale 4x 0.10 mm for samples MH (top row) and ML (bottom row) subjected to long-term degradation and UV exposure (UV T2).

3.6.5 Scanning electron microscope

Scanning electron microscopy (SEM) is an analytical technique that surface scans the microstructure of a sample to provide information about its size, shape and morphology (Wang et al., 2017). The SEM examination was carried out on 9 samples, comprising NM, ML and MH without any deterioration (T0), as well as with and without UV exposure over the degradation period T2. The images were scaled to 150x 200 m, 300x 100 m, 1500x scale 20 m, and 3000x 10 m in accordance with the usual amplifications used for geotechnical materials; however, the two latter ones were not taken into account in the interpretation of the analysis because the face mask fibers were too large to be captured by the microscope. The obtained views from the SEM can be shown in Figure 3.21, Figure 3.22 and Figure 3.23 for NM, ML and MH, respectively.

An EDS (Energy Dispersive X-ray-Spectroscopy) was also used to provide information about the chemical composition of the sample for sample NM (T0), NM (T2, UV), MH (T0) and MH (T2, UV) to see if any changes of the chemical compounds could be detected. It should be noted that the EDS only give information about the detected elements and not the chemical bonding of the elements. Due to the sensitivity of the equipment, overlap of soil particles and mask fibers may give inaccurate information about the elements present at the detected area. Figure 3.24 and Figure 3.25 show the EDS for soil that has a high concentration of face mask fibers but no degradation, and soil that has a high concentration of mask fibers but has long-term degradation and UV exposure, respectively. Appendix D contains the remaining samples that were subjected to the EDS analysis.

CHAPTER 3

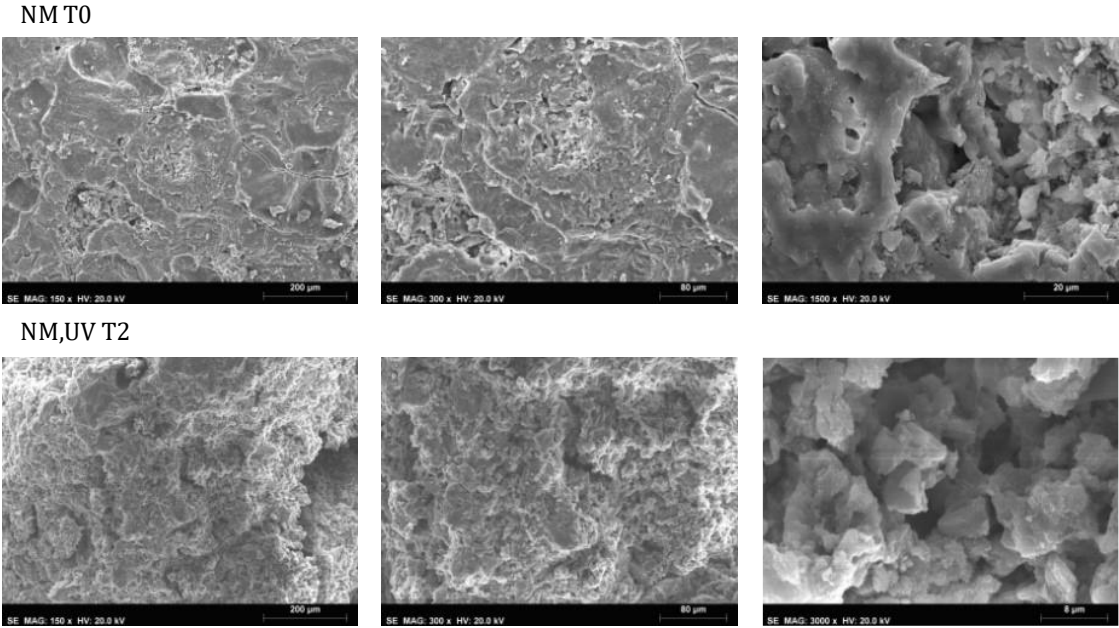


Figure 3.21. SEM views of sample containing no mask fiber concentration subjected to no degradation (NM T0) and long-term degradation with UV (NM, UV T2). Scaling of the SEM view is 150x 200 μm, 300x 100 μm and 1500 x 20 μm from left to right, respectively.

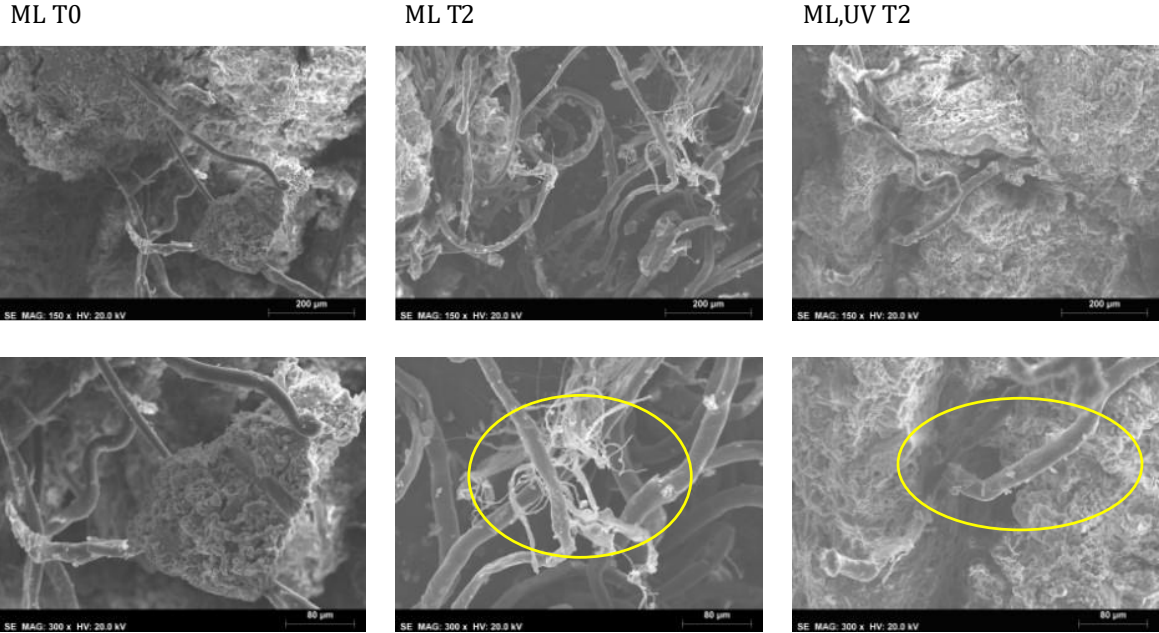


Figure 3.22. SEM views of sample containing 1 % mask fiber concentration subjected to no degradation (ML T0), long-term degradation without UV (ML T2) and long-term degradation with UV (ML, UV T2). Scaling of the SEM view is 150x 200 μm for the higher row and 300x 100 μm for the lower row.

CHAPTER 3

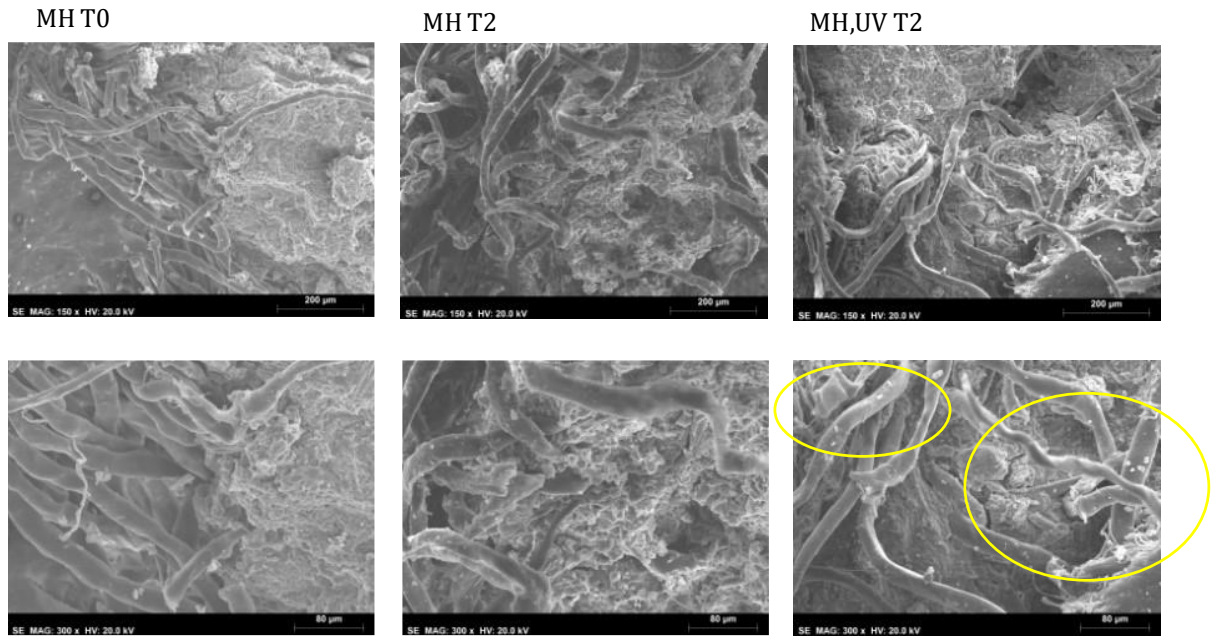
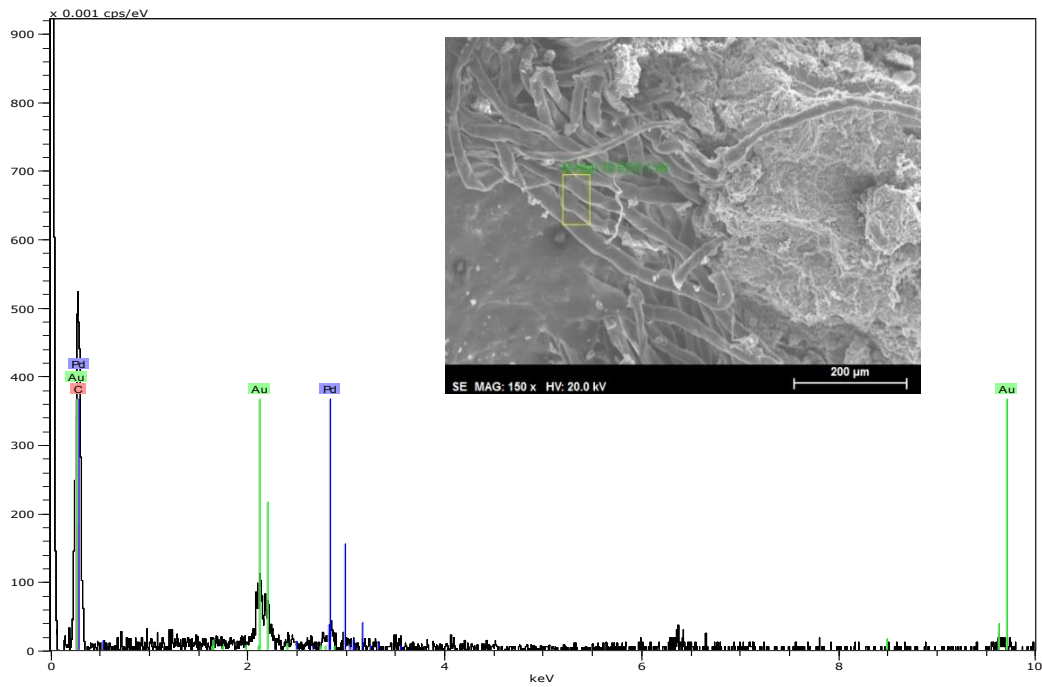


Figure 3.23. SEM views of sample containing 5 % mask fiber concentration subjected to no degradation (MH T0), long-term degradation without UV (MH T2) and long-term degradation with UV (MH, UV T2). Scaling of the SEM view is 150x 200 μm for the higher row and 300x 100 μm for the lower row.

a)

MH T0



b)

MH T0

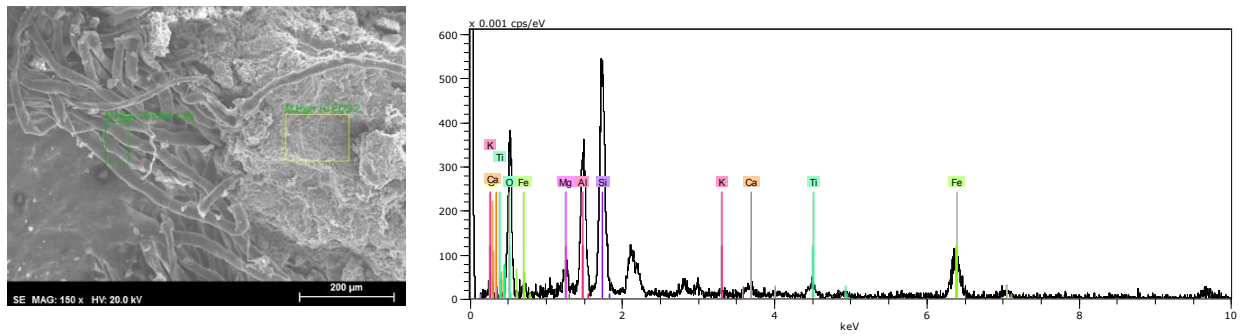
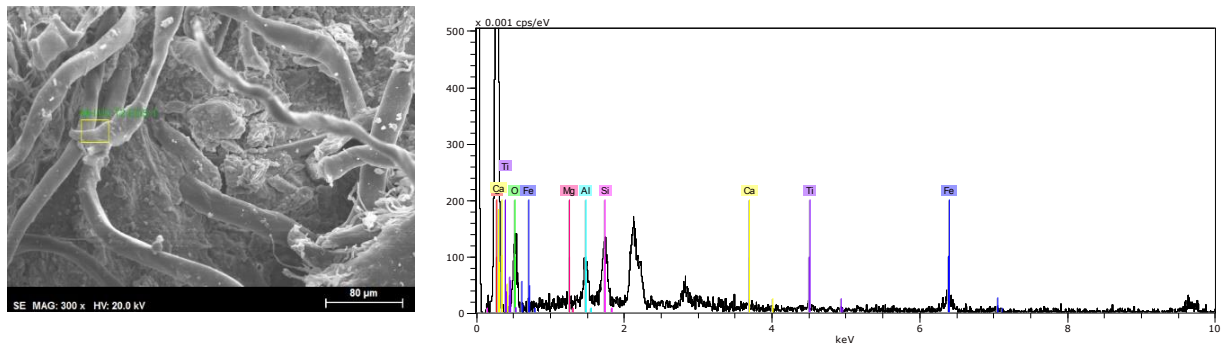


Figure 3.24. EDS spectrum (to the right) detected at the area marked with yellow for sample containing a high concentration of mask fibers with no degradation. Elements detected are Pd, Au and C (a) and O, C, Si, Al, Fe, Mg, Ti, Ca and K (b).

a)

MH, UV T2



b)

MH, UV T2

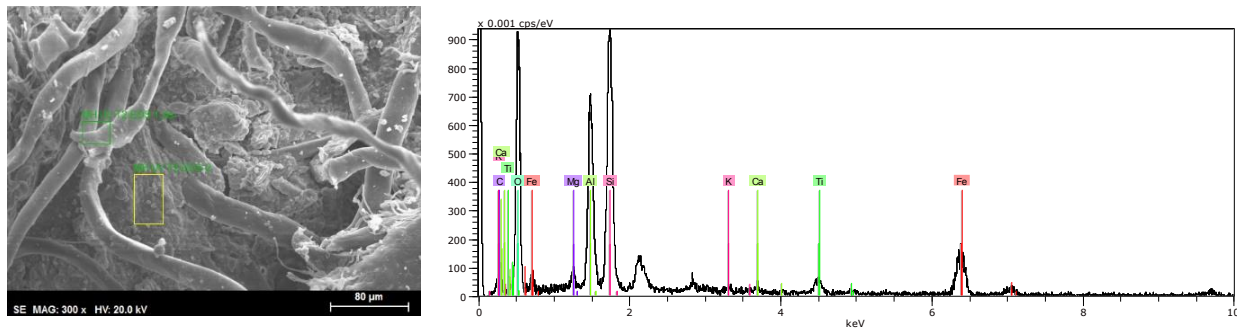


Figure 3.25. EDS spectrum (to the right) detected at the area marked with yellow for sample containing a high concentration of mask fibers subjected to long-term degradation and UV exposure. Elements detected are C, O, Fe, Si, Al, Ti, Mg and Ca (a) and O, C, Si, Al, Fe, Ti, Mg, Ca and K (b).

4 Joint Analysis of the Results and Discussion

4.1 Visual Observations

4.1.1 Soil

Observations were noted while the experiment was being conducted. During the first time-interval of the experiment (T1), it was noticed that samples with a high percentage of shredded face masks were less disturbed, with fewer soil particles accumulating at the bottom of the container, than those containing less or no mask fiber. This suggests that the fibers in the mask are practically acting as a soil stabilizer. Figure 4.1 show how the samples were changed during degradation, and how the amount of soil that was gathered at the bottom of the container varied from sample to sample. Notably, a common finding across all samples was soil swelling, which corresponds to the presence of minerals with swelling potential identified in the mineral analysis (Chapter 3.2.4). Also, samples that experienced UV exposure were more disturbed than those that did not, demonstrating that the presence of water and exposure to UV has a significant impact on the soil structure. This was particularly evident in samples without mask fibers (Figure 4.1 (2)).

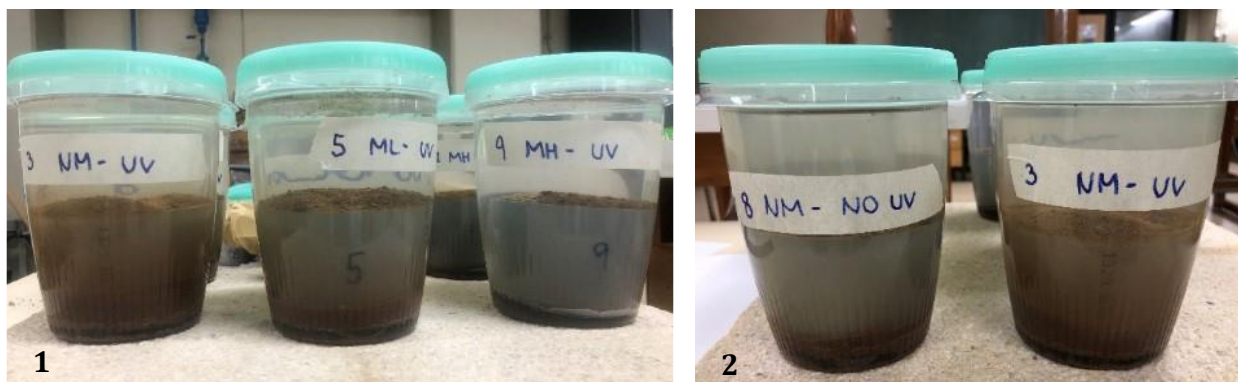


Figure 4.1. Photograph of the samples after the first period (T1) of the experiment showing that less soil was found accumulated on the bottom of the container for high concentration of masks (1, right photo) and not subjected to UV-exposure (2, left photo)

4.1.2 Water

When analysing collected extracted samples from the submersion water, it was observed that the samples with a high concentration of added mask fibers were less affected by the soil particles, as evidenced by their clearer colour when compared to the samples with low or no concentration of mask fibers. However, it was acknowledged that the colour of the samples might have been affected by the method used to obtain the water samples. To ensure a more uniform dispersion of the soil particles and fragments in the water, the soil that had gathered at the bottom of the container was mixed with the water before taking the samples. Thus, the colour variation in the samples could have been due to differences in how well each sample was blended.

During period T1, a visual inspection revealed that the samples with ML added had more mask fibers floating on the water surface than the sample with MH added (Figure 4.2). As a result, it appeared that a high concentration of added fibers was preventing soil deterioration, and the mask fibers were sustained in the soil medium. The same results were obtained during period T2 for the samples exposed to UV. However, for the samples without UV exposure, the MH samples released the largest amount of mask fibers on the water surface. Figure 4.3 illustrates the comparison of the different samples from NM to MH, and with and without UV exposure, clearly showing the differences in the leachate from each soil sample.

It is significant to highlight that the deterioration of the samples with UV exposure may account for the significant changes in mask fiber concentrations in surface water between samples exposed to UV and samples not exposed to UV. As observed during the soil inspection from period T1, UV exposure resulted in more deteriorated soil samples than without. If the degradation of the soil particles is greater, the degradation of the face mask fibers could also be greater under UV exposure and aging, causing them to degrade into even smaller pieces, like nanoplastics, and thus no longer be visible in the water. Further analysis of the water and soil samples was conducted to confirm this theory and will be discussed in subsequent chapters.

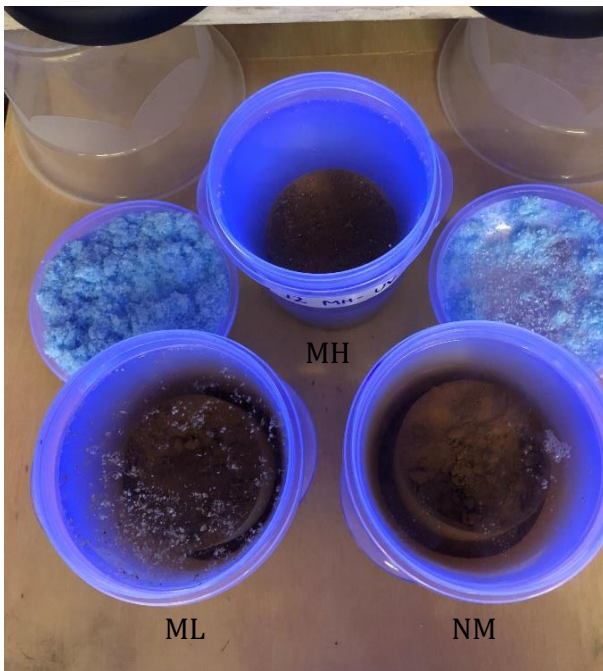


Figure 4.2. From left, ML and NM to the right. MH at the top (T1 period).

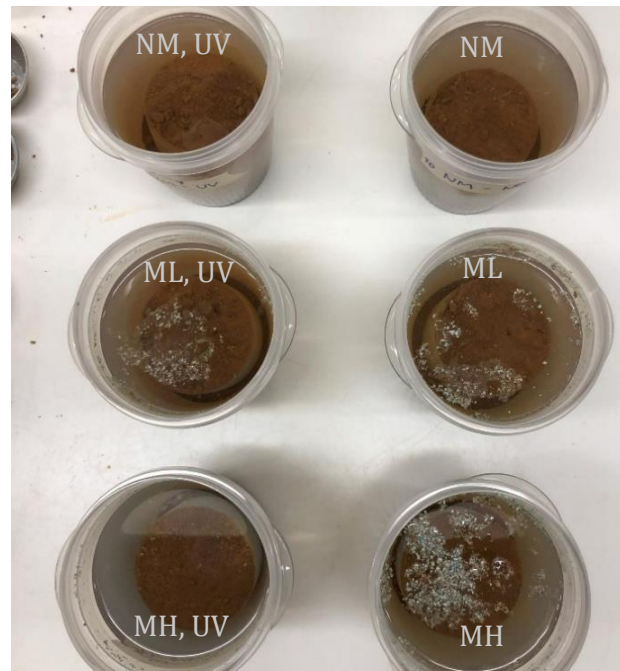


Figure 4.3. From NM to MH (top to bottom). Left column had UV exposure and right column had not (T2 period)

4.2 Mask effect on the Physical and Hydraulic Properties

4.2.1 Saturated permeability (k)

The obtained values for the saturated permeability measured for samples NM, ML and MH presented in Chapter 3.5.3, indicate that the concentration of added mask fibers affects the soil's permeability. Samples NM and MH showed a decreasing trend of the saturated permeability with increasing the concentration of face mask fibers, which aligns with the expected trend of decreased permeability, assuming that the presence of face mask fibers are occupying void spaces and reducing reduce the interconnected pathways for water flow.

However, the results for sample ML were not consistent with this trend with the smaller permeability measured for sample MH, which could be considered an error. Nevertheless, it cannot be completely disregarded since it could still be a reason for the ML sample to have such low saturated permeability. This, however, requires several analyses to be conducted, which is not covered in this study.

An experimental study by Guo et al. (2022) revealed that the presence of MPs reduced soil saturated permeability, but the degree of reduction depended on the concentration of MPs, the type of soil, and the size of MPs. The results indicated a significant decrease in permeability, particularly for smaller particles and higher concentrations, with an optimal concentration of MPs for maximum reduction in saturated permeability. This was suggested to be because a particular concentration of MPs may fill the spaces between soil particles, leading to a greater reduction in permeability. A comparison of the obtained findings with existing literature is presented in

Figure 4.4 for samples NM, ML and MH. Although the comparison is not directly applicable due to differences in size and shape of MPs added to the soil, as well as differences in soil properties, besides experimental error, it is indicative of the expected trends. To obtain more accurate and trustworthy results, several samples should have been tested.

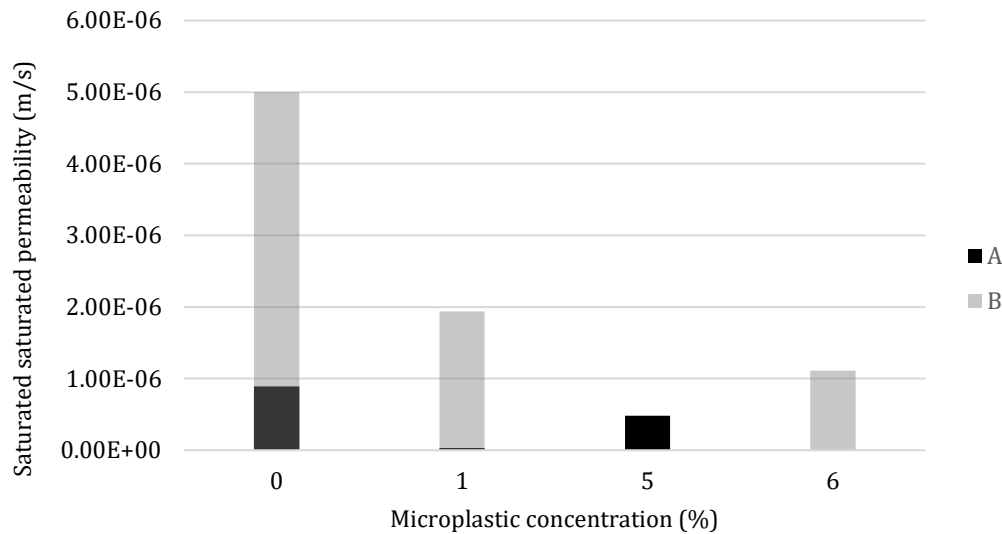


Figure 4.4. The effect of adding different concentrations of microplastics on soil saturated saturated permeability (k). Results of this experimental work using MP of size 2 mm (shredded face mask fibers) with concentrations of 0, 1, and 5 % in silty soil in the present study are shown in Bar A. In clayey soil in Keshan County, China, MP (polypropylene microfibers) of size 0.5 mm with concentrations of 0, 1, and 6 % are represented by Bar B in research results (Guo et al., 2022).

4.2.2 Water retention curves

The curve-fitting constants for soil samples mixed with varying concentrations of mask fibers and for mask fibers alone are listed in Table 3.8 and Table 3.9. On their desorption curve (drying branch), these constants represent the actual air-entry values (AEV) for each of the three soil samples, including the ones that just contain mask fibers. These AEVs represent the matric suction required to produce desaturation of the biggest soil pores (D. G. Fredlund & Xing, 1994). The reported values have been modified for curve-fitting in the data processing, therefore they do not perfectly match the AEVs generated from the WRC curves. As a result, some fluctuation in actual AEVs is expected.

From the study of Guo et al. (2022), similar results were obtained for the clay showing higher AEV values for a higher concentration of MPs. It is thus likely to assume that the presence of plastic fibers in general increases the water holding capacity of the soil. When compared to samples of soil mixed with mask fibers (Table 3.8), the samples with solely mask fibers (Table 3.9) have a much higher AEV, indicating that the addition of mask fibers to the soil is likely to increase the AEV of soil and thereby its capacity to retain water. This conclusion can be drawn from the WRC

CHAPTER 4

of solely mask fibers (Figure 3.14 and Figure 3.15), and additionally in Figure 4.5, which compares the WRC of samples including soil and various concentrations of mask fibers (NM, ML and MH) with those containing only mask fibers (ML,m and MH,m). The WRC plot for NM, ML, and MH is shown in Figure 4.6 in order to demonstrate the difference in the soils' ability to retain water when they contain no, low, and high concentrations of mask fibers.

Furthermore, it would be intriguing to explore the effects of degraded face mask fibers on soil behaviour and assess whether the combined degradation of both the soil and mask fibers would further escalate the AEV value. However, this aspect falls beyond the scope of the current research, suggesting that future studies focusing on soil-MP interactions and their implications for soil stability should consider examining this potential correlation.

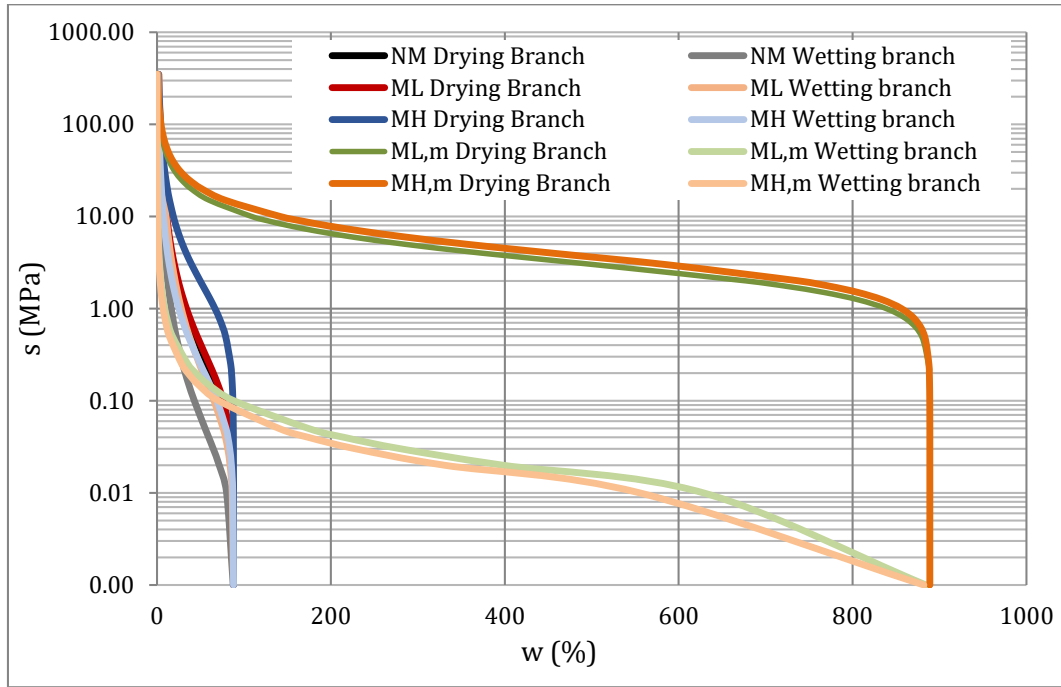


Figure 4.5. Water retention curve (WRC) obtained for samples containing concentration of 0, 1 and 5 % mask fibers and solely low- and high mask fiber mass, corresponding to NM, ML, MH, and ML,m and MH,m, respectively.

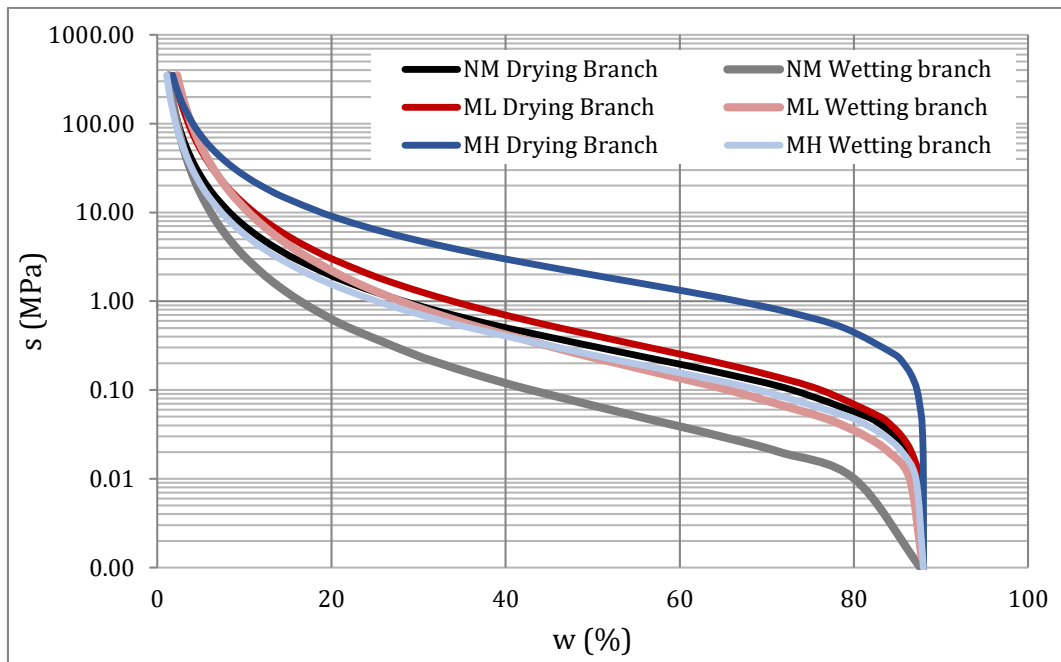


Figure 4.6. Water retention curve (WRC) obtained for samples with mask fiber concentrations of 0, 1 and 5 %, corresponding to NM, ML and MH, respectively.

4.3 Void Ratio and Effects on Soil Structure

4.3.1 Mercury Intrusion Porosimetry

Samples without degradation and water submersion

Figure 4.7 illustrates the distribution of pores for samples NM, ML, and MH under no degradation conditions. It is evident that the pore distribution is quite similar among these samples. However, an important observation is the peak of macropores located between the aggregates (displayed on the right spectrum of the plot). Macropores are defined as pores larger than 100,000 nm in size, mesopores as pores ranging from 100 to 10,000 nm, and micropores as pores smaller than 100 nm. Remarkably, this peak corresponds to a decreasing size of macropores as the concentration of mask fibers increases from 0% to 5%. This suggests that the mask fibers tend to occupy the air gaps between the soil particles, resulting in the creation of smaller pore volumes.

Furthermore, it should be noted that the pore volume distribution is larger for sample MH compared to NM and ML. This observation can be attributed to several causes. Firstly, the accumulation of mask fibers within the soil matrix results in a larger amount void space, as the particles are displaced, and voids are formed between the fibers.

Secondly, it could be caused by the interaction between the mask fibers and mercury, as the fibers are more flexible compared to the soil particles. This flexibility may allow the mercury to penetrate into the fibers or form interfacial gaps around them, resulting in a larger distribution of pore volume.

Moreover, the irregular shape and size of the face mask fibers can physically displace some soil particles during the compaction process, disrupting the packing of soil particles. This disruption leads to a higher distribution of air voids, as the fibers hinder the close arrangement of particles.

Lastly, the presence of face mask fibers can induce changes in the soil structure and porosity. These structural changes affect the compaction behavior and compactness of the soil, potentially resulting in several air voids between the soil particles.

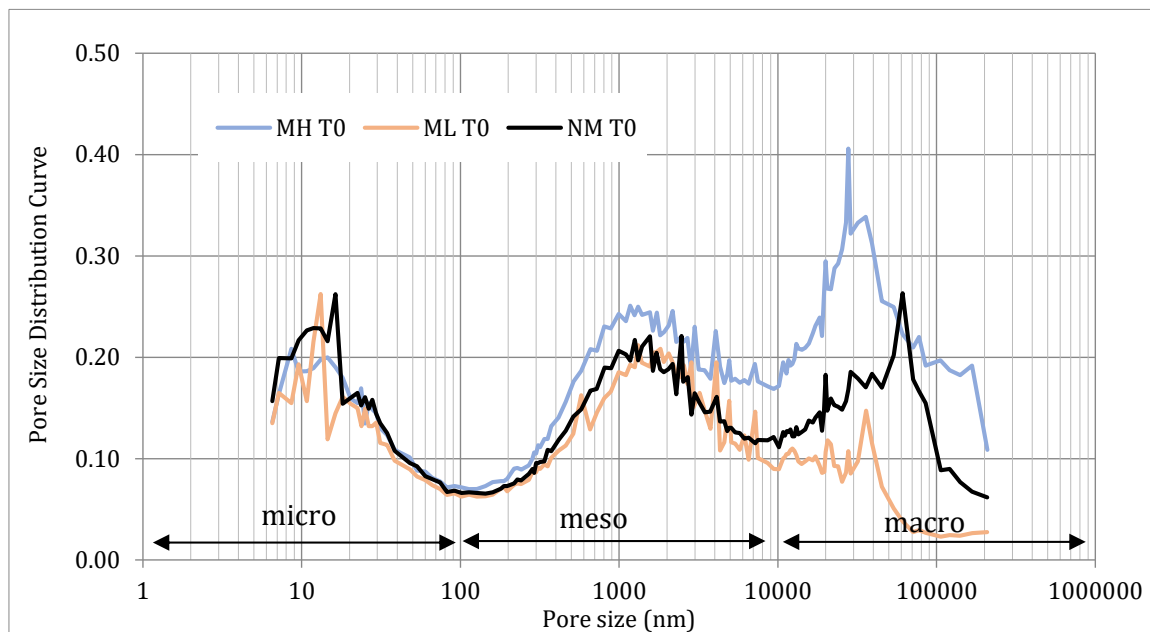


Figure 4.7. Distribution of pore sizes through the soil samples containing different concentrations of face mask fibers. NM, ML and MH corresponding to 0, 1 and 5 % concentration of face mask fibers. T0 indicates no degradation of the samples.

Samples with degradation

From Figure 3.16 illustrating the MIP for sample without any mask fibers it could be observed a decrease in meso-/macropores with long-term degradation and UV exposure. This effect could be caused by the presence of water and swelling of the sample with time, and as a result, the size of larger pores reduces.

When the samples with presence of mask fibers and degradation is analysed (Figure 4.8), it could be seen that samples NM and ML exhibit a more similar distribution of pore sizes, while sample MH stands out with notably high peaks of pore volume ranging between 5k and 50k nm. With the increasing concentration of masks, development of mesopores are thus evident. This observation could potentially be attributed to the degradation of face mask fibers, resulting in smaller fragments and consequently a broader distribution of air voids within the soil matrix.

Another possible explanation for the distinctive pore volume distribution in MH, is the formation of fiber clusters within the soil due to water submerging the sample and causing the fibers to move and aggregate. These “fiber-aggregate complexes” effectively occupy space within the soil structure, giving rise to increased pore volumes (as evident from the microscopic images in Chapter 3.2.4, Figure 3.20).

Therefore, the presence of highly prominent peaks and a more varied distribution in pore volume within sample MH (and ML) suggests a distinct behavior compared to NM sample. This behaviour could be linked to the degradation of face mask fibers and the formation of fiber-aggregate complexes (caused by water submergence), which contribute to the observed variations in pore size distribution and the overall pore volume characteristics of the soil samples.

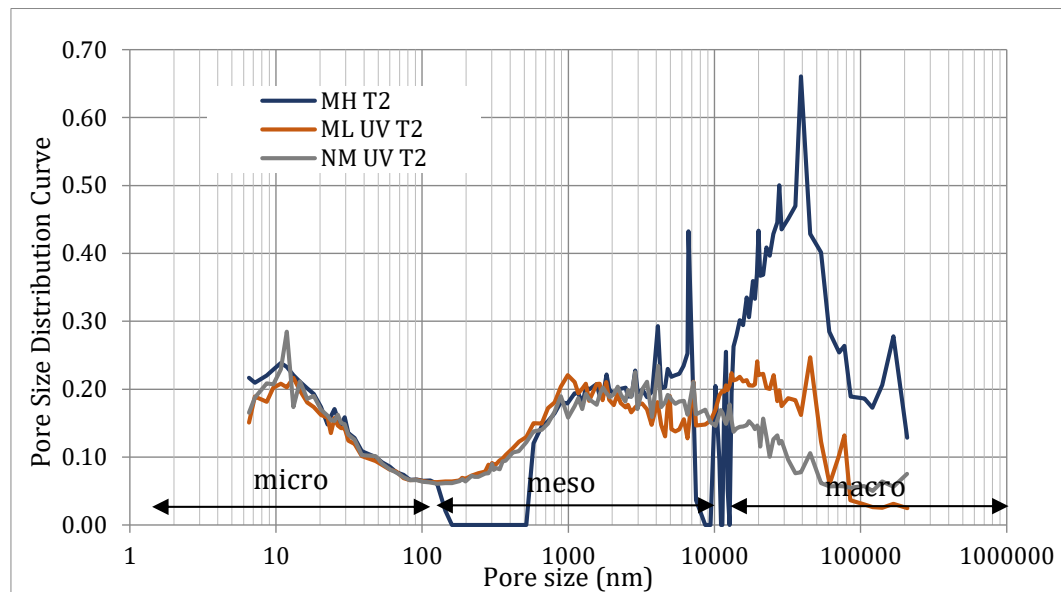


Figure 4.8. Distribution of pore sizes through the soil samples containing different concentrations of face mask fibers. NM, ML and MH corresponding to 0, 1 and 5 % concentration of face mask fibers. T2 correspond to long-term degradation and UV indicates that the sample has been exposed to UV during this period.

In conclusion, the presence of face mask fibers in soil was found to significantly affect the pore distribution and volume characteristics. The fibers occupied interparticle voids, resulting in a decrease in macropores but development of mesopores and moreover an increase in the number of voids. Degradation of face mask fibers and the formation of fiber-aggregate complexes further contributed to variations in pore size distribution and overall pore volume. Additionally, the presence of water was discovered to impact the soil itself by reducing the macropores possibly due to swelling of the soil in contact with water for a longer period. Figure 4.9 illustrates these mechanisms with the effect of water and degradation (upper row) and the effect of mask fibers and degradation (lower row).

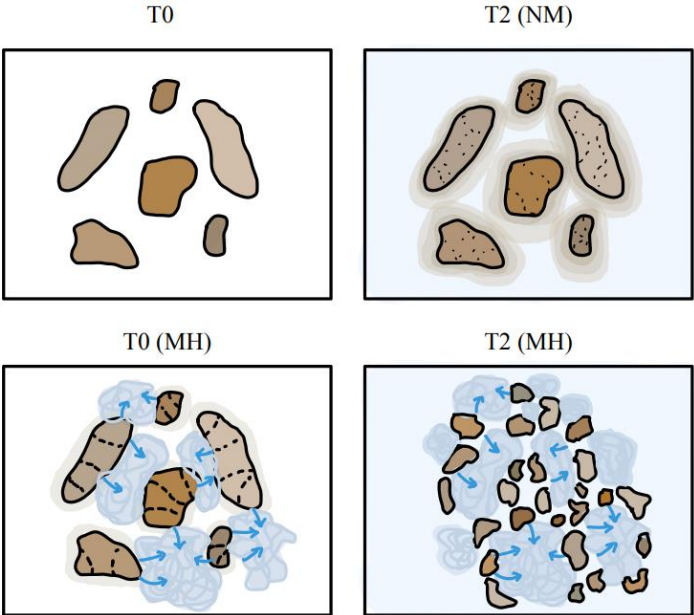


Figure 4.9. Changes in pore sizes and distribution with the presence of water and degradation in the upper row, and the presence of mask fibers and degradation in the lower row.

4.3.2 Void ratio

The void ratio, which represents the relationship between the volume of pores and that occupied by the solid particles in the soil samples, was analyzed for NM, ML, and MH. The average void ratios were determined as 1.0, 1.0, and 1.1, respectively, based on the values obtained from Table 3.5. Interestingly, these findings may not align with the saturated permeability results obtained in Chapter 3.5.2, where sample MH exhibited the least permeability. However, these observations are supported by the analysis conducted using MIP. The MIP analysis revealed that samples with a higher concentration of mask fibers exhibited a larger distribution of pore volume.

The volume of the mask fibers varies significantly across the ML and MH samples, ranging from 1% to 5%, therefore this might not be the case for samples with lower fiber concentrations, like the ML sample. For the ML samples the low amount of mask fibers is unlikely to accumulate in the soil due to their low concentration, blocking the air spaces rather than causing them.

From Table 3.10 and Table 3.11 the different void ratios after degradation period of T1 and T2, respectively, are calculated from the measurement of dry volumetric weight. Figure 4.10 illustrates the variation of these void ratios depending on if the subsamples were extracted from the top or the bottom of the sample and also their different degradation mechanisms.

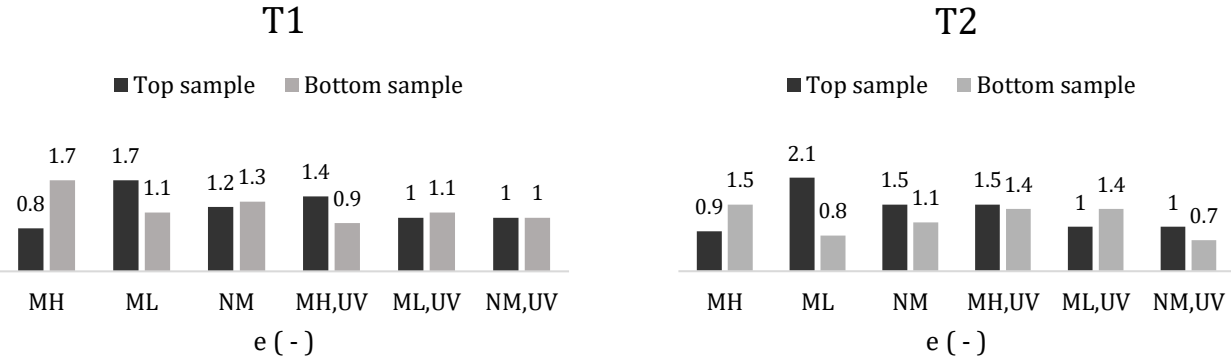


Figure 4.10. Void ratio in samples with different concentration of shredded face mask fibers with MH, ML and NM corresponding to 5,1 and 0 % respectively for sub-samples extracted from both top and bottom of cylindrical samples used in the experimental work. MH,UV, ML,UV and NM,UV are samples suffering UV exposure. T1 represents first degradation period of 2 weeks and T2 represents second degradation period of 6 weeks.

According to the findings from Figure 4.10 , the top samples, represented by the dark grey bars, tend to have higher void ratios for T2 compared to T1, indicating a change in the soil structure that causes larger spacing between the voids in the soil structure for samples that have undergone a longer period of degradation. For this trendline being substantial for the top samples, indicates that the top portion may have undergone a higher level of degradation and potentially swelling, which is explained further down in this chapter, as a result of being directly exposed to the environment, causing more disruption of the soil's surface layer.

CHAPTER 4

Table 4.1. Change in volume (Δvol) based on the difference between air void space between top and bottom sample (Δe) and the initial void ratio before any degradation (e_{init}) for period T1 and T2.

		e_{init} (-)	Δe (-)	Δvol (%)	Trend (from T1 to T2)
T1	NM	0.9	-0.17	-19.3	-
	ML	1	0.60	60.3	-
	MH	1.2	-0.89	-74.0	-
UV	NM	1.1	-0.02	-2.2	-
	ML	1.1	-0.05	-4.3	-
	MH	1	0.52	52.1	-
T2	NM	1	0.35	34.8	swelling
	ML	1	1.24	123.6	swelling ¹
	MH	1.3	-0.56	-43.0	swelling
UV	NM	1	0.24	23.9	swelling
	ML	1.1	-0.42	-37.8	collapse
	MH	1	0.08	7.6	collapse

Note 1: ML (T2) can be considered an error due to the large increase in volume.

$$\Delta vol (\%) = \frac{e_{top} - e_{bottom}}{e_{init}} \cdot 100 \%$$

(10)

Table 4.1 displays the change in volume (Δvol) for periods T1 and T2 based on the difference between the air void space between the top and bottom samples (Δe) and the initial void ratio (e_{init}) before any degradation, using equation (10). Negative values indicates that the bottom void ratio is larger than the top void ratio. This is in accordance with sign convention in traditional mechanics. The observed increase in void ratio at the bottom of the sample could be attributed to the time required for water infiltration in the submerged samples.

However, the interesting aspect is comparing the volume change from short-term to long-term degradation. The trend-column implies whether the volume change from period T1 to T2 increases (compaction) or decreases (swelling) (in accordance with soil mechanics). It is expected that the soil with no mask fibers will swell with aging, with the presence of water.

Additionally, it is evident that samples exposed to UV experienced collapse as the volume decreases from T1 to T2 in the presence of mask fibers. Moreover, it can be seen that the degree of swelling for conditions with no UV decreases with increasing concentration of mask fibers, whereas the degree of compaction for conditions with UV increases with increasing concentration of mask fibers, indicating that the fibers act as a stabilizer of the soil, resulting in a denser structure. Another probable cause is that the face mask fibers have degraded into even smaller particles with UV exposure, leading to in a more compact soil sample because the fibers occupy less space in the soil. This hypothesis can be supported by the visual examination of the soil samples (discussed in Chapter 4.1), showing that the MH sample subjected to UV degradation released fewer face mask fibers to the water surface. This finding suggests that the particles may have broken into such small fragments that they were no longer recognizably identifiable, or that the soil samples were stabilized by the fibers and emitted fewer particles as a result.

Nevertheless, factors such as inherent soil heterogeneity and differential settling due to variations in compaction can also contribute to changes in soil structure, resulting in variations in porosity and void ratio.

4.3.3 SEM Analysis

Comparing the images produced by SEM in Chapter 3.6.5 reveals that there is little variation between the various deterioration mechanisms. However, there is a very slight difference between long-term (with and without UV) degradation and no degradation in the mask fibers, The fibers appear to have a smoother surface with no degradation and some fragmentation for long-term degradation, which barely seems to be enhanced with samples being exposed to UV (see yellow marks Figure 3.21 and Figure 3.22)

The EDS analysis revealed the presence of specific chemical compounds on particular areas of the soil sample, as depicted in Figure 3.24 and Figure 3.25. The mineral analysis conducted in Chapter 3.2.4 corroborated the identification of elements such as Fe, Mg, K, O, Si, Al, and Ca in the soil samples. Furthermore, EDS detected the presence of Au, Pd, Ti, P, and C. Notably, Au and Pd were primarily detected on the mask fibers themselves in samples with a high concentration of mask fibers with no degradation. However, it is important to note that the samples used for SEM and EDS analysis represent only a small fraction of the entire soil samples. Consequently, the chemical compounds detected may vary across different samples, particularly considering that the soil employed in the experiment is classified as "natural soil" and may contain a diverse range of elements.

4.3.4 Chemical water analysis

To gain insights into the composition of submersion water in soil samples, metal component analysis was performed on 12 water samples sent to the chemical laboratory of Nova FCT. The results revealed that Cu, Ni, P, Pb, and Si were present in all samples containing face mask fibers, while Ba and Sr were detected in almost all samples except ML T2 (w) and MH T2 (w) (Table 3.12). In a study conducted by Liu et al. (2022) on leachates from disposable plastic face masks (DPFs), Co, Cu, Ni, Sr, Ti, and Zn were commonly detected. Additionally, all surgical face masks showed the presence of Cd, Cr, Mn, and Pb. However, in our study, Cd, Cr, and Mn were not detected in the leachate water from the samples.

In the NM (T1) sample, all tested components were present except Cd, Cr, and Zn. Similarly, the NM (UV T2) sample, exposed to UV radiation, showed the presence of all tested components except Cd, Co, Cr, Mn, Ti, and Zn. These findings suggest that the samples were affected by simulated degradation mechanisms, including aging, water submersion, and UV exposure. However, it is also possible that the absence of certain metals in the sample exposed to extended degradation is merely coincidental. Further testing is required to confirm this hypothesis. The mineral analysis and EDS of the NM sample (Chapter 3.2.4 and 3.6.5) also revealed the presence of Al, Fe, Si, and Ti in the bare soil with no degradation, among other compounds.

It is worth noting that Zn was consistently present in all samples containing mask fibers and water mixtures, with ML exhibiting higher concentrations (Figure 4.13). This could be attributed to more severe degradation of the ML samples due to direct and evenly distributed UV exposure on the mask fiber surfaces. However, this hypothesis lacks substantial support since the concentration of Zn is highest in the sample not subjected to UV. Zn is commonly found in face mask materials, such as melt-blown polypropylene, due to its antimicrobial properties and is considered a safe additive in many food and cosmetic products (Gonzalez et al., 2021). Thus, it poses no significant threat to animals or humans.

Previous studies have shown that aging and UV exposure increase the adsorption capacity of disposable plastic face masks (DPFs) for heavy metals like Pb, Cd, and Sr (Lin et al., 2022). Additionally, the adsorption affinity of DPFs for metals, even when not degraded, was found to be similar or even higher compared to other MPs. This trend is evident in our study when examining the concentration of Sr in Figure 4.12, where the leachate water's Sr concentration decreases with increasing face mask fiber concentration (NM to MH). However, it is worth noting that the Sr concentration is higher in samples subjected to UV, suggesting that the degradation of the sample and/or mask fibers has affected the adsorption capacity for the soil and/or mask fibers. In the

CHAPTER 4

case of the NM sample, it appears that aging and UV exposure decrease the absorption capacity or potentially increase the sorption capacity of Sr in the soil. A similar pattern could be expected for ML and MH.

In the case of mask fiber and water samples (Figure 4.13), the concentration of Sr from the mask fibers is higher in MH compared to ML (without UV), indicating a lower adsorption capacity. This could be due to the higher accumulation of mask fibers in the water of MH, which protects the fibers from degradation and allows more mask fibers to absorb metals. However, for ML and MH samples subjected to UV and aging, the concentration of Sr is higher in MH (UV T2) than in ML (UV T2), also suggesting that degradation might have affected the absorption capacity of the mask fibers. However, it would be expected that ML still has a higher concentration than MH due to the accumulation of mask fibers in MH. Thus, there is no clear evidence regarding how the adsorption and/or sorption capacity of face mask fibers is affected by degradation, and further analyses are necessary.

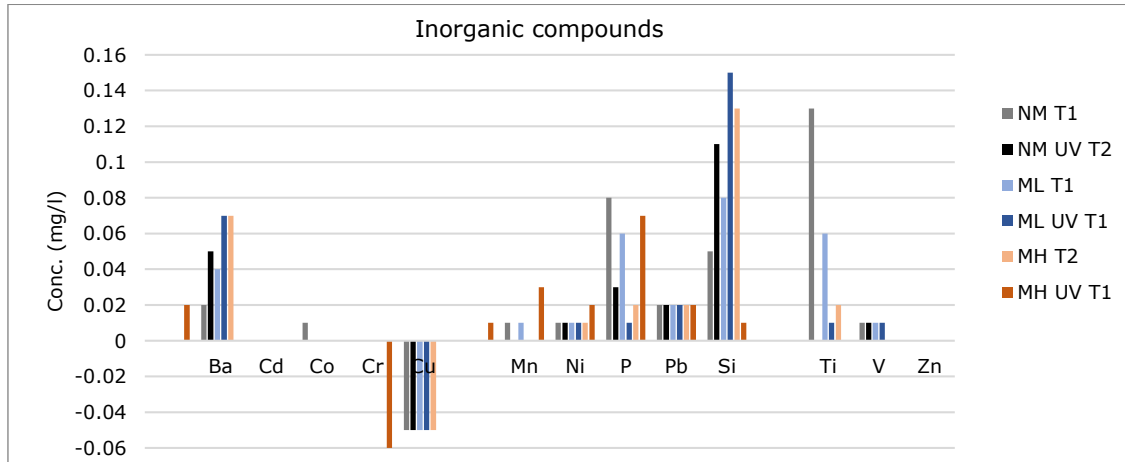


Figure 4.11. Concentrations of inorganic compounds (mg/l) of water samples submerging soil with varying concentrations of face mask fibers (NM, ML, and MH), subjected to various degradation processes such UV exposure and short- and long-term aging (T1 and T2).

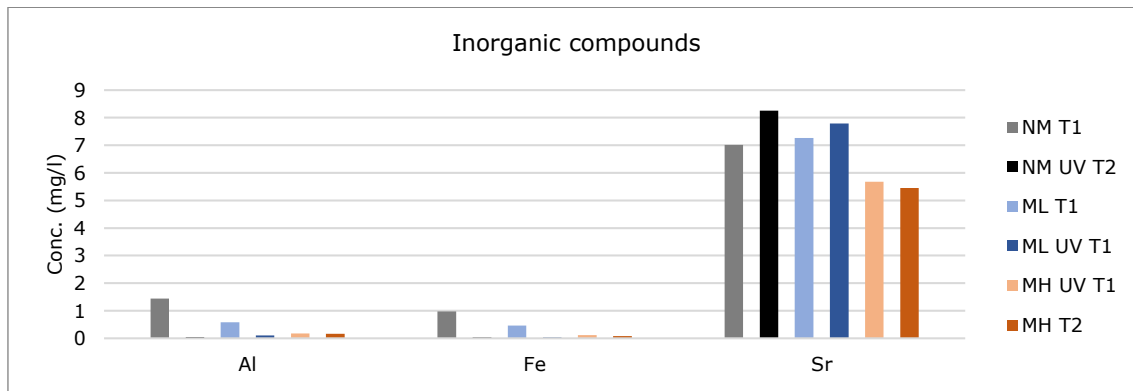


Figure 4.12. Concentrations of inorganic compounds (mg/l) of water samples submerging soil with varying concentrations of face mask fibers (NM, ML, and MH), subjected to various degradation processes such UV exposure and short- and long-term aging (T1 and T2).

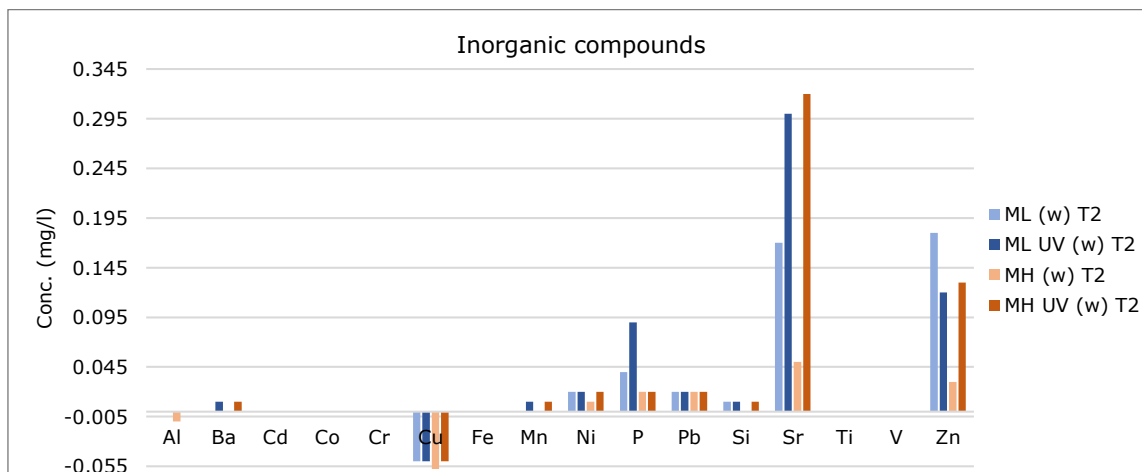


Figure 4.13. Concentrations of inorganic compounds (mg/l) in samples of water mixed with face mask fibers of concentrations (ML and MH), subjected to different degradation mechanisms such as long-term aging (T2) and UV exposure.

4.3.5 Environmental impact of single-use face masks in soils

To comprehensively analyse the environmental factors associated with the conducted experimental activity, it is crucial to consider various observations from the undertaken study. Firstly, the effects on the soil should be taken into account, as the pollution caused by MPs from shredded face masks can potentially alter the soil's characteristics. This modification may have implications for the soil's capacity to absorb and release hazardous substances, as well as its ability to sustainably support agricultural practices (Tian et al., 2022).

In light of the conducted analyses, certain results, such as the grading size distribution of the mask fibers (Chapter 3.3.2), indicated that the degradation of the face mask fibers themselves were not significantly evident within the experiment's timeline. This suggests that a longer duration may be required to observe notable changes in the fibers due to degradation mechanisms such as UV exposure, temperature and moisture. However, this also implies that the face mask fibers are "non-biodegradable" and thus capable of persisting in the environment for an extended period. Consequently, short-term degradation may not be particularly relevant to investigate for such fibers if the extent of their degradation is considered significant. Nevertheless, the persistent of these fibers in the environment for years on end raises concerns, especially considering the accumulation of smaller particles over time due to the disposal of numerous single-use face masks, and plastic in general, in the environment.

Furthermore, it is essential to examine the environmental impact on the submersion water, particularly considering the potential consequences of groundwater pollution and subsequent leaching into the marine environment. Ingestion of the contaminated water by marine species can further propagate through the food chain, ultimately posing risks of human exposure.

From the chemical water analysis, the concentration of several inorganic compounds was detected for the different samples, including Pb. Moreover, Hu et al., (2012) reported that ingesting Cd, Co, Cr and Pb was reported to have potential carcinogenic risk to both children and adults. Thus, if the leachate water has high concentrations of these components, the chance of them ending up in sources for drinking water and be ingested by humans posing a risk to our health is present.

5 Conclusions and Recommendations for Further Work

5.1 Conclusions

Based on the objective outlined in this thesis, the laboratory study conducted aimed to provide a comprehensive overview of the environmental impact of single-use face masks on terrestrial environments, particularly from the perspective of geotechnical engineering. The results shed light on the potential effects of shredded face mask fibers on soil properties and their degradation under different environmental conditions.

The findings of this study can be summarized as follows:

- Water and aging influenced the pore structure of the soil, owing to the swelling of the soil and disturbance of the soil structure.
- The presence of shredded face mask fibers in soil reduced soil permeability and increased water retaining capacity. This was attributed to the formation of fiber-aggregate complexes between the mask fibers and soil particles and thus, reducing the macropores (pores between the aggregates) while increasing the number of mesopores (pores of the aggregates) in the soil structure.
- The degradation of face mask fibers might result in the formation of finer pieces, resulting in a more compact soil structure because fibers are occupying less space in the soil, influencing the void ratio.
- Visual inspection of the water submerging the samples indicated a significant difference in the leaching potential of mask fibers, depending on the concentration and UV. Samples with high mask concentration and long-term exposure released fewer fibers, possibly due to breakdown of fibers into smaller fragments and/or the fibers acting as stabilizers withing the soil sample.

The results of this study highlight the urgent need for proper disposal and management of single-use face masks to prevent further environmental damage. The widespread use of face masks during the COVID-19 pandemic has led to a significant increase in plastic waste and the potential release of MPs into the environment. As such, it is crucial to address this issue by promoting the use of reusable face masks, proper disposal, and recycling of single-use face masks to mitigate the

CHAPTER 5

environmental impact. Additionally, further research is needed to investigate the long-term effects of face mask pollution on the environment and human health.

5.2 Recommendations for further work

As microplastic (MP) pollution in soils is a growing environmental concern, it is crucial to further investigate the fate and behaviour of MPs in different soil types. In the context of the COVID-19 pandemic, it is particularly important to investigate the fate and behaviour of MPs that originate from single-use face masks. Therefore, future research should focus on the effects of different types of face masks on MP abundance and degradation in soils. This would contribute to the development of methods for reducing their effects as well as a better understanding of the potential environmental consequences of greater face mask usage. Future mitigation efforts could be significantly impacted by research into efficient waste treatment procedures and governmental legislation regarding the disposal of single-use plastics, particularly in developing countries where waste treatment is underdeveloped due to the lack of an established economy.

Furthermore, experiments should be conducted with different depths in the soil, including deeper depths (< 1m) that are more relevant to geotechnical engineering applications. This would enable a better understanding of the vertical migration and accumulation of MPs in soils and inform the design of effective soil remediation strategies. To extend the understanding of the degradation of MPs, longer degradation periods should be tested, beyond what has been previously reported in the literature and experimental work. There is a need to perform longer ageing tests and predictive tests to evaluate the changes in strength caused by the degradation of mask fibers. These tests could include a collapse test with the presence of mask fibers, among others. In addition, different degradation mechanisms should be explored, such as wet and dry cycles, saltwater solutions to simulate marine environments, and other environmental conditions that mimic real-world scenarios. Such experiments could provide insights into how different environmental factors influence the degradation of MPs in soils.

Overall, in order to address the growing issue of MP pollution and develop practical soil remediation techniques, a thorough examination of the fate and behaviour of MPs in soils, particularly those released by single-use face masks, is essential. In the engineering industry, where cost and safety are typically prioritized over environmental concerns, this is especially crucial. Single-use plastic waste, particularly face masks, has significantly increased as a result of the COVID-19 pandemic. It is crucial to spread awareness of this problem and carry out research that can guide the development of effective long-term solutions. By comprehending the fate and behaviour of MPs in the ecosystem, we could aim to mitigate the effects of MP pollution in the environment and encourage a more sustainable future.

References

- 1 Agence européenne pour l'environnement (Organisme et agence de l'UE). (2022). *Europe's groundwater: A key resource under pressure*. Office des publications de l'Union européenne. <https://data.europa.eu/doi/10.2800/50592>
- 2 Akber Abbasi, S., Khalil, A. B., & Arslan, M. (2020). Extensive use of face masks during COVID-19 pandemic: (Micro-)plastic pollution and potential health concerns in the Arabian Peninsula. *Saudi Journal of Biological Sciences*, 27(12), 3181–3186. <https://doi.org/10.1016/j.sjbs.2020.09.054>
- 3 Armentano, I., Barbanera, M., Carota, E., Crognale, S., Marconi, M., Rossi, S., Rubino, G., Scungio, M., Taborri, J., & Calabrò, G. (2021). Polymer Materials for Respiratory Protection: Processing, End Use, and Testing Methods. *ACS Applied Polymer Materials*, 3(2), 531–548. <https://doi.org/10.1021/acsapm.0c01151>
- 4 Asadi, M. A., Ritonga, Y. A. P., Yona, D., & Hertika, A. M. S. (2019). Vertical distribution of microplastics in coastal sediments of bama resort, baluran national Park, Indonesia. *Nature Environment and Pollution Technology*, 18(4), 1169–1176. Scopus.
- 5 *ASTM D2487-17e1—Standard Practice for Classification of Soils for Engineering Purposes (Unified Soil Classification System)*. (2017). https://webstore.ansi.org/standards/astm/astmd248717e1?source=blog&_ga=2.34417314.264808458.1686140969-1759005153.1686140969&_gl=1*fqlh78*_gcl_au*MTI0ODEyODQwMC4xNjg2MTQwOTY5
- 6 Benson, N. U., Bassey, D. E., & Palanisami, T. (2021a). COVID pollution: Impact of COVID-19 pandemic on global plastic waste footprint. *Heliyon*, 7(2), e06343. <https://doi.org/10.1016/j.heliyon.2021.e06343>
- 7 Benson, N. U., Bassey, D. E., & Palanisami, T. (2021b). *COVID pollution: Impact of COVID-19 pandemic on global plastic waste footprint | Elsevier Enhanced Reader [Heliyon]*. COVID Pollution: Impact of COVID-19 Pandemic on Global Plastic Waste Footprint. <https://doi.org/10.1016/j.heliyon.2021.e06343>
- 8 Campanale, C., Massarelli, C., Savino, I., Locaputo, V., & Uricchio, V. F. (2020). A Detailed Review Study on Potential Effects of Microplastics and Additives of Concern on Human Health. *International Journal of Environmental Research and Public Health*, 17(4), Article 4. <https://doi.org/10.3390/ijerph17041212>
- 9 Cashman, M. A., Langknecht, T., El Khatib, D., Burgess, R. M., Boving, T. B., Robinson, S., & Ho, K. T. (2022). Quantification of microplastics in sediments from Narragansett Bay, Rhode Island USA using a novel isolation and extraction method. *Marine Pollution Bulletin*, 174, 113254. <https://doi.org/10.1016/j.marpolbul.2021.113254>
- 10 Chen, X., Chen, X., Liu, Q., Zhao, Q., Xiong, X., & Wu, C. (2021). Used disposable face masks are significant sources of microplastics to environment. *Environmental Pollution*, 285, 117485. <https://doi.org/10.1016/j.envpol.2021.117485>
- 11 *Comparison of mask types for COVID-19 | Safe Work Australia*. (2022). <https://covid19.swa.gov.au/comparison-mask-types-covid-19>
- 12 CORPORATIVA, I. (n.d.). *How to dispose of masks and protect the environment?* Iberdrola. Retrieved 10 February 2023, from <https://www.iberdrola.com/social-commitment/how-to-dispose-of-face-masks>

BIBLIOGRAPHY

- 13 Cutting Mill SM 200—Retsch—Operational safety and convenience. (n.d.). Retrieved 15 May 2023, from <https://www.retsch.com/products/milling/cutting-mills/sm-200/>
- 14 D18 Committee. (n.d.-a). *Practice for Classification of Soils for Engineering Purposes (Unified Soil Classification System)*. ASTM International. <https://doi.org/10.1520/D2487-17>
- 15 D18 Committee. (n.d.-b). *Test Methods for Laboratory Compaction Characteristics of Soil Using Modified Effort (56,000 ft-lbf/ft³ (2,700 kN-m/m³))*. ASTM International. <https://doi.org/10.1520/D1557-12R21>
- 16 D18 Committee. (n.d.-c). *Test Methods for Liquid Limit, Plastic Limit, and Plasticity Index of Soils*. ASTM International. <https://doi.org/10.1520/D4318-17>
- 17 D18 Committee. (n.d.-d). *Test Methods for Specific Gravity of Soil Solids by Water Pycnometer*. ASTM International. <https://doi.org/10.1520/D0854-02>
- 18 Disposing of disposable masks properly. (2022, July 14). *Sustainable Industry*. <https://brazilsustainableindustry.com.br/sustainable-hints/disposing-of-disposable-masks-properly/>
- 19 Drabek, J., & Zatloukal, M. (2019). Meltblown technology for production of polymeric microfibers/nanofibers: A review. *Physics of Fluids*, 31(9), 091301. <https://doi.org/10.1063/1.5116336>
- 20 *Estimated 1.56 billion face masks will have entered oceans in 2020—OceansAsia Report*. (2020). OCEANS ASIA. <https://oceansasia.org/covid-19-facemasks/>
- 21 Fadare, O. O., & Okoffo, E. D. (2020). Covid-19 face masks: A potential source of microplastic fibers in the environment. *Science of The Total Environment*, 737, 140279. <https://doi.org/10.1016/j.scitotenv.2020.140279>
- 22 Fava, M. F. (2022, May 9). Plastic pollution in the ocean: Data, facts, consequences. *Ocean Literacy Portal*. <https://oceanliteracy.unesco.org/plastic-pollution-ocean/>
- 23 Fredlund, D. G., & Xing, A. (1994). Equations for the soil-water characteristic curve. *Canadian Geotechnical Journal*, 31(4), 521–532. <https://doi.org/10.1139/t94-061>
- 24 Fredlund, M. D., Tran, D., & Fredlund, D. G. (2016). Methodologies for the Calculation of Actual Evaporation in Geotechnical Engineering. *International Journal of Geomechanics*, 16(6), D4016014. [https://doi.org/10.1061/\(ASCE\)GM.1943-5622.0000730](https://doi.org/10.1061/(ASCE)GM.1943-5622.0000730)
- 25 *From Pollution to Solution*. (2022). United Nations Environment Programme (UNEP). <https://www.unep.org/interactives/pollution-to-solution/>
- 26 Fu, W., Min, J., Jiang, W., Li, Y., & Zhang, W. (2020). Separation, characterization and identification of microplastics and nanoplastics in the environment. *Science of The Total Environment*, 721, 137561. <https://doi.org/10.1016/j.scitotenv.2020.137561>
- 27 Gabisa, E. W., & Gheewala, S. H. (2022). Microplastics in ASEAN region countries: A review on current status and perspectives. *Marine Pollution Bulletin*, 184, 114118. <https://doi.org/10.1016/j.marpolbul.2022.114118>
- 28 Geyer, R., Jambeck, J., & Law, K. (2017). Production, use, and fate of all plastics ever made. *Science Advances*, 3, e1700782. <https://doi.org/10.1126/sciadv.1700782>
- 29 Gilbert, M. (2017). Chapter 1 - Plastics Materials: Introduction and Historical Development. In M. Gilbert (Ed.), *Brydson's Plastics Materials (Eighth Edition)* (pp. 1–18). Butterworth-Heinemann. <https://doi.org/10.1016/B978-0-323-35824-8.00001-3>
- 30 Gonzalez, A., Aboubakr, H. A., Brockgreitens, J., Hao, W., Wang, Y., Goyal, S. M., & Abbas, A. (2021). Durable nanocomposite face masks with high particulate filtration and rapid inactivation of coronaviruses. *Scientific Reports*, 11, 24318. <https://doi.org/10.1038/s41598-021-03771-1>
- 31 *Growing plastic pollution in wake of COVID-19: How trade policy can help | UNCTAD*. (2020, July 27). <https://unctad.org/news/growing-plastic-pollution-wake-covid-19-how-trade-policy-can-help>

BIBLIOGRAPHY

- 32 Guerrero, L. A., Maas, G., & Hogland, W. (2013). Solid waste management challenges for cities in developing countries. *Waste Management*, *33*(1), 220–232. <https://doi.org/10.1016/j.wasman.2012.09.008>
- 33 Guo, Z., Li, P., Yang, X., Wang, Z., Lu, B., Chen, W., Wu, Y., Li, G., Zhao, Z., Liu, G., Ritsema, C., Geissen, V., & Xue, S. (2022). Soil texture is an important factor determining how microplastics affect soil hydraulic characteristics. *Environment International*, *165*, 107293. <https://doi.org/10.1016/j.envint.2022.107293>
- 34 Gupta, P., Kumar, A., & Sinhamahapatra, A. (2022). Liquid Fuel From Plastic Waste. In *Encyclopedia of Materials: Plastics and Polymers* (pp. 904–916). Elsevier. <https://doi.org/10.1016/B978-0-12-820352-1.00128-0>
- 35 Haugen, H. J., & Bertoldi, S. (2017). Characterization of morphology—3D and porous structure. In *Characterization of Polymeric Biomaterials* (pp. 21–53). Elsevier. <https://doi.org/10.1016/B978-0-08-100737-2.00002-9>
- 36 Horton, A. A., Walton, A., Spurgeon, D. J., Lahive, E., & Svendsen, C. (2017). Microplastics in freshwater and terrestrial environments: Evaluating the current understanding to identify the knowledge gaps and future research priorities. *Science of The Total Environment*, *586*, 127–141. <https://doi.org/10.1016/j.scitotenv.2017.01.190>
- 37 Hu, X., Zhang, Y., Ding, Z., Wang, T., Lian, H., Sun, Y., & Wu, J. (2012). Bioaccessibility and health risk of arsenic and heavy metals (Cd, Co, Cr, Cu, Ni, Pb, Zn and Mn) in TSP and PM_{2.5} in Nanjing, China. *Atmospheric Environment*, *57*, 146–152. <https://doi.org/10.1016/j.atmosenv.2012.04.056>
- 38 Jambeck, J. R., Geyer, R., Wilcox, C., Siegler, T. R., Perryman, M., Andrady, A., Narayan, R., & Law, K. L. (2015). Plastic waste inputs from land into the ocean. *Science*, *347*(6223), 768–771. <https://doi.org/10.1126/science.1260352>
- 39 Konda, A., Prakash, A., Moss, G. A., Schmoldt, M., Grant, G. D., & Guha, S. (2020). Aerosol Filtration Efficiency of Common Fabrics Used in Respiratory Cloth Masks. *ACS Nano*, *14*(5), 6339–6347. <https://doi.org/10.1021/acsnano.0c03252>
- 40 Kontrick, A. V. (2018). Microplastics and Human Health: Our Great Future to Think About Now. *Journal of Medical Toxicology*, *14*(2), 117–119. <https://doi.org/10.1007/s13181-018-0661-9>
- 41 Kuller, L. (1969). Sudden death in arteriosclerotic heart disease. *The American Journal of Cardiology*, *24*(5), 617–628. [https://doi.org/10.1016/0002-9149\(69\)90450-0](https://doi.org/10.1016/0002-9149(69)90450-0)
- 42 Kumar, M., Xiong, X., He, M., Tsang, D. C. W., Gupta, J., Khan, E., Harrad, S., Hou, D., Ok, Y. S., & Bolan, N. S. (2020). Microplastics as pollutants in agricultural soils. *Environmental Pollution*, *265*, 114980. <https://doi.org/10.1016/j.envpol.2020.114980>
- 43 Kundra, Y. (2022, November 18). Specific Gravity of Plastic Laboratories, Specific Gravity of Plastic Testing Services in California, USA. *Infinita Lab*. <https://infinitalab.com/material-testing-service/specific-gravity-of-plastic/>
- 44 Kwak, J. I., & An, Y.-J. (2021). Post COVID-19 pandemic: Biofragmentation and soil ecotoxicological effects of microplastics derived from face masks. *Journal of Hazardous Materials*, *416*, 126169. <https://doi.org/10.1016/j.jhazmat.2021.126169>
- 45 Lin, L., Yuan, B., Zhang, B., Li, H., Liao, R., Hong, H., Lu, H., Liu, J., & Yan, C. (2022). Uncovering the disposable face masks as vectors of metal ions (Pb(II), Cd(II), Sr(II)) during the COVID-19 pandemic. *Chemical Engineering Journal*, *439*, 135613. <https://doi.org/10.1016/j.cej.2022.135613>
- 46 Liu, Z., Wang, J., Yang, X., Huang, Q., Zhu, K., Sun, Y., Van Hulle, S., & Jia, H. (2022). Generation of environmental persistent free radicals (EPFRs) enhances ecotoxicological effects of the disposable face mask waste with the COVID-19 pandemic. *Environmental Pollution*, *301*, 119019. <https://doi.org/10.1016/j.envpol.2022.119019>

BIBLIOGRAPHY

- 47 LNEC E 239—1970 Solos—Análise Granulométrica Por Peneiração Húmida | PDF. (n.d.). Scribd. Retrieved 1 March 2023, from <https://pt.scribd.com/document/420087993/LNEC-E-239-1970-Solos-Analise-Granulometrica-Por-Peneiracao-Humida>
- 48 Moharir, R. V., Gautam, P., & Kumar, S. (2019). Waste Treatment Processes/Technologies for Energy Recovery. In *Current Developments in Biotechnology and Bioengineering* (pp. 53–77). Elsevier. <https://doi.org/10.1016/B978-0-444-64083-3.00004-X>
- 49 *More than 8.3 billion tons of plastics made: Most has now been discarded.* (2017, July 19). ScienceDaily. <https://www.sciencedaily.com/releases/2017/07/170719140939.htm>
- 50 *Munnbind.* (2020, August 25). <https://www.helsenorge.no/en/coronavirus/face-masks/>
- 51 Novák, V., & Hlaváčiková, H. (2019). Soil-Water Retention Curve. In V. Novák & H. Hlaváčiková (Eds.), *Applied Soil Hydrology* (pp. 77–96). Springer International Publishing. https://doi.org/10.1007/978-3-030-01806-1_7
- 52 Nurhasanah, Cordova, M. R., & Riani, E. (2021). Micro- and mesoplastics release from the Indonesian municipal solid waste landfill leachate to the aquatic environment: Case study in Galuga Landfill Area, Indonesia. *Marine Pollution Bulletin*, *163*, 111986. <https://doi.org/10.1016/j.marpolbul.2021.111986>
- 53 Panno, S. V., Kelly, W. R., Scott, J., Zheng, W., McNeish, R. E., Holm, N., Hoellein, T. J., & Baranski, E. L. (2019). Microplastic Contamination in Karst Groundwater Systems. *Groundwater*, *57*(2), 189–196. <https://doi.org/10.1111/gwat.12862>
- 54 Parker, L. (2019, July 6). *Plastic pollution facts and information.* Environment. <https://www.nationalgeographic.com/environment/article/plastic-pollution>
- 55 Pizarro-Ortega, C. I., Dioses-Salinas, D. C., Fernández Severini, M. D., Forero López, A. D., Rimondino, G. N., Benson, N. U., Dobaradaran, S., & De-la-Torre, G. E. (2022). Degradation of plastics associated with the COVID-19 pandemic. *Marine Pollution Bulletin*, *176*, 113474. <https://doi.org/10.1016/j.marpolbul.2022.113474>
- 56 Polyolefins • Plastics Europe. (n.d.). *Plastics Europe.* Retrieved 18 May 2023, from <https://plasticseurope.org/plastics-explained/a-large-family/polyolefins/>
- 57 Poudel, S. (2021). *Disposing of face masks: The next environmental problem?* UNICEF. <https://www.unicef.org/nepal/stories/disposing-face-masks-next-environmental-problem>
- 58 *Qualities to Look for in Face Mask Protection—Safe 'N' Clear, Inc. | The Communicator™ clear face mask.* (n.d.). Retrieved 22 May 2023, from <https://safenclear.com/qualities-to-look-for-in-face-mask-protection/>
- 59 Queensland, c=AU; o=The S. of. (n.d.). *Soil colour | Soil properties* [Text]. corporateName=The State of Queensland; jurisdiction=Queensland. Retrieved 16 April 2023, from <https://www.qld.gov.au/environment/land/management/soil/soil-properties/colour>
- 60 Sarijan, S., Azman, S., Said, M. I. M., & Jamal, M. H. (2021). Microplastics in freshwater ecosystems: A recent review of occurrence, analysis, potential impacts, and research needs. *Environmental Science and Pollution Research*, *28*(2), 1341–1356. <https://doi.org/10.1007/s11356-020-11171-7>
- 61 Selvaranjan, K., Navaratnam, S., Rajeev, P., & Ravintherakumar, N. (2021). Environmental challenges induced by extensive use of face masks during COVID-19: A review and potential solutions. *Environmental Challenges*, *3*, 100039. <https://doi.org/10.1016/j.envc.2021.100039>
- 62 Sendra, M., Rodriguez-Romero, A., Yeste, M. P., Blasco, J., & Tovar-Sánchez, A. (2022). Products released from surgical face masks can provoke cytotoxicity in the marine diatom *Phaeodactylum tricornutum*. *Science of The Total Environment*, *841*, 156611. <https://doi.org/10.1016/j.scitotenv.2022.156611>

BIBLIOGRAPHY

- 63 Shekaraiah, S., & Suresh, K. (2021). Effect of Face Mask on Voice Production During COVID-19 Pandemic: A Systematic Review. *Journal of Voice*, S0892199721003271. <https://doi.org/10.1016/j.jvoice.2021.09.027>
- 64 Singh, N., Tang, Y., & Ogunseitan, O. A. (2020). Environmentally Sustainable Management of Used Personal Protective Equipment. *Environmental Science & Technology*, 54(14), 8500–8502. <https://doi.org/10.1021/acs.est.0c03022>
- 65 Singh, S., & Bhagwat, A. (2022). Microplastics: A potential threat to groundwater resources. *Groundwater for Sustainable Development*, 19, 100852. <https://doi.org/10.1016/j.gsd.2022.100852>
- 66 *Standard Test Methods for Laboratory Compaction Characteristics of Soil Using Standard Effort (12,400 ft-lbf/ft³ (600 kN-m/m³))*. (n.d.). Retrieved 7 June 2023, from <https://www.astm.org/d0698-12r21.html>
- 67 *Standard Test Methods for Liquid Limit, Plastic Limit, and Plasticity Index of Soils*. (n.d.). Retrieved 15 May 2023, from <https://www.astm.org/d4318-17.html>
- 68 *Standard Test Methods for Measurement of Saturated permeability of Saturated Porous Materials Using a Flexible Wall Permeameter*. (n.d.). Retrieved 15 May 2023, from <https://www.astm.org/d5084-16a.html>
- 69 Statista. (2016). *Regional consumption of plastic materials per capita 2015*. Statista. <https://www.statista.com/statistics/270312/consumption-of-plastic-materials-per-capita-since-1980/>
- 70 Su, L., Xiong, X., Zhang, Y., Wu, C., Xu, X., Sun, C., & Shi, H. (2022). Global transportation of plastics and microplastics: A critical review of pathways and influences. *Science of The Total Environment*, 831, 154884. <https://doi.org/10.1016/j.scitotenv.2022.154884>
- 71 Tian, L., Jinjin, C., Ji, R., Ma, Y., & Yu, X. (2022). Microplastics in agricultural soils: Sources, effects, and their fate. *Current Opinion in Environmental Science & Health*, 25, 100311. <https://doi.org/10.1016/j.coesh.2021.100311>
- 72 Wang, Z.-M., Wagner, J., Ghosal, S., Bedi, G., & Wall, S. (2017). SEM/EDS and optical microscopy analyses of microplastics in ocean trawl and fish guts. *Science of The Total Environment*, 603–604, 616–626. <https://doi.org/10.1016/j.scitotenv.2017.06.047>
- 73 Watt-Smith, M. J., Rigby, S. P., Chudek, J. A., & Fletcher, R. S. (2007). Simulation of mercury porosimetry using MRI images of porous media. In P. L. Llewellyn, F. Rodriguez-Reinoso, J. Rouquerol, & N. Seaton (Eds.), *Studies in Surface Science and Catalysis* (Vol. 160, pp. 177–184). Elsevier. [https://doi.org/10.1016/S0167-2991\(07\)80024-3](https://doi.org/10.1016/S0167-2991(07)80024-3)
- 74 *WHO publish report on microplastics in drinking water*. (2019, August 28). <https://www.medicalnewstoday.com/articles/326144>
- 75 Xiang, S., Xie, Y., Sun, X., Du, H., & Wang, J. (2022). Identification and Quantification of Microplastics in Aquaculture Environment. *Frontiers in Marine Science*, 8, 804208. <https://doi.org/10.3389/fmars.2021.804208>
- 76 Yao, P., Zhou, B., Lu, Y., Yin, Y., Zong, Y., Chen, M.-T., & O'Donnell, Z. (2019). A review of microplastics in sediments: Spatial and temporal occurrences, biological effects, and analytic methods. *Quaternary International*, 519, 274–281. <https://doi.org/10.1016/j.quaint.2019.03.028>
- 77 Zhang, K., Hamidian, A. H., Tubić, A., Zhang, Y., Fang, J. K. H., Wu, C., & Lam, P. K. S. (2021). Understanding plastic degradation and microplastic formation in the environment: A review. *Environmental Pollution*, 274, 116554. <https://doi.org/10.1016/j.envpol.2021.116554>
- 78 Zhou, Y., Wang, J., Zou, M., Jia, Z., Zhou, S., & Li, Y. (2020). Microplastics in soils: A review of methods, occurrence, fate, transport, ecological and environmental risks. *Science of The Total Environment*, 748, 141368. <https://doi.org/10.1016/j.scitotenv.2020.141368>

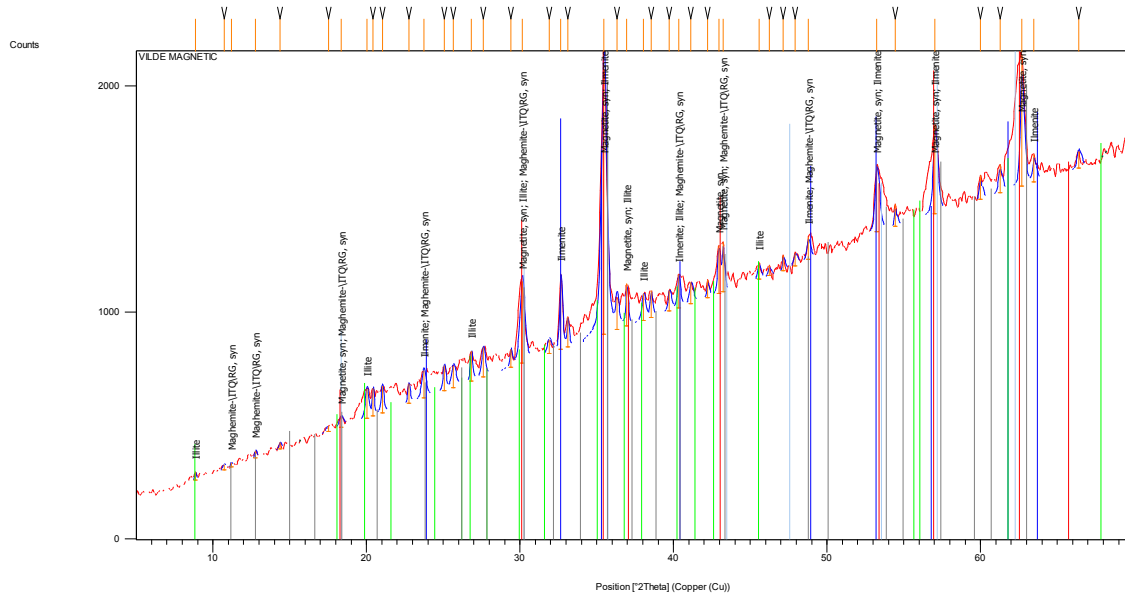
Appendix A

Laboratory Results – Mineral Analysis of the Soil

This is the simple example template containing only headers for each report item and the bookmarks. The invisible bookmarks are indicated by text between brackets.
Modify it according to your own needs and standards.

Measurement Conditions: (Bookmark 1)

Dataset Name	VILDE MAGNETIC
File name	C:\X'Pert Data\MF\Rafaela\VILDE MAGNETIC.xrdml
Comment	Configuration=PW3064/60, Owner=User-1, Creation
date=3/2/2007 4:22:01 PM	
	Goniometer=PW3050/60 (Theta/Theta); Minimum step size
2Theta:0.001; Minimum step size	Omega:0.001
step size Phi:0.1	Sample stage=Transmission Spinner PW3064/60; Minimum
	Diffraction system=XPRT-PRO
	Measurement program=Training1, Owner=User-1, Creation
date=4/2/2007 11:10:47 AM	
Measurement Date / Time	5/10/2023 6:21:26 PM
Operator	Administrador
Raw Data Origin	XRD measurement (*.XRDML)
Scan Axis	Gonio
Start Position [°2Th.]	5.0437
End Position [°2Th.]	69.9547
Step Size [°2Th.]	0.0330
Scan Step Time [s]	74.0162
Scan Type	Continuous
PSD Mode	Scanning
PSD Length [°2Th.]	2.12
Offset [°2Th.]	0.0000
Divergence Slit Type	Automatic
Irradiated Length [mm]	3.00
Specimen Length [mm]	10.00
Measurement Temperature [°C]	25.00
Anode Material	Cu
K-Alpha1 [Å]	1.54060
K-Alpha2 [Å]	1.54443
K-Beta [Å]	1.39225
K-A2 / K-A1 Ratio	0.50000
Generator Settings	35 mA, 40 kV
Diffraction Type	0000000011019195
Diffraction Number	0
Goniometer Radius [mm]	240.00
Dist. Focus-Diverg. Slit [mm]	100.00
Incident Beam Monochromator	No
Spinning	Yes

Main Graphics, Analyze View: (Bookmark 2)**Peak List:** (Bookmark 3)

Pos. [°2Th.]	Height [cts]	FWHM [°2Th.]	d-spacing [Å]	Rel. Int. [%]
8.8505	37.41	0.1299	9.99158	3.20
10.7262	24.08	0.2598	8.24821	2.06
11.1972	20.12	0.1624	7.90229	1.72
12.7786	31.75	0.1948	6.92771	2.71
14.3683	28.87	0.1948	6.16461	2.47
17.5263	25.44	0.3897	5.06030	2.17
18.3604	48.35	0.3247	4.83224	4.13
20.0240	128.45	0.2598	4.43439	10.98
20.4297	121.33	0.1299	4.34722	10.37
21.0302	118.93	0.1948	4.22444	10.16
22.7537	85.41	0.1624	3.90820	7.30
23.7289	121.65	0.3247	3.74975	10.39
25.0688	112.33	0.1948	3.55228	9.60
25.6686	94.90	0.3247	3.47062	8.11
26.8224	133.25	0.1624	3.32389	11.39
27.6084	129.45	0.2598	3.23102	11.06
29.4175	79.27	0.1299	3.03631	6.77
30.1438	359.55	0.3572	2.96479	30.72
31.8983	60.55	0.3247	2.80561	5.17
32.6662	333.25	0.1948	2.74139	28.48
33.1134	133.83	0.1299	2.70539	11.44
35.4602	1170.30	0.3897	2.53154	100.00
36.3166	141.76	0.1948	2.47378	12.11
36.9562	188.14	0.1624	2.43242	16.08
38.0444	117.84	0.2598	2.36531	10.07

38.5370	119.63	0.1624	2.33620	10.22
39.7364	91.28	0.2273	2.26841	7.80
40.3323	147.51	0.1948	2.23626	12.60
41.1422	94.31	0.2598	2.19409	8.06
42.2246	78.94	0.1299	2.14032	6.75
42.9512	213.18	0.1948	2.10578	18.22
43.2333	220.21	0.1299	2.09269	18.82
45.5634	73.04	0.1948	1.99095	6.24
46.2347	44.61	0.1624	1.96359	3.81
47.1586	69.25	0.1624	1.92725	5.92
47.9288	53.76	0.2598	1.89807	4.59
48.7804	95.92	0.2273	1.86691	8.20
53.2530	297.94	0.2922	1.72018	25.46
54.4539	98.34	0.1299	1.68505	8.40
57.0362	391.55	0.2922	1.61474	33.46
59.9925	106.74	0.1624	1.54205	9.12
61.2649	126.80	0.2273	1.51304	10.84
62.6832	581.51	0.2273	1.48217	49.69
63.4878	122.02	0.1948	1.46532	10.43
66.3889	74.13	0.2376	1.40698	6.33

Pattern List: (Bookmark 4)

Visible	Ref. Code	Score	Compound Name	Displacement [°2Th.]	Scale Factor	Chemical Formula
*	00-019-0629	48	Magnetite, syn	0.000	0.980	Fe Fe ₂ O ₄
*	00-003-0778	22	Ilmenite	0.000	0.473	Fe Ti O ₃
*	00-002-0050	6	Illite	0.000	0.074	2 K ₂ O !3 Mg O ! Al ₂ O ₃ !24 Si O ₂ !12 H ₂ O
*	00-025-1402	13	Maghemite- \ITQ\RG, syn	0.000	0.512	Fe ₂ O ₃

Document History: (Bookmark 5)

Insert Measurement:

- File name = "VILDE MAGNETIC.xrdml"
- Modification time = "5/10/2023 6:59:56 PM"
- Modification editor = "Administrador"

Default properties:

- Measurement step axis = "None"
- Internal wavelengths used from anode material: Copper (Cu)
- Original K-Alpha1 wavelength = "1.54060"
- Used K-Alpha1 wavelength = "1.54060"
- Original K-Alpha2 wavelength = "1.54443"
- Used K-Alpha2 wavelength = "1.54443"

- Original K-Beta wavelength = "1.39225"
- Used K-Beta wavelength = "1.39225"
- Incident beam monochromator = "No"
- Fixed div. slit size = "1.00000"
- Receiving slit size = "0.10000"
- Step axis value = "0.00000"
- Offset = "0.00000"
- Sample length = "10.00000"
- Modification time = "5/10/2023 6:59:56 PM"
- Modification editor = "Administrador"

Interpolate Step Size:

- Step Size = "Derived"
- Modification time = "9/1/2006"
- Modification editor = "PANalytical"

Smooth:

- Type of smoothing = "Polynomial"
- Polynomial type = "Cubic"
- Convolution range = "11"
- Modification time = "5/10/2023 5:23:50 PM"
- Modification editor = "Administrador"

Search Peaks:

- Minimum significance = "0.25"
- Minimum tip width = "0.05"
- Maximum tip width = "0.50"
- Peak base width = "2.00"
- Method = "Minimum 2nd derivative"
- Modification time = "5/10/2023 5:24:52 PM"
- Modification editor = "Administrador"

Correct Displacement:

- Known displacement = "-0.300 [mm]"
- Modification time = "5/10/2023 7:00:16 PM"
- Modification editor = "Administrador"

Search & Match:

- Data source = "Profile and peak list"
 - Restriction = "Restriction set"
 - Description = "Minerals subfile only"
 - All of: elements = ""
 - At least one of: elements = ""
 - None of: elements = ""
 - Maximum no. of elements = "105"
 - Skip marked as deleted by ICDD = "No"
 - Skip marked as deleted by a user = "No"
 - Skip non ambient pressure = "No"
 - Skip non ambient temperature = "No"
 - Skip alternate patterns = "No"
 - Quality marks set = ""
-

- Subfiles = "Mineral"
- Scoring schema = "Multi phase"
- Auto residue = "Yes"
- Match intensity = "Yes"
- Demote unmatched strong = "No"
- Allow pattern shift = "No"
- Two theta shift = "0"
- Identify = "No"
- Modification time = "1/11/2001 10:27:07 AM"
- Modification editor = "PANalytical"

More items... (Bookmark 6)

More items... (Bookmark 7)

More items... (Bookmark 8)

More items... (Bookmark 9)

More items... (Bookmark 10)

More items... (Bookmark 11)

More items... (Bookmark 12)

More items... (Bookmark 13)

More items... (Bookmark 14)

More items... (Bookmark 15)

Appendix B

Report – Laser Diffraction of Face Mask Fibers



Analysis Report

Laser Diffraction

Customer: IST

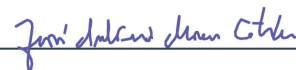
Contact Person: Rafaela Cardoso

Date: 25/05/2023

Doc N°: 7066



(Hugo Gonçalves – Applications Specialist)



(Ver. José A. M. Catita – Technical Manager)

www.paralab.pt • www.paralab.es • analises@paralab.pt

Rua Dr. Joaquim Manuel Costa, 946
Armazém B e C • 4420-437 Valbom, Gondomar

PORTO • LISBOA • SANTANDER • MADRID • BARCELONA

Introduction

Laser Diffraction is an experimental analysis technique that allows the measurement of particle sizes and size distribution in a range from a few nanometres to a few millimetres. A quantitative size distribution of the whole particle population is obtained, thus enabling the determination of the diameters that represent a certain percentage of the referred population. Size distribution can be represented by number or, more frequently, by volume. As the laser hits a particle with a random orientation, the laser diffraction pattern of a population is the combination of every diffraction from every single possible particle orientation. Because of this fact, the size of a particle is reported as the diameter of a sphere that has the same volume as that particle, defined as equivalent spherical diameter or, simply, equivalent diameter.

The theoretical models that allow the calculation of particle diameters from a diffraction pattern are Fraunhofer and Mie. According to ISO 13320, the Fraunhofer theory produces good results for particle sizes above 50 μm . For smaller sizes, the Mie theory offers the best general solution.

The Mie theory is more complete and more accurate, because it takes into account a certain degree of transparency of the particle towards the laser, but in this case one must know the optical properties of the sample, namely the Refractive and Absorption Indexes (RI and AI).

The analysis performed in this work follow the international standards guidelines, namely: ISO 13320, USP 429 and EP 2.9.31.

Experimental Parameters and Procedures

Samples

Four samples were sent for analysis. The goal is to determine the particle size and particle size distribution.

	Samples			
NAME:	Bentonite	Kaolin	Mask no degradation	MH UV T2
SAMPLING PROCEDURE:	Costumer			
APPEARANCE:	Brownish powder	White powder	blue and white fibres	

Sample Reception Date: 18/05/2023

Sample Storage: Room temperature

Instrument

Mastersizer 3000; MalvernPanalytical®; Serial Number: MAL1125347;

Analysis conditions

The samples were analysed in a wet medium by using the Hydro MV accessory. The analysis parameters were the following.

PARAMETER	Value / Description / OBS
Sample	Bentonite
Dispersant:	Ethanol
Dispersant RI:	1.36
Surfactant:	N/A
Sample RI:	1.503
Sample AI:	0.1
Sample amount	N/A
Stirring Speed:	3500 rpm
Optical Pathlength	N/A
Obscuration:	5-15%
Ultrasound:	N/A
Theoretical Model:	Mie
Analysis Model:	General Purpose
Type of Distribution:	Volume

PARAMETER	Value / Description / OBS
Sample	Kaolin, Mask no degradation, MH UV T2
Dispersant:	Water
Dispersant RI:	1.330
Surfactant:	N/A
Sample RI:	1.560
Sample AI:	0.01
Sample amount	N/A
Stirring Speed:	3500 rpm
Optical Pathlength	N/A
Obscuration:	5 – 15%
Ultrasound:	N/A
Theoretical Model:	Mie
Analysis Model:	General Purpose
Type of Distribution:	Volume

Obtained Results

The results (in μm) of the most relevant percentiles are presented in the table below. The percentiles are the average of 6 consecutive measurements and the respective Coefficient of Variation¹ (CV).

Sample:	Dv 10	CV	Dv 50	CV	Dv 90	CV
Bentonite	8.33	2.32	43.2	0.8	110	1.1
Kaolin	2.61	0.84	11.5	3.4	40.7	3.6
Mask no degradation	532	2.7	1370	1.4	2500	0.5
HM UV T2	533	4.3	1400	0.1	2530	1.8

The original analysis report as delivered by the software (version 3.81) is sent in Annex.

¹ Relative standard deviation (deprecated), commonly reported as a percentage.

Measurement Details

Operator Name Regina Torre
Sample Name Average of 'HM UV T2'
SOP File Name HydroMV.cfg

Measurement Details

Analysis Date Time 22/05/2023 11:20:52
Measurement Date Time 22/05/2023 11:20:52
Result Source Averaged

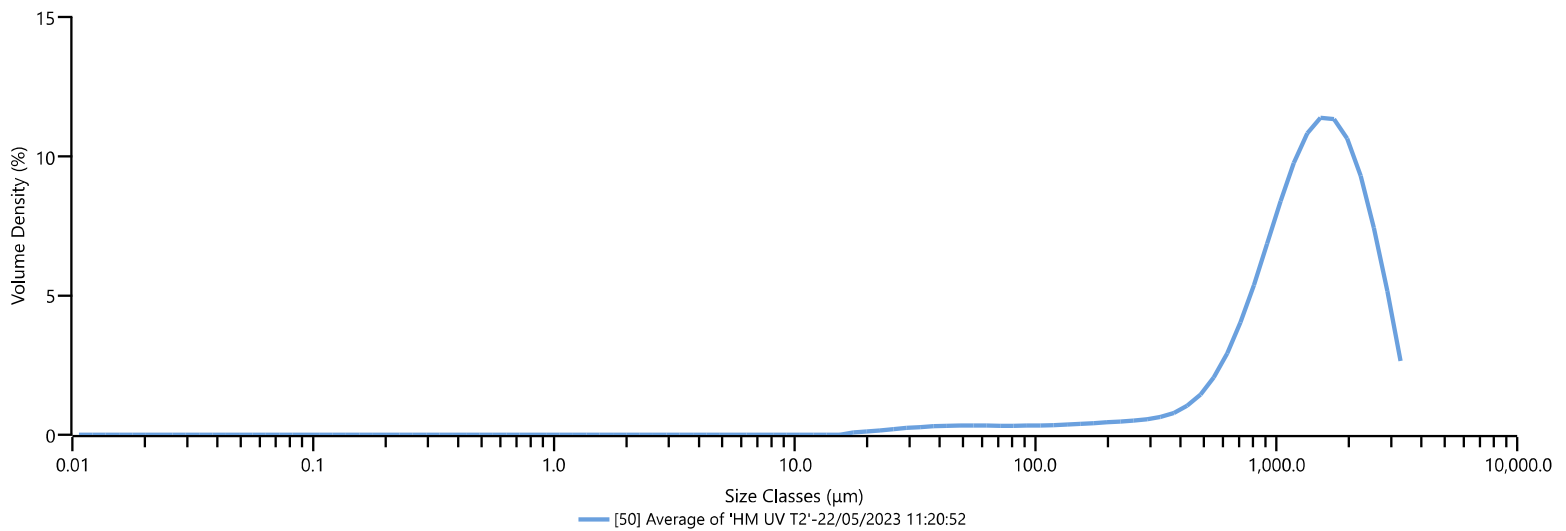
Analysis

Particle Name Material 2
Particle Refractive Index 1.560
Particle Absorption Index 0.010
Dispersant Name Water
Dispersant Refractive Index 1.330
Scattering Model Mie
Analysis Model General Purpose
Weighted Residual 1.74 %
Laser Obscuration 12.80 %

Result

Concentration 1.0281 %
Span 1.422
Uniformity 0.434
Specific Surface Area 10.18 m²/kg
D [4,3] 1470 μm
D [5,3] 1650 μm
Dv (10) 532 μm
Dv (50) 1400 μm
Dv (90) 2530 μm

Frequency (compatible)



Result

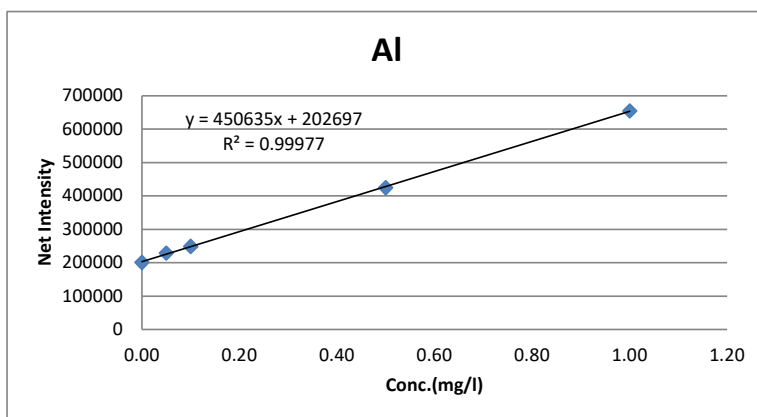
Size (μm)	% Volume In	Size (μm)	% Volume In	Size (μm)	% Volume In	Size (μm)	% Volume In	Size (μm)	% Volume In	Size (μm)	% Volume In	Size (μm)	% Volume In
0.0100	0.00	0.0597	0.00	0.357	0.00	2.13	0.00	12.7	0.00	76.0	0.27	454	1.19
0.0114	0.00	0.0679	0.00	0.405	0.00	2.42	0.00	14.5	0.00	86.4	0.28	516	1.70
0.0129	0.00	0.0771	0.00	0.460	0.00	2.75	0.00	16.4	0.07	98.1	0.28	586	2.42
0.0147	0.00	0.0876	0.00	0.523	0.00	3.12	0.00	18.7	0.10	111	0.29	666	3.35
0.0167	0.00	0.0995	0.00	0.594	0.00	3.55	0.00	21.2	0.14	127	0.31	756	4.47
0.0189	0.00	0.113	0.00	0.675	0.00	4.03	0.00	24.1	0.17	144	0.33	859	5.73
0.0215	0.00	0.128	0.00	0.767	0.00	4.58	0.00	27.4	0.21	163	0.35	976	7.00
0.0244	0.00	0.146	0.00	0.872	0.00	5.21	0.00	31.1	0.24	186	0.37	1110	8.17
0.0278	0.00	0.166	0.00	0.991	0.00	5.92	0.00	35.3	0.26	211	0.40	1260	9.06
0.0315	0.00	0.188	0.00	1.13	0.00	6.72	0.00	40.1	0.27	240	0.43	1430	9.54
0.0358	0.00	0.214	0.00	1.28	0.00	7.64	0.00	45.6	0.28	272	0.47	1630	9.50
0.0407	0.00	0.243	0.00	1.45	0.00	8.68	0.00	51.8	0.28	310	0.53	1850	8.91
0.0463	0.00	0.276	0.00	1.65	0.00	9.86	0.00	58.9	0.28	352	0.65	2100	7.79
0.0526	0.00	0.314	0.00	1.88	0.00	11.2	0.00	66.9	0.27	400	0.86	2390	6.22



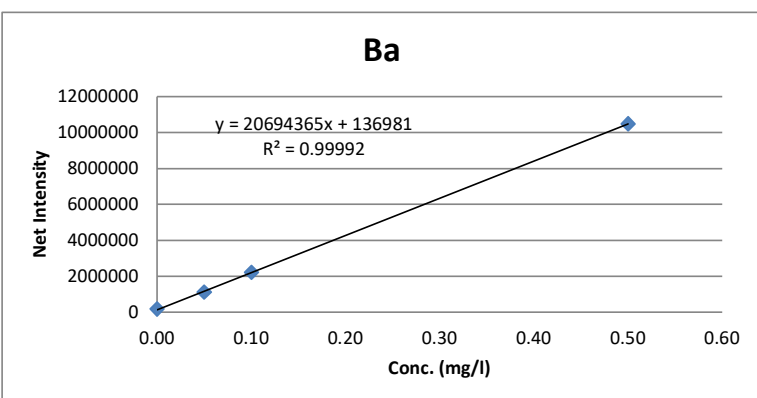
Appendix C

Report – Chemical Analysis of Water Samples

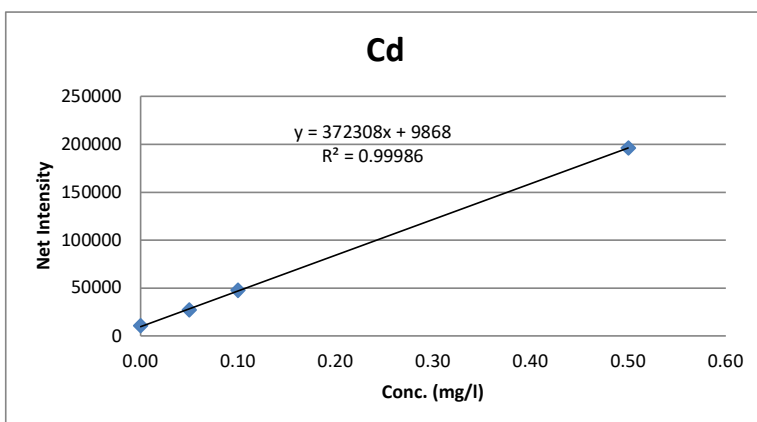
Sample Name	Conc. (mg/l)	Net Intensity	RSD(%)
Padrões	0.00	200263	0.29
	0.05	228813	0.44
	0.10	248579	0.23
	0.50	424602	0.06
	1.00	654778	0.94
pure water	-0.01	196640	0.39
2 MH-NOUV	0.16	274236	1.14
4 ML-NOUV	0.58	462847	5.83
6 ML-UV	0.10	246129	2.15
7 NM-UV	0.05	226122	0.11
8 NM-NOUV	1.44	853381	5.51
9 MH-UV	0.18	283991	3.16
12 MH-UV	0.03	218154	2.06
13 VMH-UV T2	0.00	203422	0.34
14 MH T2	-0.01	200274	0.37
15 ML-UV T2	0.00	201173	0.50
16 ML T2	0.00	204487	0.21



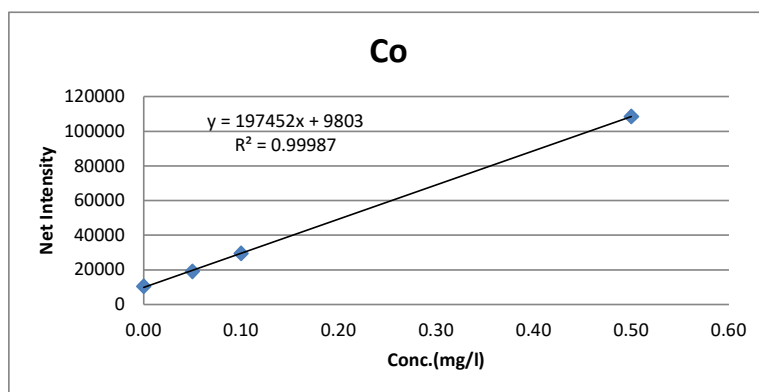
Sample Name	Conc. (mg/l)	Net Intensity	RSD(%)
Padrões	0.00	179852	0.49
	0.05	1112697	1.41
	0.10	2219206	1.76
	0.50	10487506	0.15
pure water	0.00	177677	0.29
2 MH-NOUV	0.07	1490036	1.51
4 ML-NOUV	0.04	947648	1.04
6 ML-UV	0.07	1539510	2.37
7 NM-UV	0.05	1185931	1.84
8 NM-NOUV	0.02	498895	1.58
9 MH-UV	0.02	639425	2.18
12 MH-UV	0.09	1975129	1.57
13 VMH-UV T2	0.01	289755	0.50
14 MH T2	0.00	200003	0.46
15 ML-UV T2	0.01	323542	0.37
16 ML T2	0.00	233122	0.28



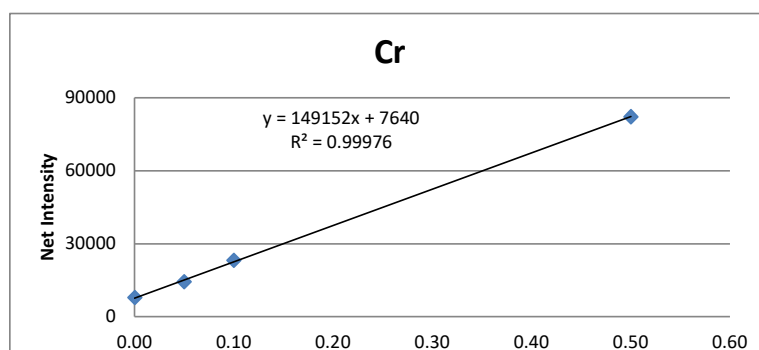
Sample Name	Conc. (mg/l)	Net Intensity	RSD(%)
Padrões	0.00	10734	1.06
	0.05	27073	1.71
	0.10	47603	1.98
	0.50	196062	3.71
pure water	0.00	10978	2.04
2 MH-NOUV	0.00	10902	0.78
4 ML-NOUV	0.00	11019	1.41
6 ML-UV	0.00	10920	2.41
7 NM-UV	0.00	10985	0.49
8 NM-NOUV	0.00	11034	1.82
9 MH-UV	0.00	11066	0.41
12 MH-UV	0.00	10842	2.11
13 VMH-UV T2	0.00	10971	0.58
14 MH T2	0.00	11034	0.73
15 ML-UV T2	0.00	11224	0.56
16 ML T2	0.00	11022	2.44



Sample Name	Conc. (mg/l)	Net Intensity	RSD(%)
Padrões	0.00	10420	0.88
	0.05	19042	2.18
	0.10	29489	2.52
	0.50	108604	0.71
pure water	0.00	10728	1.23
2 MH-NOUV	0.00	10730	0.53
4 ML-NOUV	0.00	10765	0.81
6 ML-UV	0.00	10577	1.22
7 NM-UV	0.00	10647	0.53
8 NM-NOUV	0.01	10873	0.89
9 MH-UV	0.00	10649	0.72
12 MH-UV	0.00	10538	0.86
13 VMH-UV T2	0.00	10701	1.68
14 MH T2	0.00	10724	2.63
15 ML-UV T2	0.00	10756	0.57
16 ML T2	0.00	10666	0.28



Sample Name	Conc. (mg/l)	Net Intensity	RSD(%)
Padrões	0.00	7824	1.21
	0.05	14403	1.45
	0.10	23106	1.44
	0.50	82175	0.96
pure water	0.00	8118	0.97
2 MH-NOUV	0.00	8046	1.32
4 ML-NOUV	0.00	8204	1.45
6 ML-UV	0.00	8154	0.99
7 NM-UV	0.00	7954	0.82
8 NM-NOUV	0.00	8375	1.11
9 MH-UV	0.00	8007	2.50
12 MH-UV	0.00	8016	0.65
13 VMH-UV T2	0.00	7924	1.57
14 MH T2	0.00	8080	1.71

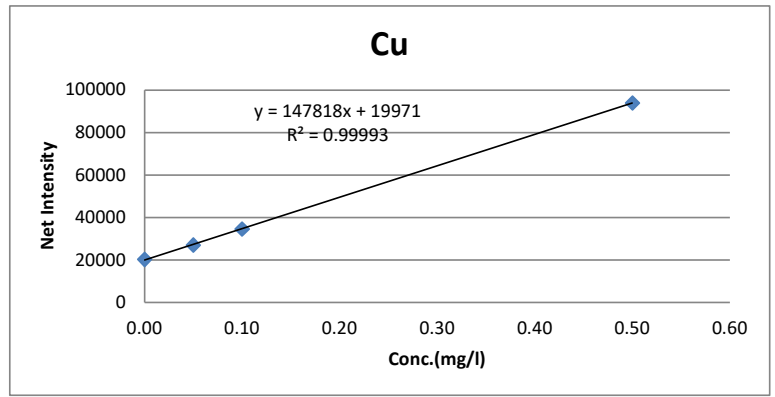


15 ML-UV T2	0.00	8046	0.78
16 ML T2	0.00	8083	0.90

Conc. (mg/l)

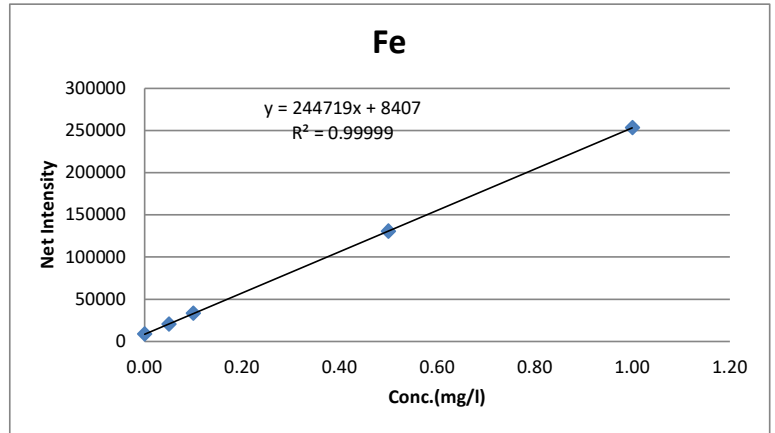
Cu 224.700

Sample Name	Conc. (mg/l)	Net Intensity	RSD(%)
Padrões	0.00	20342	1.05
	0.05	27046	1.03
	0.10	34643	1.75
	0.50	93933	2.19
pure water	-0.05	12607	0.54
2 MH-NOUV	-0.05	12098	0.68
4 ML-NOUV	-0.05	12150	1.04
6 ML-UV	-0.05	11889	1.15
7 NM-UV	-0.05	11873	1.08
8 NM-NOUV	-0.05	11933	0.21
9 MH-UV	-0.06	11768	0.69
12 MH-UV	-0.06	11793	0.68
13 VMH-UV T2	-0.05	11934	0.62
14 MH T2	-0.06	11657	0.86
15 ML-UV T2	-0.05	12370	0.29
16 ML T2	-0.05	12090	1.69



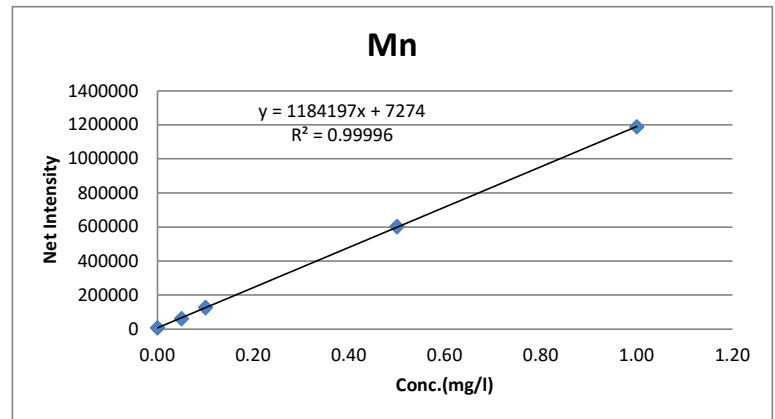
Fe 259.940

Sample Name	Conc. (mg/l)	Net Intensity	RSD(%)
Padrões	0.00	8521	1.06
	0.05	20416	0.60
	0.10	33166	1.96
	0.50	130455	1.77
	1.00	253265	1.52
pure water	0.00	8735	1.46
2 MH-NOUV	0.08	27450	1.60
4 ML-NOUV	0.46	120380	4.33
6 ML-UV	0.03	16379	1.82
7 NM-UV	0.03	15097	1.06
8 NM-NOUV	0.97	246780	1.15
9 MH-UV	0.12	37065	1.73
12 MH-UV	0.01	11648	1.99
13 VMH-UV T2	0.00	8585	0.91
14 MH T2	0.00	8609	0.92
15 ML-UV T2	0.00	9475	0.66
16 ML T2	0.00	8592	0.37



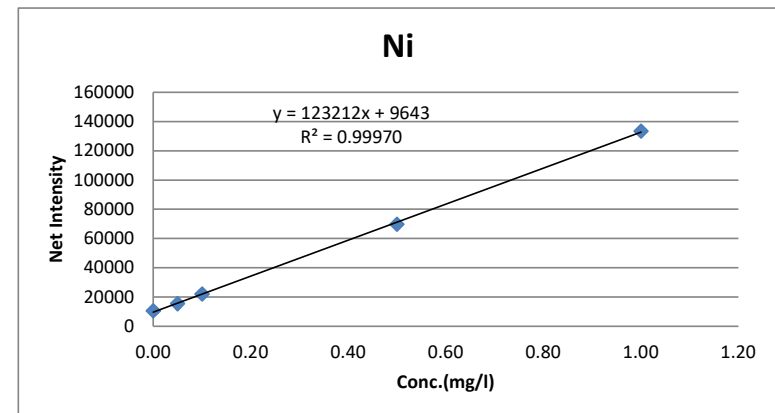
Mn 257.610

Sample Name	Conc. (mg/l)	Net Intensity	RSD(%)
Padrões	0.00	8404	1.15
	0.05	61808	0.98
	0.10	127518	0.95
	0.50	602710	2.36
	1.00	1189853	1.45
pure water	0.00	9204	0.78
2 MH-NOUV	0.00	9449	4.03
4 ML-NOUV	0.01	22609	2.05
6 ML-UV	0.00	9094	1.54
7 NM-UV	0.00	10176	0.83
8 NM-NOUV	0.01	17808	1.12
9 MH-UV	0.00	10821	4.05
12 MH-UV	0.00	12495	1.21
13 VMH-UV T2	0.01	15486	1.46
14 MH T2	0.00	9681	0.73
15 ML-UV T2	0.01	14852	0.72
16 ML T2	0.00	12982	1.22



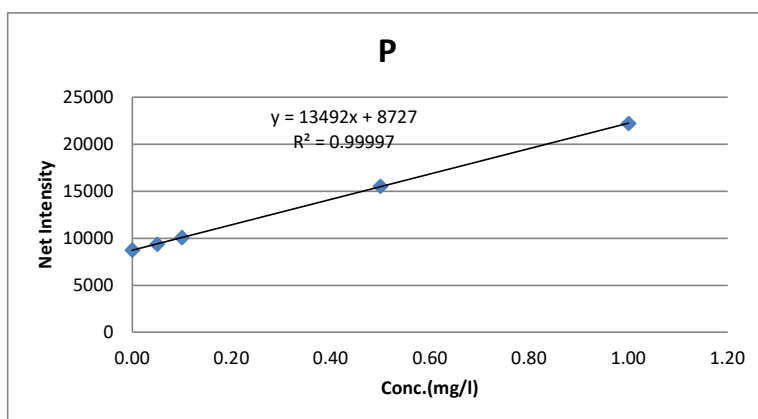
Ni 231.604

Sample Name	Conc. (mg/l)	Net Intensity	RSD(%)
Padrões	0.00	10524	2.50
	0.05	15488	1.90
	0.10	22085	1.16
	0.50	69869	1.62
	1.00	133549	1.45
pure water	0.01	10745	2.69
2 MH-NOUV	0.01	10896	0.46
4 ML-NOUV	0.01	10963	1.27
6 ML-UV	0.01	10518	3.11
7 NM-UV	0.01	10522	4.22
8 NM-NOUV	0.01	10905	1.23
9 MH-UV	0.01	10891	1.51
12 MH-UV	0.01	10739	2.22
13 VMH-UV T2	0.02	12342	1.44
14 MH T2	0.01	10775	2.11
15 ML-UV T2	0.02	12603	0.65
16 ML T2	0.02	12160	1.49



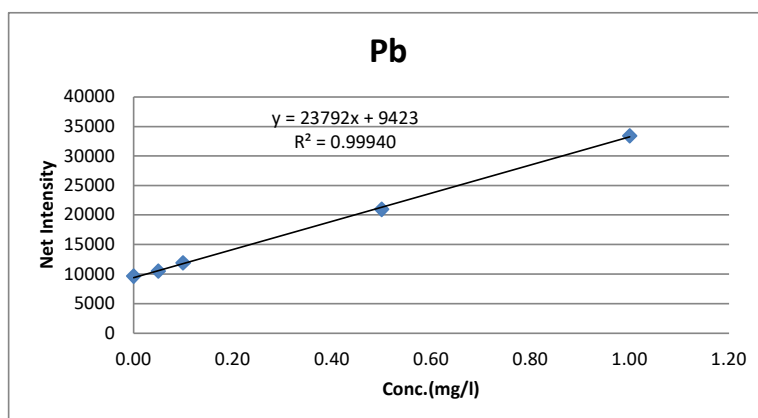
P 214.914

Sample Name	Conc. (mg/l)	Net Intensity	RSD(%)
Padrões	0.00	8740	1.92
	0.05	9369	1.62
	0.10	10072	0.59
	0.50	15514	2.35
	1.00	22200	0.89
pure water	0.00	8775	1.56
2 MH-NOUV	0.02	9048	0.47
4 ML-NOUV	0.06	9541	5.60
6 ML-UV	0.01	8852	0.26
7 NM-UV	0.03	9109	0.53
8 NM-NOUV	0.08	9778	0.92
9 MH-UV	0.03	9099	0.79
12 MH-UV	0.02	9039	1.21
13 VMH-UV T2	0.02	8930	1.16
14 MH T2	0.02	8938	1.06
15 ML-UV T2	0.09	9967	0.18
16 ML T2	0.04	9257	2.31



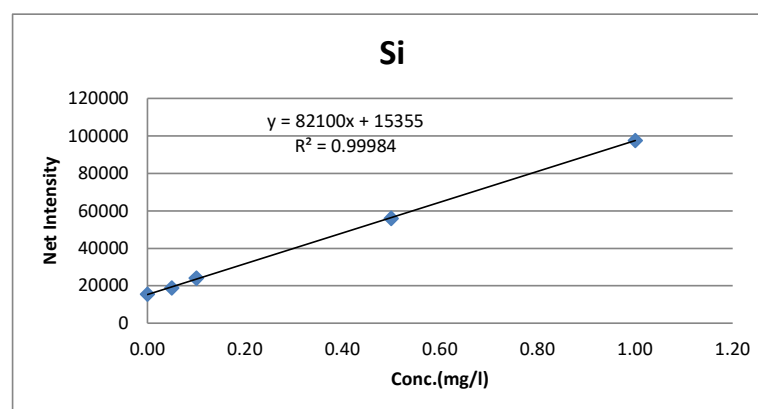
Pb 220.353

Sample Name	Conc. (mg/l)	Net Intensity	RSD(%)
Padrões	0.00	9647	0.90
	0.05	10509	1.07
	0.10	11871	1.52
	0.50	20941	2.82
	1.00	33402	1.37
pure water	0.01	9754	0.18
2 MH-NOUV	0.02	9836	1.14
4 ML-NOUV	0.02	9877	0.64
6 ML-UV	0.02	9809	0.86
7 NM-UV	0.02	9915	1.74
8 NM-NOUV	0.02	9873	0.91
9 MH-UV	0.02	9873	0.66
12 MH-UV	0.02	9811	0.91
13 VMH-UV T2	0.02	9787	1.52
14 MH T2	0.02	9848	1.15
15 ML-UV T2	0.02	9831	0.50
16 ML T2	0.02	9839	0.88



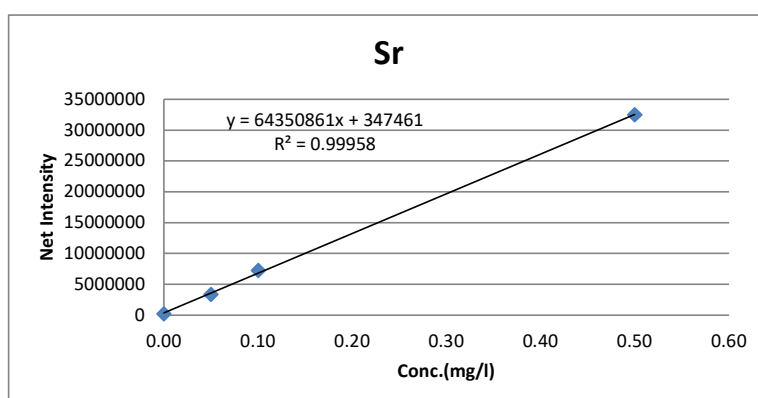
Si 251.611

Sample Name	Conc. (mg/l)	Net Intensity	RSD(%)
Padrões	0.00	15585	0.83
	0.05	18902	1.17
	0.10	24089	1.69
	0.50	56061	1.08
	1.00	97602	3.02
pure water	0.00	15715	0.44
2 MH-NOUV	5.45	462816	0.90
4 ML-NOUV	7.27	611874	3.11
6 ML-UV	7.79	654843	2.56
7 NM-UV	8.26	693767	0.70
8 NM-NOUV	7.01	590781	3.06
9 MH-UV	5.68	481350	0.74
12 MH-UV	8.07	678206	0.53
13 VMH-UV T2	0.32	41870	0.56
14 MH T2	0.05	19183	0.19
15 ML-UV T2	0.30	39942	2.03
16 ML T2	0.17	29548	0.85



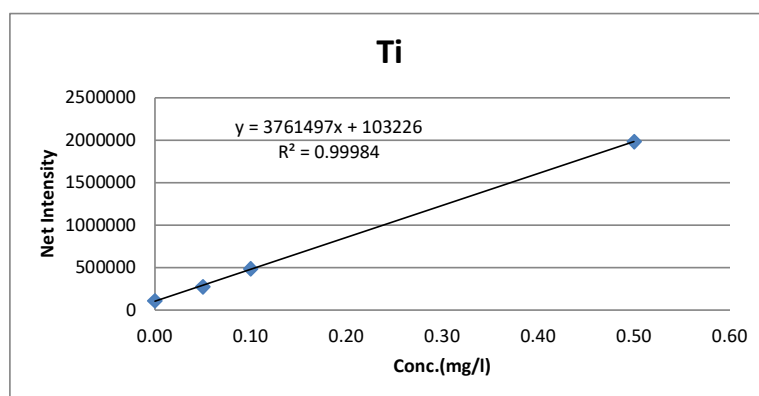
Sr 407.771

Sample Name	Conc. (mg/l)	Net Intensity	RSD(%)
Padrões	0.00	192495	0.42
	0.05	3346037	0.40
	0.10	7222592	1.32
	0.50	32456779	1.65
	1.00	64350861	1.65
pure water	0.00	209299	0.47
2 MH-NOUV	0.13	8953337	0.66
4 ML-NOUV	0.08	5678189	0.45
6 ML-UV	0.15	9808905	2.66
7 NM-UV	0.11	7596280	0.54
8 NM-NOUV	0.05	3476119	1.46
9 MH-UV	0.07	5071124	0.74
12 MH-UV	0.16	10407395	1.28
13 VMH-UV T2	0.01	947918	2.23
14 MH T2	0.00	344852	1.46
15 ML-UV T2	0.01	747851	1.67
16 ML T2	0.01	729659	1.80



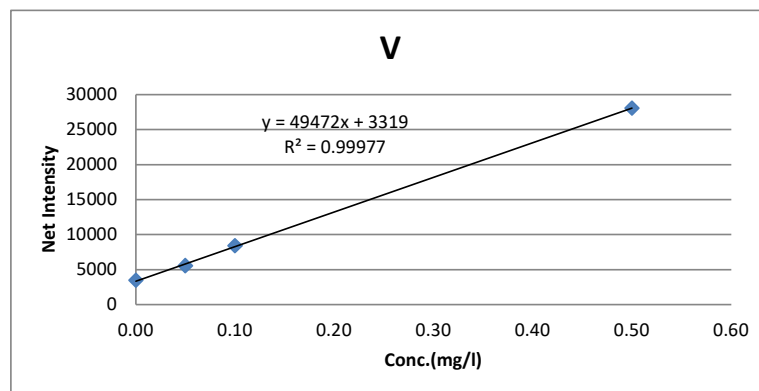
Ti 334.941

Sample Name	Conc. (mg/l)	Net Intensity	RSD(%)
Padrões	0.00	110239	0.58
	0.05	276062	0.25
	0.10	487754	2.52
	0.50	1983823	0.73
pure water	0.00	107991	0.29
2 MH-NOUV	0.02	165186	1.18
4 ML-NOUV	0.06	317787	7.90
6 ML-UV	0.01	136190	4.63
7 NM-UV	0.00	121205	0.67
8 NM-NOUV	0.13	594467	1.92
9 MH-UV	0.02	177964	6.17
12 MH-UV	0.00	113839	2.18
13 VMH-UV T2	0.00	108783	0.29
14 MH T2	0.00	109007	0.43
15 ML-UV T2	0.00	110249	0.52
16 ML T2	0.00	109506	0.66



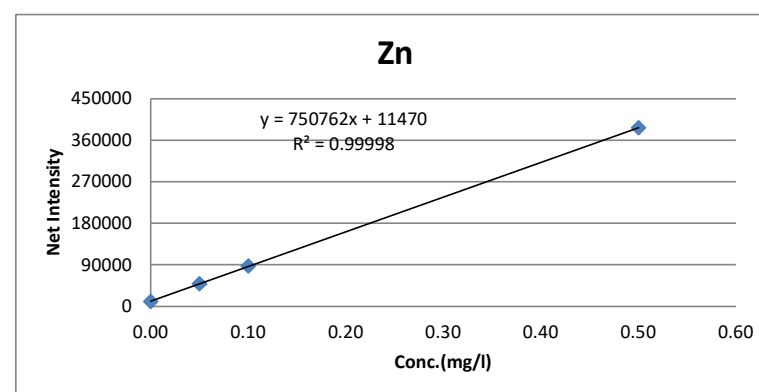
V 292.402

Sample Name	Conc. (mg/l)	Net Intensity	RSD(%)
Padrões	0.00	3441	1.73
	0.05	5551	1.50
	0.10	8385	2.91
	0.50	28055	0.36
pure water	0.00	3416	2.44
2 MH-NOUV	0.00	3556	0.57
4 ML-NOUV	0.01	3632	1.69
6 ML-UV	0.01	3616	0.28
7 NM-UV	0.01	3582	1.32
8 NM-NOUV	0.01	3802	0.91
9 MH-UV	0.01	3632	1.35
12 MH-UV	0.01	3575	1.48
13 VMH-UV T2	0.00	3439	0.78
14 MH T2	0.00	3521	2.00
15 ML-UV T2	0.00	3435	1.20
16 ML T2	0.00	3443	1.58



Zn 213.856

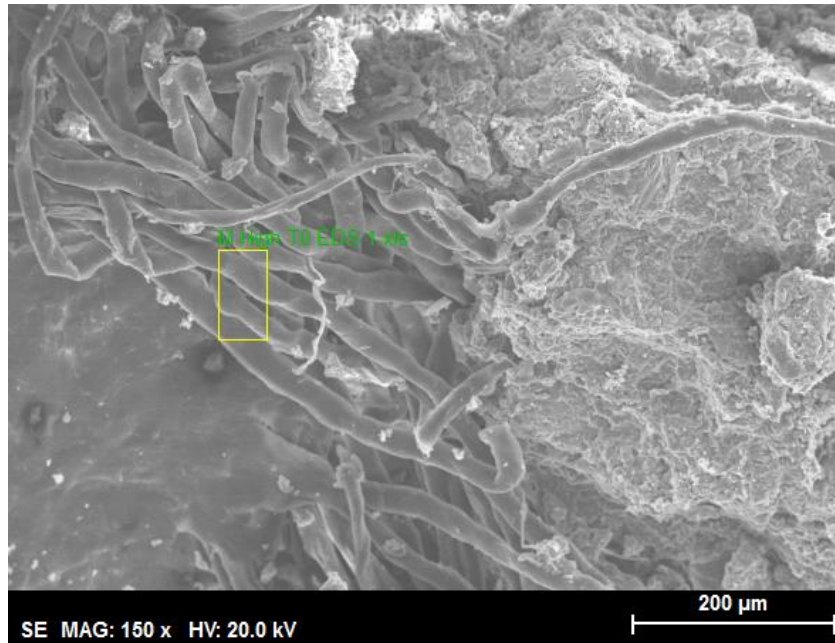
Sample Name	Conc. (mg/l)	Net Intensity	RSD(%)
Padrões	0.00	10449	1.13
	0.05	49355	0.98
	0.10	87432	0.34
	0.50	386639	0.73
pure water	0.00	13746	1.78
2 MH-NOUV	0.00	11337	1.59
4 ML-NOUV	0.00	10436	0.98
6 ML-UV	0.00	9910	0.90
7 NM-UV	0.00	9909	0.89
8 NM-NOUV	0.00	10837	9.65
9 MH-UV	0.00	9862	2.74
12 MH-UV	0.00	9633	1.50
13 VMH-UV T2	0.13	109405	1.52
14 MH T2	0.03	36433	5.14
15 ML-UV T2	0.12	102102	0.84
16 ML T2	0.18	149808	1.40



Appendix D

Energy-Dispersive X-ray Spectroscopy

MH T0



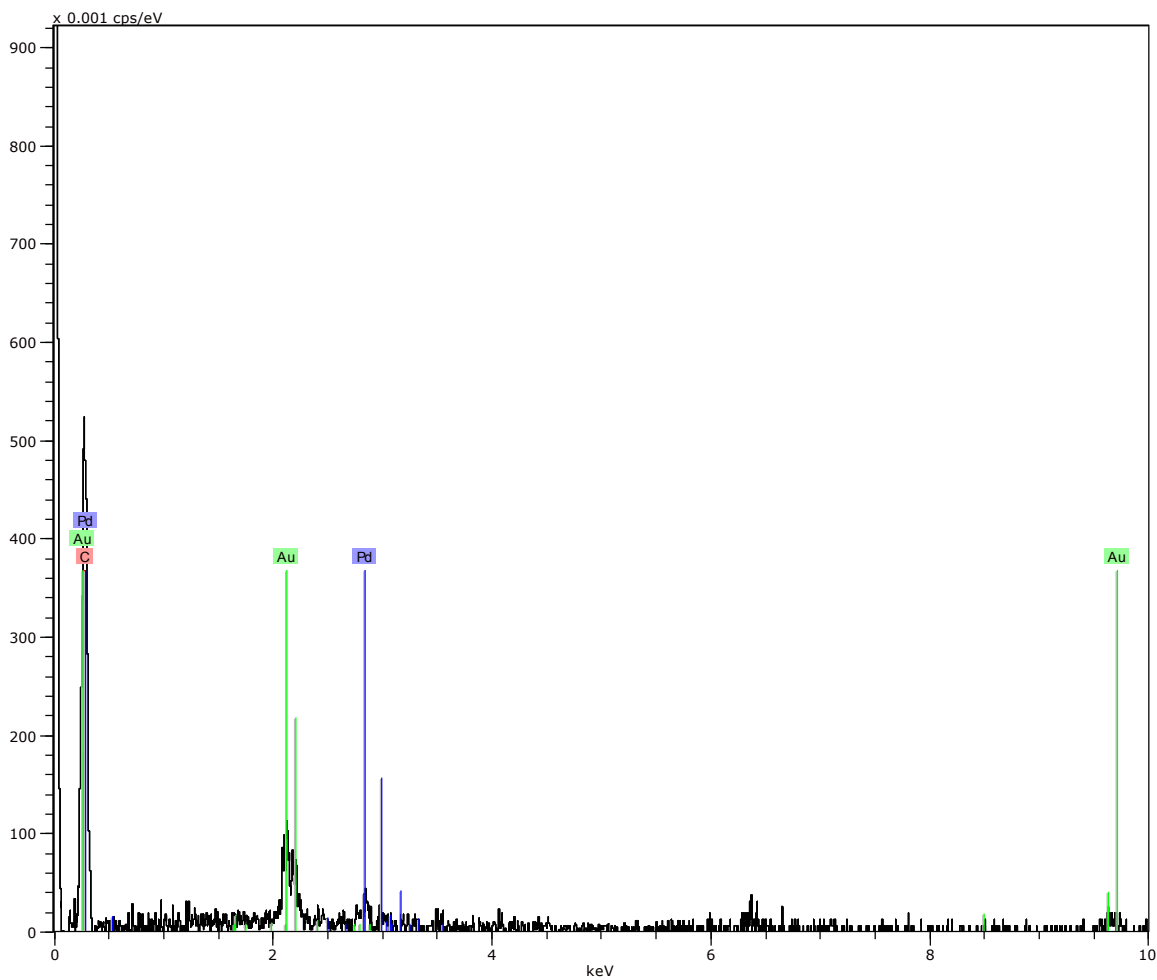
1 1

Date:22-05-2023 09:39:31

Image size:2400 x 1800

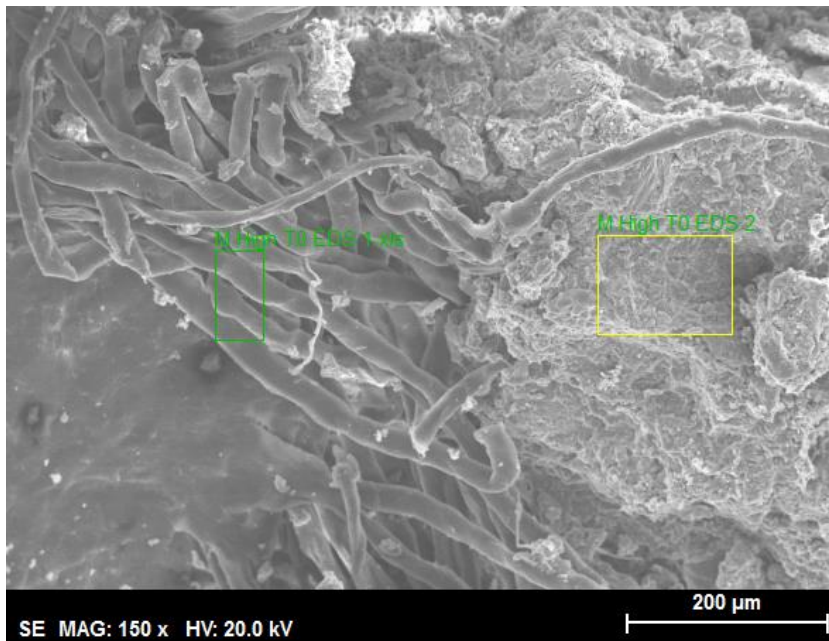
Mag:150x

HV:20.0kV

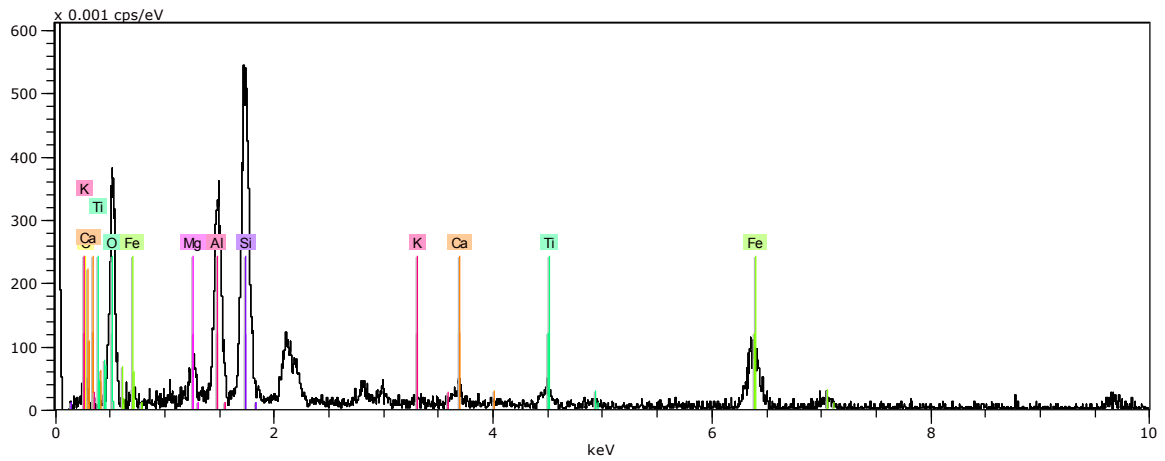


M High T0 EDS 1.xls
th.:0.30kcps

Date:22-05-2023 09:41:11 HV:20.0kV Puls



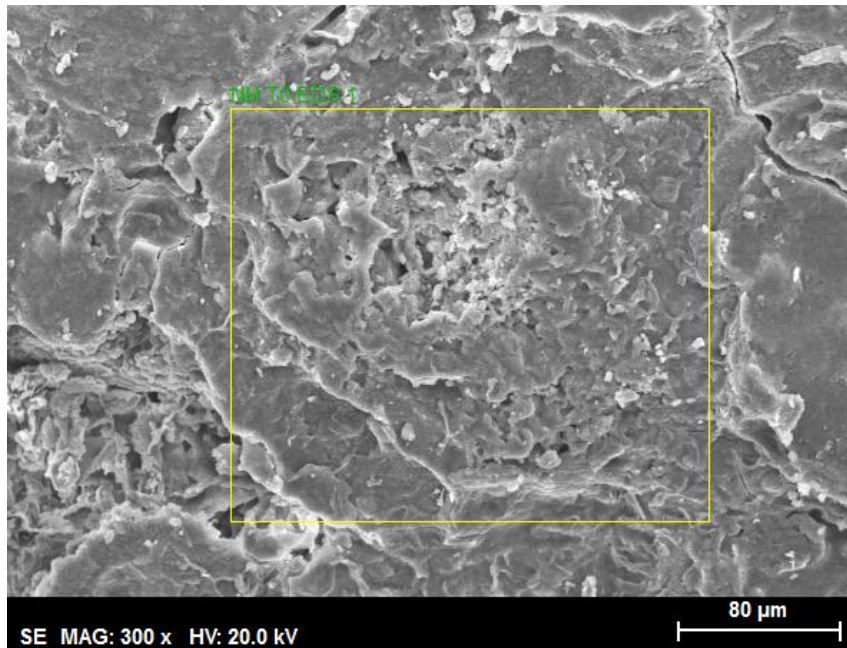
M High TO
 Date:22-05-2023 09:39:31
 Image size:2400 x 1800
 Mag:150x
 HV:20.0kV



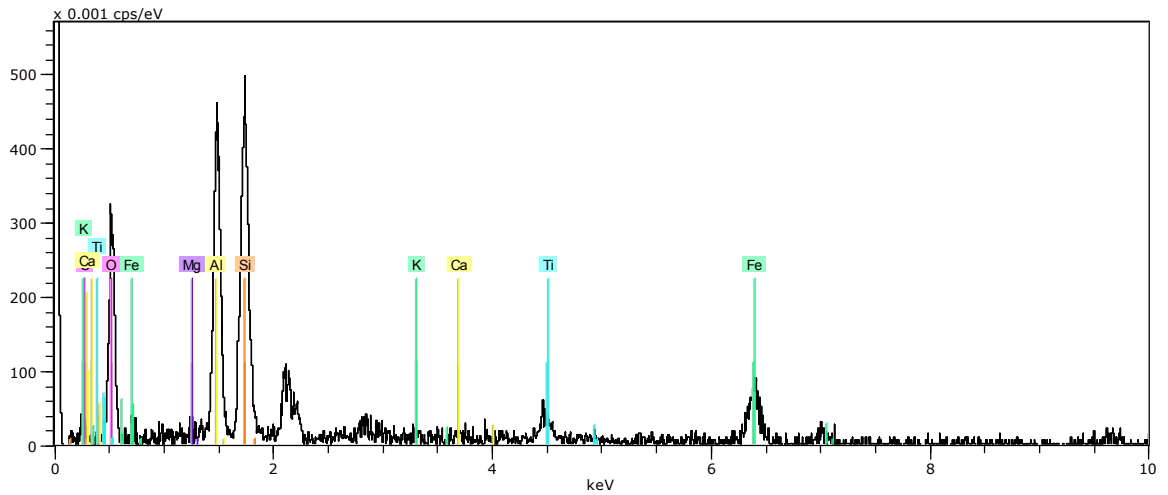
M High TO EDS 2.spx Date:22-05-2023 09:42:11 HV:20.0kV Puls
 th.:0.43kcps

El	AN	Series	unn. C [wt.%]	norm. C [wt.%]	Atom. C [at.%]	Error (1 Sigma) [wt.%]
O	8	K-series	27.84	40.34	53.75	6.07
C	6	K-series	6.29	9.12	16.19	3.46
Si	14	K-series	10.16	14.73	11.18	0.54
Al	13	K-series	6.56	9.51	7.51	0.43
Fe	26	K-series	13.39	19.41	7.41	0.66
Mg	12	K-series	1.08	1.56	1.37	0.14
Ti	22	K-series	1.99	2.89	1.28	0.19
Ca	20	K-series	1.36	1.97	1.05	0.14
K	19	K-series	0.33	0.48	0.26	0.08
Total:			69.02	100.00	100.00	

NM T0



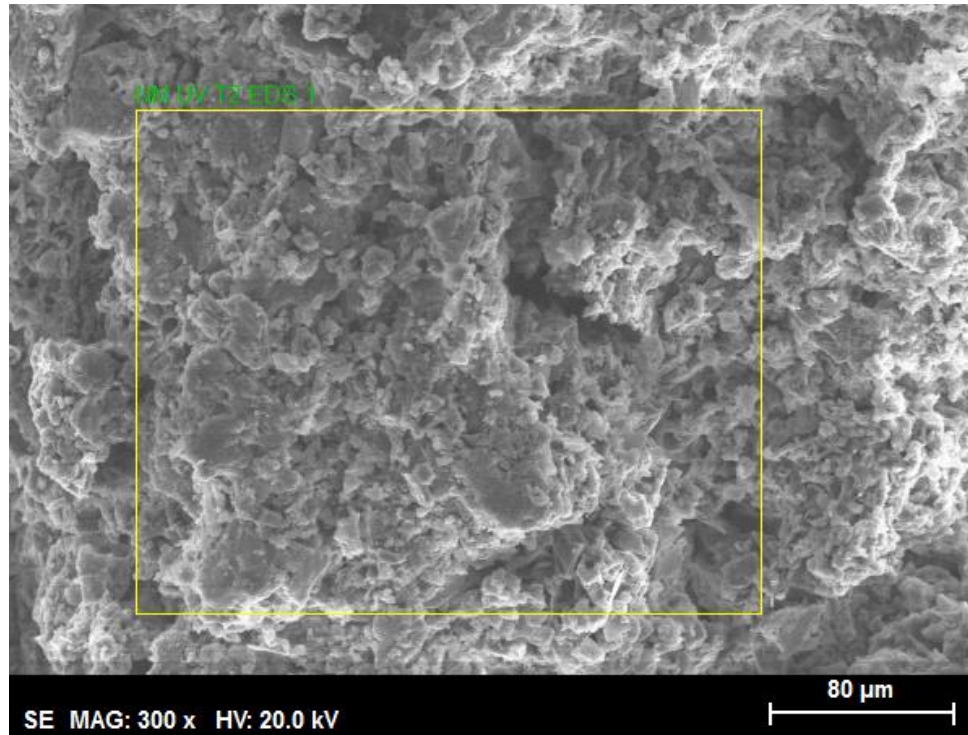
NM T0 2
 Date:22-05-2023 09:48:36
 Image size:2400 x 1800
 Mag:300x
 HV:20.0kV



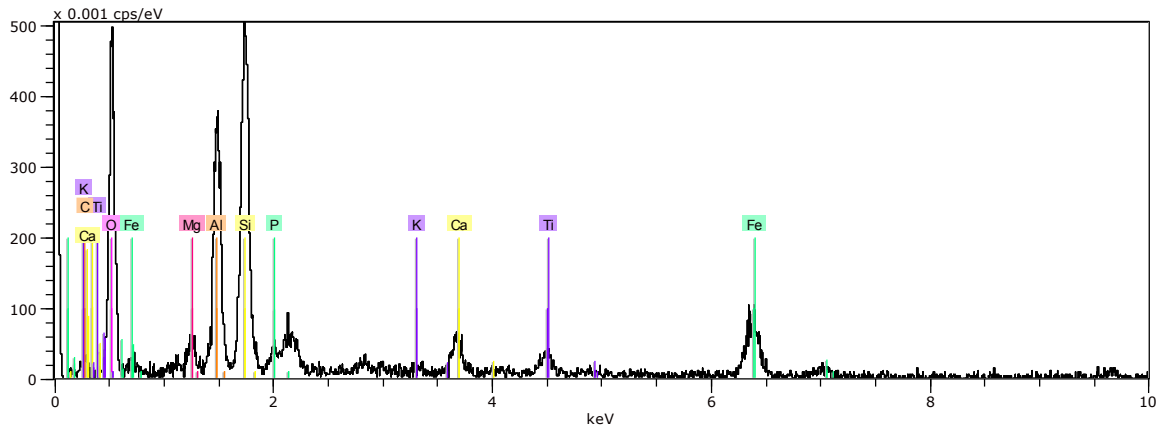
NM T0 EDS 1.xls Date:22-05-2023 09:49:06 HV:20.0kV Puls th.:0.41kcps

El	AN	Series	unn. C [wt.%]	norm. C [wt.%]	Atom. C [at.%]	Error (1 Sigma) [wt.%]
O	8	K-series	22.37	40.70	59.94	5.27
Si	14	K-series	10.08	18.33	15.38	0.56
Al	13	K-series	8.26	15.02	13.12	0.52
Fe	26	K-series	11.01	20.03	8.45	0.61
Ti	22	K-series	2.59	4.72	2.32	0.23
Ca	20	K-series	0.29	0.53	0.31	0.08
K	19	K-series	0.27	0.50	0.30	0.07
Mg	12	K-series	0.10	0.17	0.17	0.05
C	6	K-series	0.00	0.00	0.00	0.00
Total:			54.96	100.00	100.00	

NM T2



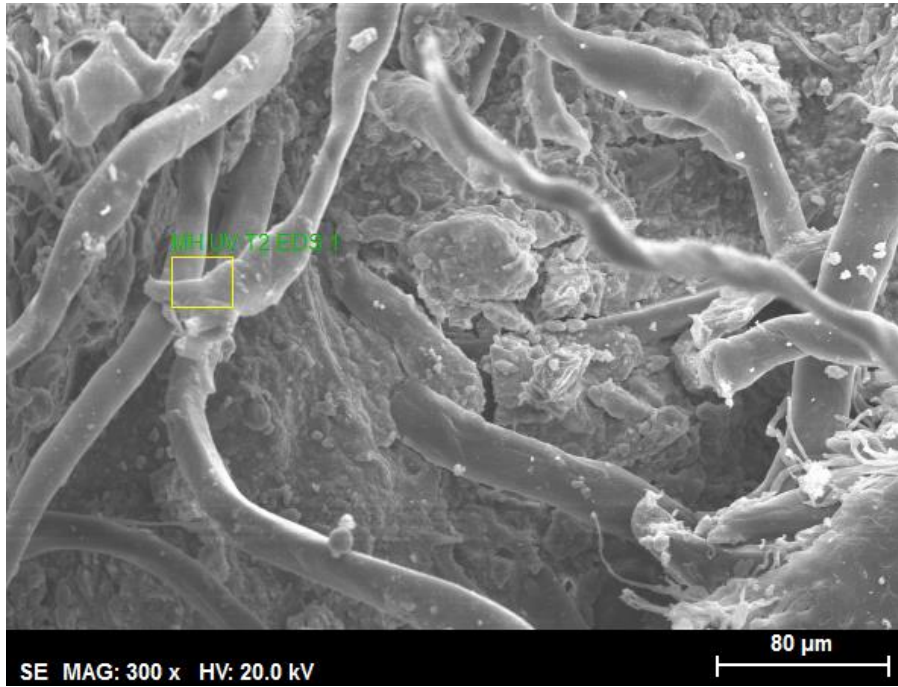
NM UV T2 2
 Date:22-05-2023 09:57:45
 Image size:2400 x 1800
 Mag:300x
 HV:20.0kV



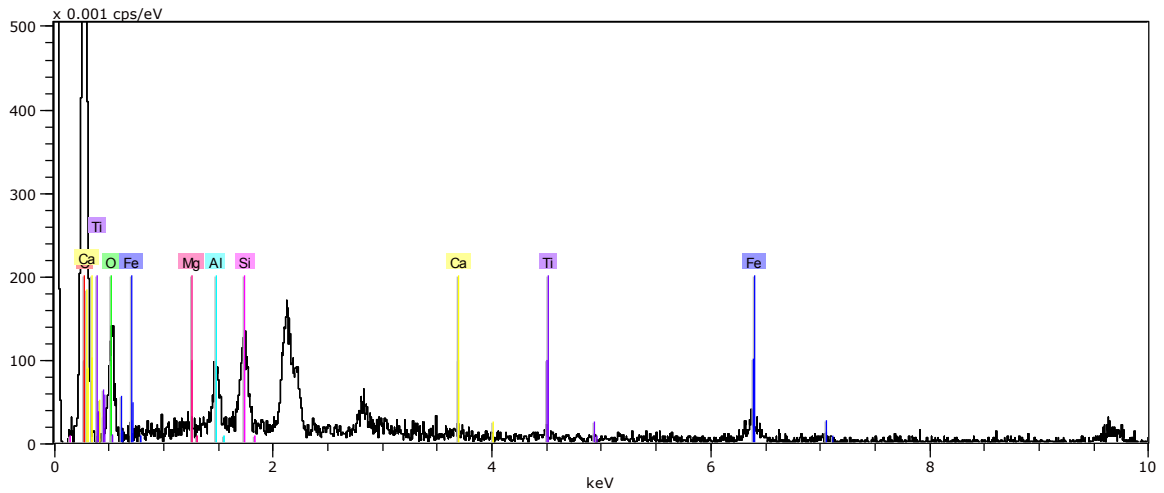
NM UV T2 EDS 1.spx Date:22-05-2023 09:58:16 HV:20.0kV Puls
 th.:0.43kcps

El	AN	Series	unn. C [wt.%]	norm. C [wt.%]	Atom. C [at.%]	Error (1 Sigma) [wt.%]
O	8	K-series	50.14	46.02	58.93	9.36
Si	14	K-series	17.43	16.00	11.67	0.88
C	6	K-series	6.88	6.31	10.76	3.64
Al	13	K-series	13.80	12.67	9.62	0.81
Fe	26	K-series	11.35	10.41	3.82	0.52
Mg	12	K-series	2.19	2.01	1.69	0.24
P	15	K-series	2.25	2.06	1.36	0.20
Ca	20	K-series	2.43	2.23	1.14	0.17
Ti	22	K-series	2.27	2.08	0.89	0.18
K	19	K-series	0.22	0.21	0.11	0.06
Total:			108.95	100.00	100.00	

MH, UV T2



SE MAG: 300 x HV: 20.0 kV
 MH UV T2 2
 Date:22-05-2023 10:07:39
 Image size:2400 x 1800
 Mag:300x
 HV:20.0kV

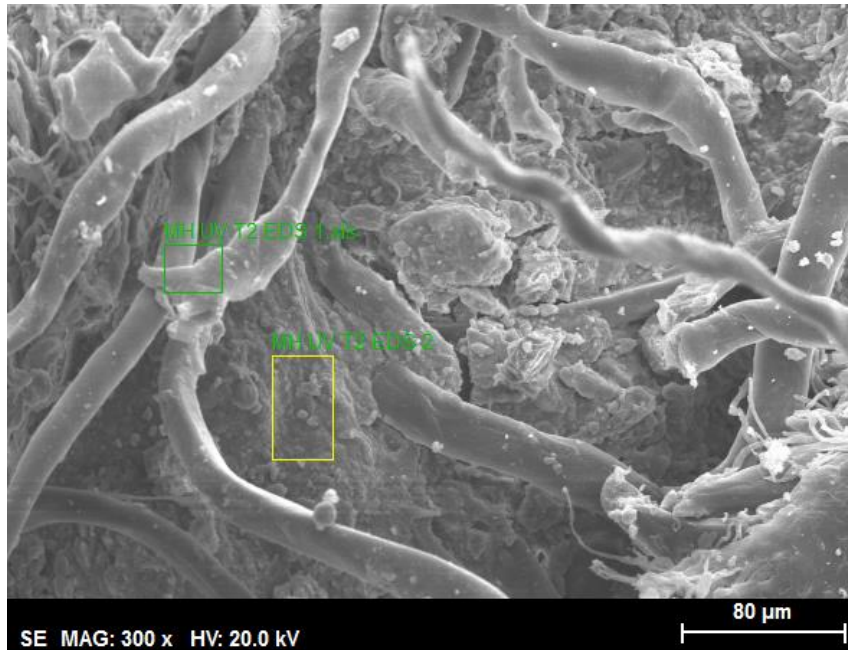


MH UV T2 EDS 1.xls
 th.:0.40kcps

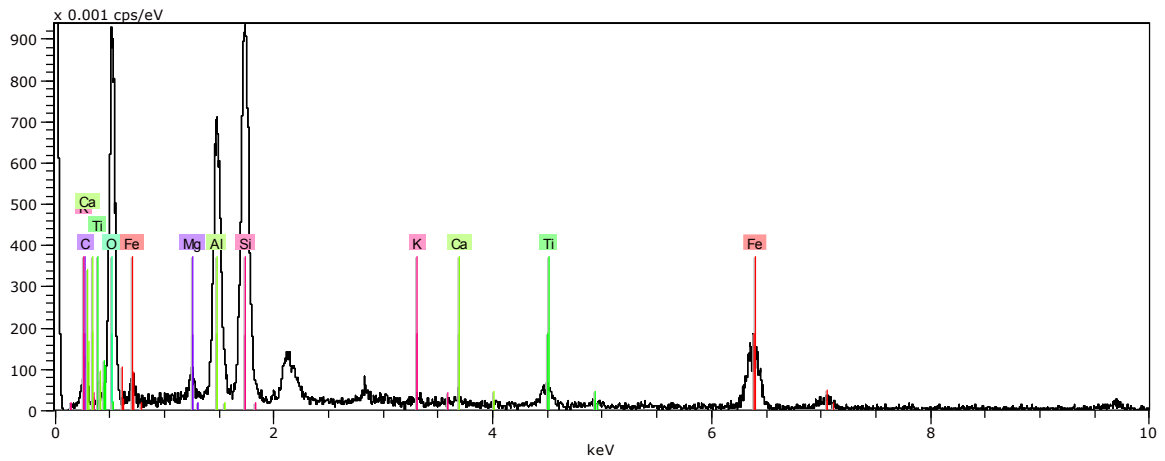
Date:22-05-2023 10:08:25 HV:20.0kV Puls

El	AN	Series	unn. C [wt.%]	norm. C [wt.%]	Atom. C [at.%]	Error (1 Sigma) [wt.%]
C	6	K-series	71.88	71.88	79.72	11.61
O	8	K-series	21.64	21.64	18.02	5.66
Fe	26	K-series	3.25	3.25	0.77	0.25
Si	14	K-series	1.54	1.54	0.73	0.13
Al	13	K-series	1.17	1.17	0.58	0.12
Ti	22	K-series	0.31	0.31	0.09	0.07
Mg	12	K-series	0.08	0.08	0.05	0.05
Ca	20	K-series	0.12	0.12	0.04	0.05

Total: 100.00 100.00 100.00

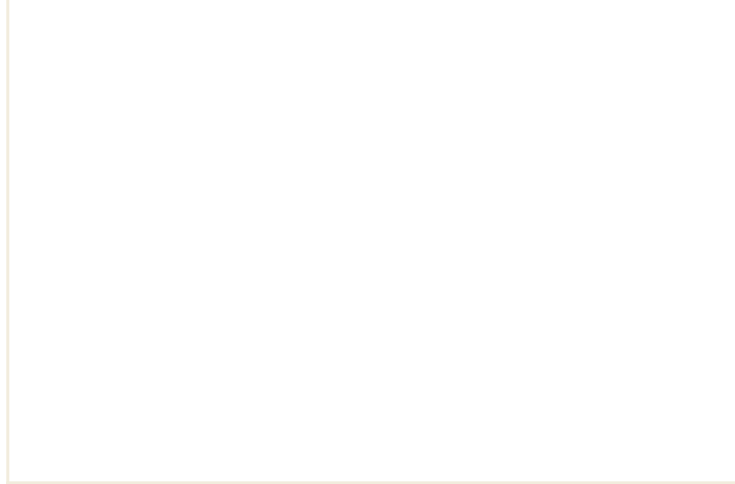


SE MAG: 300 x HV: 20.0 kV
 MH UV T2 2
 Date:22-05-2023 10:07:39
 Image size:2400 x 1800
 Mag:300x
 HV:20.0kV



MH UV T2 EDS 2.spx Date:22-05-2023 10:10:28 HV:20.0kV Puls
 th.:0.60kcps

El	AN	Series	unn. C [wt.%]	norm. C [wt.%]	Atom. C [at.%]	Error (1 Sigma) [wt.%]
O	8	K-series	44.18	46.34	55.67	7.10
C	6	K-series	13.62	14.29	22.86	3.92
Si	14	K-series	10.53	11.04	7.56	0.51
Al	13	K-series	8.88	9.32	6.64	0.49
Fe	26	K-series	13.71	14.38	4.95	0.54
Ti	22	K-series	2.39	2.51	1.01	0.16
Mg	12	K-series	0.91	0.96	0.76	0.11
Ca	20	K-series	0.60	0.63	0.30	0.08
K	19	K-series	0.52	0.55	0.27	0.07
Total:			95.34	100.00	100.00	



 **NTNU**

Norwegian University of
Science and Technology